THE
PHYSICAL REVIEW
A Journal of Experimental and Theoretical Physics Established by E. L. Nichols in 1893
VOL. 55, NO. 3 FEBRUARY 1, 1939 SECOND SERIES

Energies of the Soft Beta-Radiations of Rubidium and Other Bodies. Method for Their Determination

W. F. LIBBY AND D. D. LEE
Department of Chemistry, University of California, Berkeley, California
(Received September 6, 1938)

A method for measuring the upper limits of soft beta-spectra by use of screen wall tube counters filled with hydrogen gas is described. Illustrative results are given for Rb^{87}, Na^{22}, S^{35}, and Au^{198}.

INTRODUCTION

THE necessity of checking any relation between the decay constants of beta-radioactive nuclei and the energies of the emitted radiations of the type Sargent[1] has suggested makes data on the energies of soft beta-spectra valuable. The difficulties of such a measurement, arising principally from the high probability of scattering for low energy electrons, have previously prevented our obtaining of data of desirable reliability for the rather numerous long-lived soft emitters.

The following discussion is intended to be a brief presentation of a method which apparently will serve for beta-radiation harder than about ten or twenty kilovolts. Illustrative data are given.

APPARATUS AND METHOD

The method[2] employs a screen-wall Geiger-Müller counter placed along the axis of a surrounding cylinder which has the radioactive body mounted on its inner surface. Fig. 1 shows the counter. The whole chamber is evacuated and filled with hydrogen gas at a few centimeters of Hg pressure and is placed in a solenoidal magnet with its axis parallel to the field. The effect of the sample on the counter (obtained by movement of the sample cylinder inside the counter chamber) is studied as a function of the field and, in general, is found to disappear at a certain value of the field. If gamma-radiation is present there is a constant residual effect. The maximum energy of the beta-spectrum is determined by the field at which the effect of the sample on the counter is just eliminated. The $H\rho$ (product of field and radius of curvature of electron track) value for the upper limit of the spectrum is this limiting field multiplied by half of the shortest distance from the sample surface to the counter, because any smaller field allows some of the curved tracks to penetrate the counter. The geometrical arrangement used in this method was suggested and used by Bocciarelli and Occhialini[3] on the potassium radiation with a solid-wall counter as detector.

The amplifying and recording units used with the counters are of conventional design for use with solid-wall counters. In fact, screen-wall

[1] B. W. Sargent, Proc. Roy. Soc. **A139**, 659 (1933).
[2] W. F. Libby, Phys. Rev. **46**, 196 (1934).
[3] D. Bocciarelli, Nature **128**, 375 (1931).

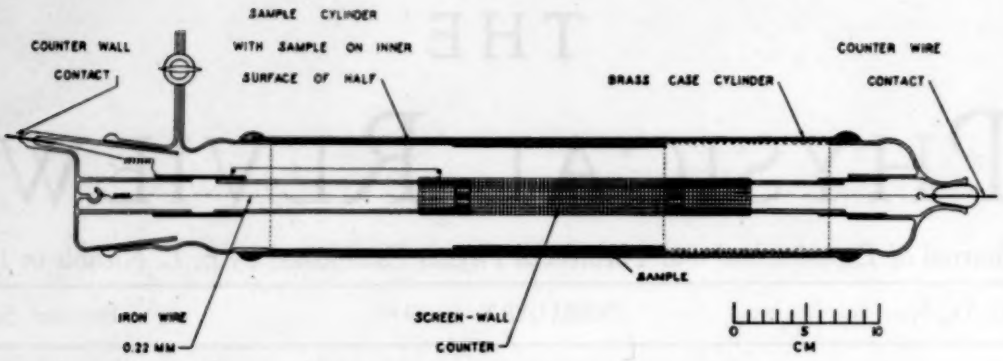

FIG. 1. Screen wall counter assembly.

counters differ in only one essential respect from solid-wall counters insofar as operation is concerned. It is necessary to provide an electric field between the counter and the surrounding chamber wall, presumably to prevent the accumulation of ions in the intervening space some of which would be free to move back into the counting volume and trip the counter. Under normal operating conditions the chamber wall (and sample cylinder) is kept about fifty volts positive relative to the counter wall by means of an insulated battery. The size of this potential drop seems to be rather unimportant providing it is sufficiently small to prevent sparking across the gap. It is convenient occasionally to ground the chamber for purposes of handling and to allow the full counter voltage to serve as a clearing voltage. Fig. 2 shows the effects produced by changing the sign and magnitude of this clearing field for a standard counter with diameter of 2.5 cm and sample cylinder diameter of 6 cm. The gas was helium at a pressure of 6 cm of mercury, with a trace of air impurity. The three curves are for the background, potassium radiation plus background, and aluminum photoelectrons plus background. The aluminum photoelectrons were obtained by illuminating an aluminum sample cylinder with visible light. The rise observed with the chamber wall more negative than the counter was due to an effective increase in size of the counter. In a certain sense, the screen is replaced as the counter wall by the chamber wall and sample cylinder. Various uses of this arrangement for construction of large sensitive counters suggested themselves. In particular, a soft radiation incident at the wall of a counter of large diameter might not produce enough ion pairs to initiate the counter discharge in the case of the ordinary counter. However, in the case of the arrangement described above with a sufficiently large negative potential on the sample cylinder with respect to the screen, the initial ionization will be increased more than it would have been in the standard counter because of the larger fields near the outer wall. The chances of counting are necessarily increased. Evidence for this appears in the figure in the relative effects of changing the sign of the clearing field on the potassium beta-radiation and the aluminum photoelectrons. The effect on the latter is an increase of considerable size while that on the potassium-plus-background radiation is little more than is observed with the background radiation alone. When the clearing voltage is removed entirely the counters have a tendency to develop high backgrounds which finally grow until they prevent the counter's operating at all. This may require only a few seconds with small assemblies.

The magnetic fields used (6000 gauss at most) have two effects on the operation of the counter which, though small, must be considered. The operating voltage is reduced by placing the

TABLE I. *Counter dimensions.*

Counter Name	Counter Diameter (cm)	Counter Length (cm)	Counter Wire Diameter (mm)	Sample Cylinder Diameter (cm)	Value of ρ (cm)
Large	2.5	14	0.22	13.5	2.75
Medium	2.5	14	0.22	10.1	1.90
Small	2.5	14	0.22	6.1	0.90

screen-wall counter in a field; the effect is about two percent at 6000 gauss. The explanation of this fact is not clear, though it is possible that it is due to an increase in probability of recombination of ion pairs formed in the space between the counter wall and the chamber walls before the positive ions so formed have time to move to the negatively charged counter wall. In the absence of the field these ions would tend to collect on the screen and reduce the negative

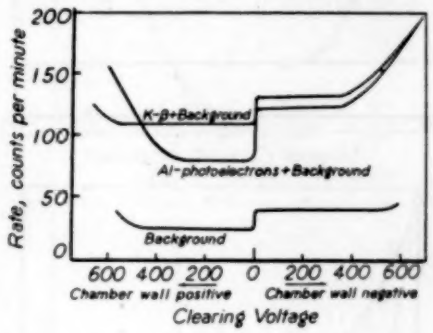

FIG. 2. Effects of clearing fields in small counter (6 cm He as gas).

potential. The effect apparently is associated with the curving of the paths traversed by the ions and the consequent decrease in their chance of reaching the walls before recombination occurs. The result is that the field allows the screen to maintain a higher average negative potential and requires a reduction of the applied voltage relative to the field-free value. This effect is not observed with solid-wall counters. The adjustment is made in practice by setting the voltage so the shape of the kicks, as shown on an oscillograph, remains constant over the whole range of variation of the field.

The other effect of the field is a linear reduction of the background as the field is applied which has an obvious explanation in the elimination of electron secondaries ejected from the chamber wall and sample cylinder by background gamma-radiation, etc. This effect amounts to a reduction of about thirty percent in most cases. The data presented later show this effect and are quite typical.

THE MAGNET

The magnet used was a solenoid with central hole six inches in diameter and one foot long.

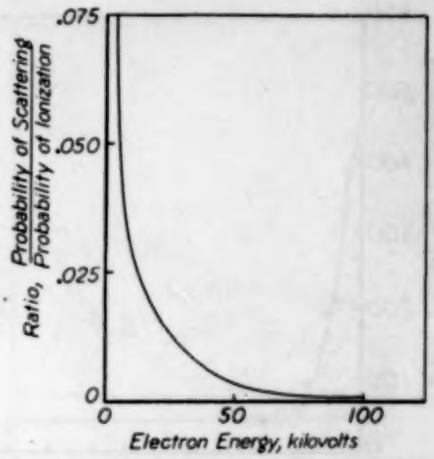

FIG. 3. Relative probabilities of scattering (≧5°) and production of one ion pair in H_2.

The coil is cooled by a kerosene circulation system. The assembly is of standard type for obtaining the fields used in Zeeman effect work. The pole pieces were removed and only one of the two coils used in any one determination in this work. Both coils were calibrated, however (by bismuth spiral and flip coil measurements), and both used in the course of the work. Maps were made of the fields in the cylindrical holes which showed them to be homogeneous within five percent over a distance of about 20 cm along the axis of the solenoid. The variations along the perpendicular direction in this region were smaller.

THE COUNTERS

Counters of the type shown in Fig. 1 with the characteristics given in Table I were used. All counters were constructed of copper screen with fourteen wires (0.010″ diameter) to the inch. The counter gas was hydrogen at a pressure of about 4 cm of mercury with a little air, water, or ethyl alcohol vapor introduced to improve the counting characteristics.[4] The sixth column of Table I gives the value of the radius of curvature, ρ, of the electrons which leave the sample surface tangentially and hit the counter surface tangentially, traveling in a plane perpendicular to the direction of the magnetic field. This is half of the shortest distance between the sample and counter surfaces. As given in the table it is computed for thin samples. In the cases where

[4] A. Trost, Zeits f. Physik **105**, 399 (1937).

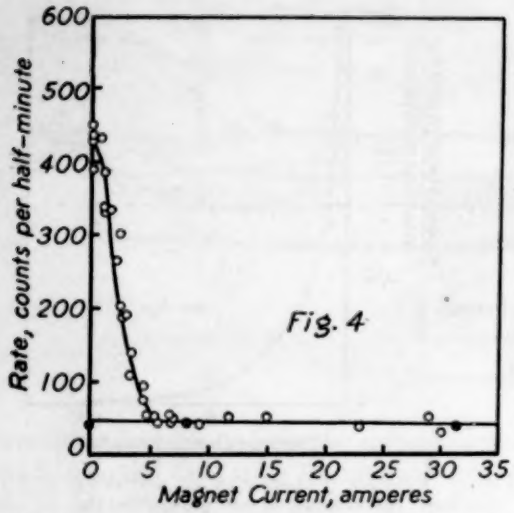

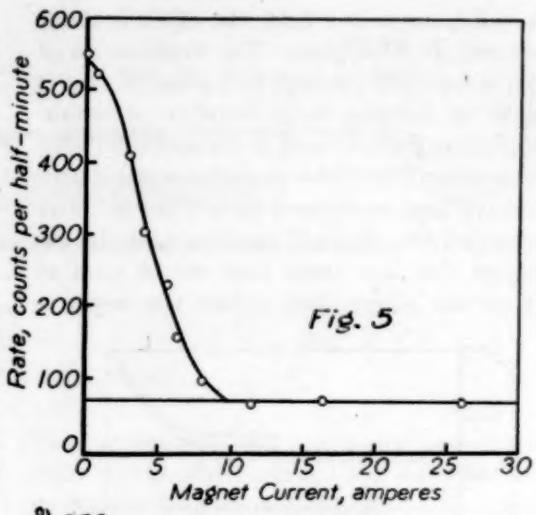

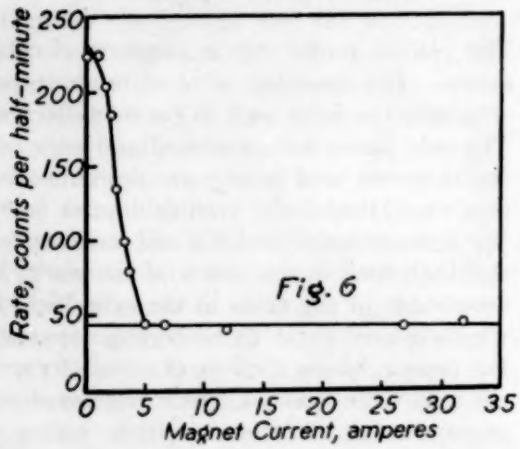

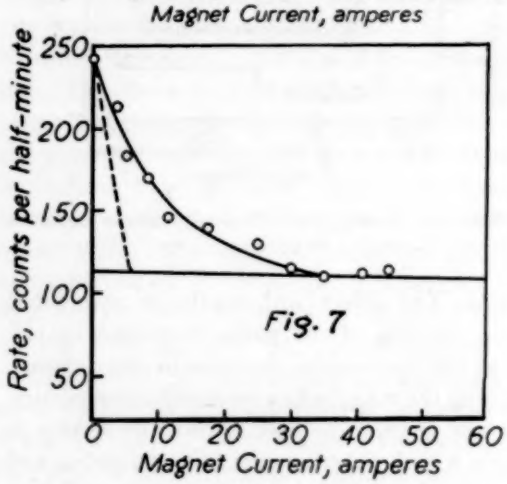

FIG. 4. Beryllium sample in medium counter. (1.85 cm H_2). Open circle, exposed. Solid circle, unexposed. $i_{max}=5.5\pm1$ amperes. $H_{max}=220\pm40$ gauss. $(H\rho)_{max}=410\pm75$. $E_{max}=15{,}000\pm7{,}000$ ev.

FIG. 6. Beryllium sample in medium counter. (5.1 cm H_2 as gas). $\rho=1.85$ cm. $i_{max}=5.0\pm1$ amperes. $H_{max}=200\pm40$ gauss. $(H\rho)_{max}=370\pm75$. $E_{max}=12{,}000\pm6{,}000$ ev.

FIG. 5. Beryllium sample in small counter. (2.8 cm H_2 as gas). $\rho=0.85$ cm. $i_{max}=10\pm2$ amperes. $H_{max}=400\pm$gauss. $(H\rho)_{max}=340\pm70$. $E_{max}=11{,}000\pm5{,}000$ ev.

FIG. 7. Straggling effect. Beryllium sample in medium counter. (4.0 cm A as gas).

the samples were of appreciable thickness, the proper ρ value was computed and used. The uncertainty of this quantity seems to be about 0.5 mm. This information was obtained by running a given spectrum in counters with different ρ values. The uncertainty of measurement of the distance from sample to counter is of that order.

The Straggling Effect and Theoretical Limitations of the Method

The problem of fixing the curvature in a magnetic field and recording a low energy electron is difficult because the probability of scattering is high. The method used in this research requires that the number of collisions along the path from the sample to the counter be as small as is compatible with the production of one or more ion pairs in the counter volume proper. Obvious steps in this direction are the reduction of the distance from sample to counter and the use of hydrogen as counter gas.

Since the essential quantity involved is the ratio of the probability of serious scattering ($\geq 5°$, for example) to the probability of production of an ion pair, this quantity has been

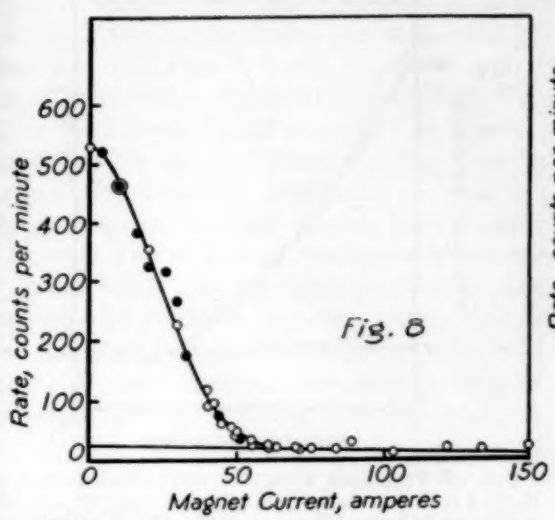

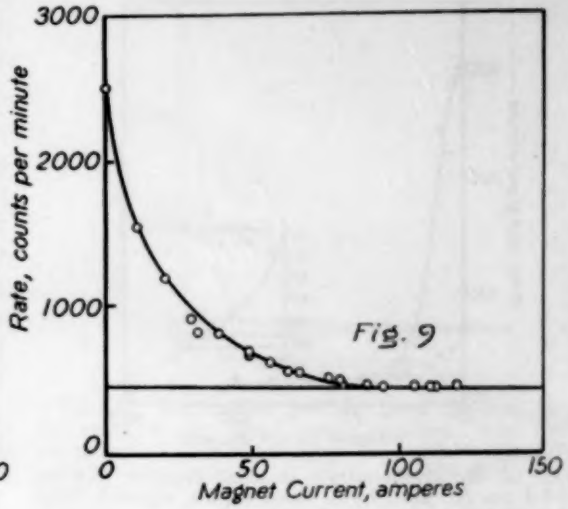

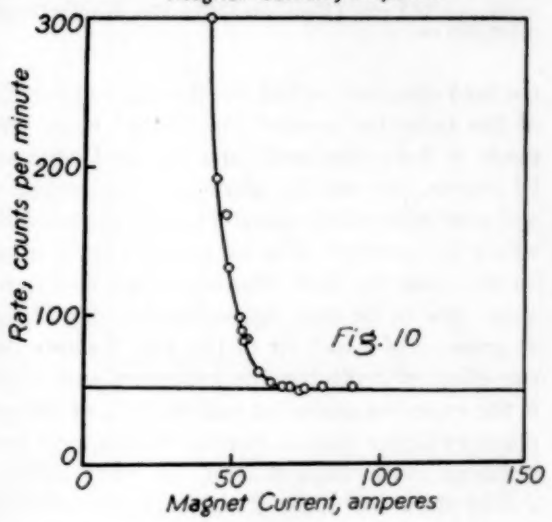

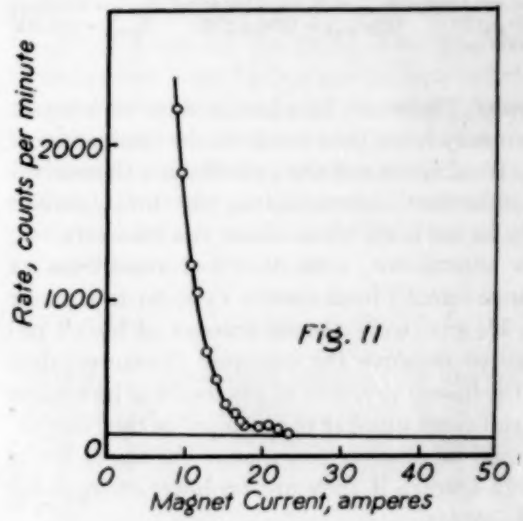

FIG. 8. Radioactive phosphorus in large counter. (3.8 cm H_2+0.2 cm C_2H_5OH). $i_{max}=65\pm5$ amperes. $H_{max}=2600\pm200$. $\rho=2.75$ cm. $(H\rho)_{max}=7150\pm550$. $E_{max}=1.69\pm0.08$ Mev.

FIG. 10. RaE in medium counter. (Approximately 4 cm H_2+trace of C_2H_5OH). $\rho=1.90$ cm. $i_{max}=68\pm3$ amperes. $H_{max}=2720\pm120$. $(H\rho)_{max}=5150\pm250$. $E_{max}=1.16\pm0.06$ Mev.

FIG. 9. Mesothorium 2 in medium counter. (Approximately 4 cm H_2+trace of C_2H_5OH). $\rho=1.90$ cm. $i_{max}=88\pm5$ amperes. $H_{max}=3520\pm200$. $(H\rho)_{max}=6680\pm380$. $E_{max}=1.55\pm0.07$ Mev.

FIG. 11. RaD in small counter. $(H\rho)_{max}=750\pm50$. $E_{max}=48{,}000\pm6000$ ev.

calculated approximately for hydrogen gas from the formula for energy loss given by Bethe,[5] as modified by Bloch's summation method, and the formulae for electronic and nuclear scattering given by Mott.[6] Fig. 3 shows the results as a function of the energy of the electrons. This curve allows an estimate to be made of the energy of the softest beta-radiation for which the method will be valid. The ratio of path length through the counter to the path length before reaching the counter must be at least as large as the ratio of the probability of serious scattering to the probability of ionization. For the small counter used this ratio is about one to twenty; the chief uncertainty arises from the estimation of the path length through the counter. This corresponds to an electron energy of about six

[5] H. Bethe, *Handbuch der Physik* Vol. 24, No. 1 (Berlin, 1933), p. 519.
[6] N. F. Mott, Proc. Roy. Soc. **125**, 222; **126**, 259 (1929).

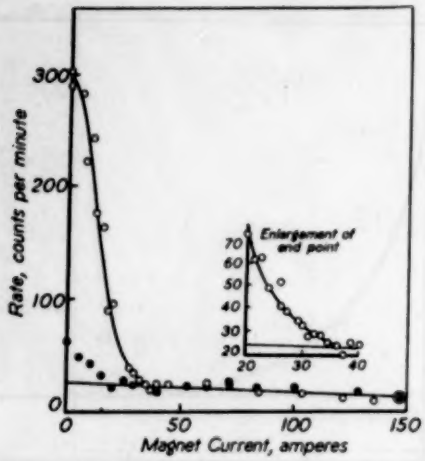

FIG. 12. Rubidium nitrate in small counter. (3.6 cm H_2+0.4 cm A). ρ=0.9 cm. Open circles, exposed. Solid circles, unexposed. i_{max}=36.0±3 amperes. H_{max}=40.0i_{max} =1440±120. $(H\rho)_{max}$=1296±110. E_{max}=132,000 ±20,000 ev.

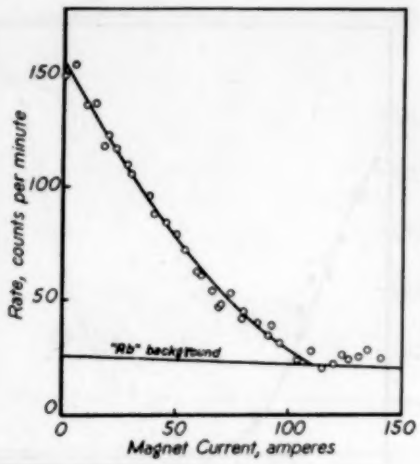

FIG. 13. Potassium nitrate in small counter. (3.6 cm H_2+0.4 cm A). i_{max}=110±10 amperes. H_{max}=4400 ±400. ρ=0.85 cm. $(H\rho)_{max}$=3740±340. E_{max}=725,000 ±100,000 ev.

kilovolts. However, because an error of a factor of two may have been made in the estimation of the critical ratio and the calculations themselves are somewhat approximate, the limit cannot safely be set lower than about ten kilovolts.

To summarize, with the best conditions of distance (small) from sample cylinder to counter wall, H_2 gas (with a small amount of heavy impurity to improve the counting characteristics) and the lowest pressure of gas insuring formation of a sufficient number of ion pairs in the counter, it should be possible to measure the upper limits of beta-spectra if they are no lower than about ten kilovolts.

These conclusions were tested experimentally by means of a source of soft electrons (kindly loaned by Professor E. M. McMillan of the Physics Department). It was a piece of metallic beryllium which had been bombarded for several months with deuterons in the cyclotron. The radiation consists of negative electrons (determined by placing sloping vanes between the sample cylinder and the counter and reversing the field direction to find the direction of bending of the radiation around the vanes.[1] Runs were made in both the small and medium counters. Of course, the test for absence of the straggling and scattering effect was to find conditions under which the product $(H\rho)$ for the end point would be the same for both counters. Figs. 4, 5 and 6 show this to be true approximately for H_2 gas at pressure of 2 to 5 cm of Hg. Fig. 7 shows that the effect of replacing the hydrogen with argon is the expected smearing and shifting of the end point to higher values. Similar results have been obtained with oxygen and air. The $(H\rho)_{max}$ values show the upper limit to be 13,000±5000 electron volts.

TABLE II. *Energy of β-rays.*

ELEMENT	ENERGY (THIS RESEARCH) (Mev)	ENERGY (OTHER METHODS) (Mev)
Pa	1.69 ±0.08	1.69
MsTh 2	1.55 ±0.07	1.60
RaE	1.16 ±0.06	1.16
RaD	0.048±0.006	0.046

The mechanism of counting for the electrons of maximum energy when the field is set for them to hit the edge of the counter may not involve the production of ions in the gas by single collisions so seriously as reflection by the screen into the counter volume or possibly the ejection of electrons from the screen itself. The data afford some evidence for this. It seems difficult to account for the observed counting near the end point at some of the gas pressures used without invoking some mechanism of this sort. Of course such an effect makes the effect of scattering less important.

CHECKS AGAINST KNOWN SPECTRA

In order to prove that the upper limits determined by this method are not seriously in error

a number of determinations have been made for spectra whose upper limits are obtainable by other methods. Figs. 8, 9 and 10 present typical determinations for P^{32}, MsTh 2, and RaE. Fig. 11 for RaD gives the upper limit of 46 kilovolts found by the standard semi-circular focusing method[7, 8, 9] which is applicable in this low energy range in this case because the radiation is intense. The 46 kilovolt radiation is emitted by conversion of a 47.1-kilovolt gamma-ray. The semi-circular focusing method which uses a photographic plate is inherently a very good apparatus for studying low energy spectra providing there is sufficient intensity available

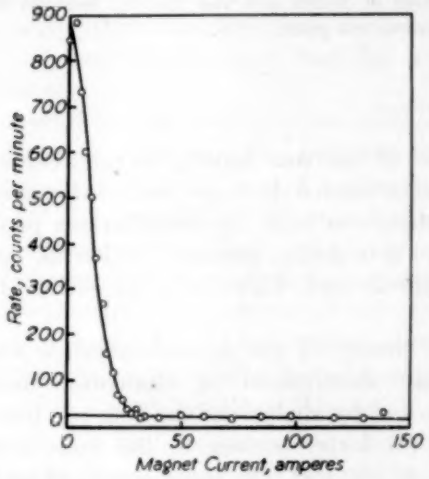

FIG. 14. Radioactive sulfur ($BaSO_4$) in small counter. (3.6 cm H_2+0.4 cm C_2H_5OH). ρ=0.9 cm. i_{max}=32±3 amperes. $H_{max}=40.0i_{max}=1280\pm120$. $(H\rho)_{max}=1152\pm108$. $E_{max}=107{,}000\pm20{,}000$ ev.

TABLE III. *Summary of results.*

ELEMENT	HALF-LIFE	ENERGY OF UPPER LIMIT (Mev)	REFERENCE
Ac	13.4 yr.	0.220±0.05	D. E. Hull, W. F. Libby and W. M. Latimer, J. Am. Chem. Soc. **57**, 1649 (1935)
MsThI	6.7 yr.	0.053±0.005	D. D. Lee and W. F. Libby, following article
S^{35}	88 days	0.107±0.020	This paper*
Au^{198}	2.7 days	0.77 ±0.16	This paper
Rb^{87}	10^{11} yr.	0.132±0.02	This paper

* The authors are indebted to Professor D. M. Yost of the California Institute of Technology for communicating this value of the half-life of radioactive sulfur checking that given first by E. B. Andersen, Zeits. f. physik. Chemie, **32**, 237 (1936).

[7] L. Danysz, Le Radium **9**, 1 (1911).
[8] L. Meitner, Zeits. f. Physik **11**, 35 (1922).
[9] D. H. Black, Proc. Roy. Soc. **A109**, 166 (1925).

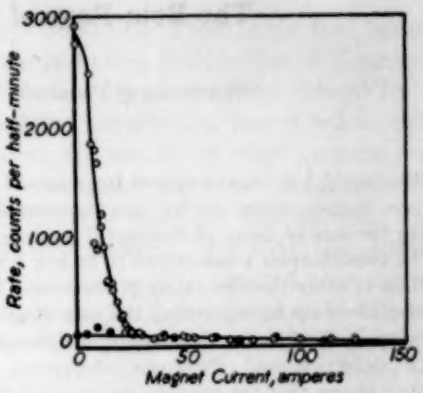

FIG. 15. Radioactive gold in large counter. (4 cm H_2+trace of air). Open circles, exposed. Solid circles, unexposed. i_{max}=33±4 amperes. ρ=2.70 cm. $H_{max}=41.1i+80=1440\pm165$. $(H\rho)_{max}=3890\pm450$. $E_{max}=770{,}000\pm160{,}000$ ev.

to give a trace on the plate. The whole space between source and plate can be evacuated and the scattering by the gas eliminated. There certainly is little reason to doubt the correctness of its result on the RaD conversion electrons.

Table II presents the results obtained by the present method together with the accepted values from other methods.

RESULTS

Figure 12 gives data obtained for the natural radioactivity of rubidium, due to Rb^{87}. The result is 132,000±20,000 ev and is considerably lower than the value of 250,000 ev previously used.[10]

Figure 13 shows the data for the natural activity of potassium, due to K^{40}, which give a value of 725,000±100,000 ev in agreement with the older determinations. No serious attempt was made to make this accurate because of the agreement with the older work and the low intensity of the radiation.

Figure 14 presents data for radioactive sulfur (S^{35}) and Fig. 15 for radioactive gold. The result on radioactive sulfur is new; that for radioactive gold checks the value given by McMillan, Kamen, and Ruben[11] from absorption.

Table III is a summary of results obtained by this method.

[10] O. Klemperer, Proc. Roy. Soc. **148**, 638 (1935).
[11] E. McMillan, M. Kamen and S. Ruben, Phys. Rev. **52**, 375 (1937).

The Beta-Rays of Mesothorium 1 and Radium D

D. D. Lee and W. F. Libby
Department of Chemistry, University of California, Berkeley, California
(Received September 6, 1938)

Mesothorium 1 has been prepared from an old sample of thorium sulfate whose purity was demonstrated by measuring the rate of decay of thorium B prepared therefrom. The mesothorium 1 was shown to be free from contaminations of other thorium decay products and isotopic radioactive elements by measuring the rate of growth of mesothorium 2, and proving the absence of alpha-emitters. Magnetic deflection and aluminum absorption experiments have shown that the particles emitted are electrons whose maximum energy is 53,000±4000 electron volts. Samples of RaD and RaE, pure to within 0.3 percent, have been prepared. The momentum of the most energetic conversion beta-ray of RaD has been determined as 765±32 gauss cm, and the upper limit of the RaE continuous spectrum was found to be 5150±250 gauss cm. The upper limit apparently to be assigned to the primary beta-ray spectrum of RaD was determined as 546±10 gauss cm, or 25,500±1000 ev, in agreement with the determination of Richardson and Leigh-Smith. An estimate of the observed number of secondary beta-rays arising from the conversion of the 47.2-kev gamma-rays of RaD indicates the emission of five to ten such electrons per 100 disintegrations, in rough agreement with the results of Kikuchi and the predictions of Fisk for the *L* conversion of dipole radiation, but in complete disagreement with the conclusions of Stahel and von Droste. Reasons for this disagreement are given.

AMONG the naturally occurring radioactive bodies about which there is very little, or only controversial, information available at present are mesothorium 1 and radium D.

The emission of ionizing radiation from the first of these has never been definitely established, although it was discovered in 1907, and it was for a long time considered to be "rayless." However, from the chemical properties of mesothorium 1[1] and its product, mesothorium 2 (which have been found to be isotopes of radium, and actinium, respectively) and the displacement law, it is assumed that a weak beta-particle is emitted in the decay of mesothorium 1.

The decay of radium D to form radium E is known to occur by the emission of primary beta-rays, gamma-rays, secondary beta-rays from the internal conversion of gamma-rays, x-rays, and perhaps tertiary, or Auger, electrons from the internal conversion of the x-rays.

The first definite information about the primary beta-particles of radium D was furnished by a very recent cloud-chamber investigation by Richardson and Leigh-Smith,[2] who found a large number of electrons having energies below four kv, and estimated the upper limit of the spectrum, by comparison with the distributions predicted in the beta-decay theories of Fermi, and of Konopinski and Uhlenbeck, as either 16, or 24, kv.

The energy of the gamma-radiation emitted has been determined by absorption measurements, and by analysis of the beta-ray line spectrum, the latter leading to the most accurate value, 47,200 ev.[3] The more recent of such determinations[4] have been done in such a manner as to determine not only the energy of this gamma-ray, but the energy of the accompanying x-radiation and to estimate the quantities of each emitted. The x-rays have been found to have energies corresponding rather closely to the *L* x-rays of bismuth, with which they have been identified, although determination of their ener-

[1] O. Hahn, Ber. **40**, 1462 (1907), Physik. Zeits. **8**, 277 (1907); B. Boltwood, Physik. Zeits. **8**, 556 (1907); H. N. McCoy and W. Ross, J. Am. Chem. Soc. **29**, 1709 (1907); L. Haitinger, K. Peters and St. Meyer, Vienna, Akad. Sitz.-Ber. **120** [*2a*], 1199 (1911); L. Meitner, Physik. Zeits. **19**, 257 (1918).

[2] H. O. W. Richardson and A. Leigh-Smith, Proc. Roy. Soc. **A160**, 454 (1937).

[3] J. Danysz, Le Rad. **2**, 1, 6 (1912); E. Rutherford and H. Richardson, Phil. Mag. **26**, 324, 937 (1913); C. D. Ellis, Proc. Camb. Phil. Soc. **21**, 121 (1921–23); L. Meitner, Zeits. f. Physik **9**, 131, 145 (1922); **11**, 35 (1922); I. Curie and G. Fournier, Comptes rendus **176**, 1301 (1923); D. H. Black, Proc. Roy. Soc. **A109**, 166 (1925); L. F. Curtiss, Phys. Rev. [*2*]**27**, 672 (1926).

[4] S. Kikuchi, Jap. J. of Phys. **4**, 143 (1925–27); L. H. Gray and O'Leary, Nature **123**, 568 (1929); L. H. Gray, Nature **130**, 738 (1932); J. Petrova, Zeits. f. Physik **55**, 628 (1929); S. Bramson, Zeits. f. Physik **66**, 721 (1930); E. Stahel and G. J. Sizoo, Zeits. f. Physik **66**, 741 (1930); H. O. W. Richardson, Proc. Roy. Soc. **A133**, 367 (1931); G. von Droste zu Vischering, Zeits. f. Physik **84**, 17 (1933); E. Stahel, Helv. Phys. Acta **8**, 651 (1935).

gies have given only average values. The number of such photons has been found to be 22 to 30 per 100 disintegrations, and the number of 47,000-ev gamma-rays, about 3.5 per 100.[5] We shall assume that the x-rays are excited by the conversion of 47,000-ev gamma-rays in L shells, (the K shell could not be excited because the energy of the gamma-ray is too low). The number observed, considered with the fluorescence yield of bismuth, has led to the conclusion that each primary beta emitted leaves the resulting RaE nucleus in an excited state 47 kv above the ground state of RaE, and that all such nuclei emit gamma-rays of this energy. Of these, 96 or 97 percent are internally converted in L, M and N shells of extranuclear electrons, the remaining three or four percent are emitted without conversion.

In a series of experiments, wherein were used a point counter covered with a collodion foil and a source of RaD, RaE and Po placed in an evacuated chamber, Stahel[6] measured the number of electrons from RaD. He distinguished these from the beta-rays of RaE, the alphas of Po, and the general background radiation by means of a magnetic field and various aluminum foils. The absorption of the RaD betas in one, two and three of his collodion foils led Stahel to the conclusion that he was observing, through the first permanent foil, only the secondary electrons due to the conversion of the 47,200-ev gamma-ray; but, as it was pointed out by Feather and Richardson,[7] the absorption which Stahel observed did not agree with the absorption which would be calculated from the known energies and intensities of these electrons, and the range-energy relations of Williams.[8] In fact, the observed absorption could be accounted for only by the assumption that Stahel was getting a relatively large number of low energy (4 to 20 kv) electrons through the first foil. From the work of Richardson and Leigh-Smith,[2] and the fact that Stahel's first foil could completely stop only electrons of less than 4500 ev, it is clear that more than half of these might have been primary beta-rays. From this fact alone and without estimating the number of observed electrons which might have been caused by Auger effect of the x-radiation, one is led to conclude that there are not 83 or more gamma-ray conversion electrons per 100 disintegrations as Stahel believed, but that this number must be considerably smaller, and that the number of 47,200-ev gamma-rays (emitted plus converted) is less than one per disintegration. It follows from this that since no beta-rays of RaD having energies corresponding to a transition from ground state to ground state have been observed, there may occur the emission of two or more gamma-rays of less than 47,200 ev energy (nuclear x-rays) in a "cascade" process involving more than the one known excited level of the RaE nucleus. It is not at all improbable, that such nuclear x-rays may have been observed by Kikuchi, Gray and O'Leary, von Droste and Stahel, and their corresponding conversion electrons may have been observed by Kikuchi, Petrova, Richardson, and Richardson and Leigh-Smith, only to be confused with the L rays and Auger electrons arising therefrom.

From the work of Kikuchi one finds only about twenty electrons attributable to the conversion of 47,200-ev gamma-rays per 100 disintegrations. Since about thirteen of these are from the L orbits, the L conversion coefficient calculated from this value is 13/3.5, or about 3.7. A theoretical calculation by Fisk[9] gives the values 1.8 and 2.9 for the L conversion coefficients of dipole and quadrupole radiation, respectively. Only the assumption of multipole, or magnetic multipole radiation could have accounted for the coefficient 17.1 calculated by Stahel.

The subsequently described experiments with RaD were intended to furnish information regarding the upper limit of the primary beta-rays, and to permit an estimate of the number of secondary electrons produced by the conversion of 47,200-ev gamma-rays.

Preparation of Samples

All mesothorium preparations were made from a thirteen-year-old sample of Kahlbaum thorium sulfate, the purity of which was determined by

[5] H. Lay, Zeits. f. Physik **91**, 533 (1934).
[6] E. Stahel, Zeits. f. Physik **68**, 1 (1931).
[7] N. Feather and H. O. W. Richardson, Nature **129**, 314 (1932).
[8] E. J. Williams, Proc. Roy. Soc. **A130**, 310 (1931).
[9] J. B. Fisk, Proc. Roy. Soc. **143**, 674 (1934).

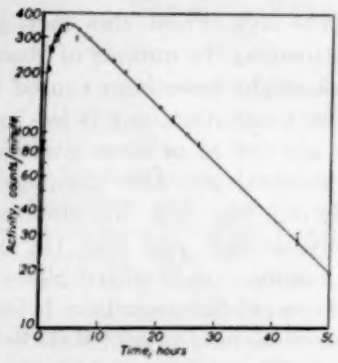

FIG. 1. Growth and decay curve for ThB precipitate to test purity of thorium sample.

following the growth and subsequent decay of gamma- and strong beta-ray activity in a sample of thorium B prepared from about one-half gram of thorium sulfate. The activity was measured with a solid-wall Geiger-Müller counter and increased in the first four hours after at exactly the rate to be expected for the growth of ThC from ThB preparation. After six hours, the activity decayed with the half-life of thorium B. This indicates the absence of more than three to five percent of any radium B, actinium B, or radium D contamination (see Fig. 1).

Mesothorium 1 and 2 were removed from a solution of thorium sulfate by precipitating barium sulfate. To remove from this precipitate any traces of occluded thorium or radiothorium, the $BaSO_4$ was converted to $BaCl_2$ by heating with carbon, digestion of the residue in concentrated sodium carbonate solution, and leaching of the resulting solid with dilute hydrochloric acid. To the resulting solution a trace of ferric chloride was added, and the ferric ion removed as ferric hydroxide by the addition of a slight excess of sodium hydroxide solution. This procedure removed thorium, radiothorium, mesothorium 2, and the elements of the thorium active deposit. As thorium X is isotopic with mesothorium 1, it cannot be removed by chemical separations but must be allowed to decay. About one month is necessary for the removal of 99.6 percent of ThX and its decay products.

From such a month-old sample of mesothorium 1 and 2, either of these two elements could be removed by simple chemical precipitations. The addition of ferric ion as the chloride and its removal as ferric hydroxide leaves a solution containing only about ten percent of its original content of mesothorium 2. Two further treatments of this kind suffice to remove all noticeable amounts of mesothorium 2 and the precipitation of the barium ion as barium carbonate removes mesothorium 1 for experimentation. The growth of activity of such a sample, as observed with a screen wall counter, is shown in Fig. 2. Comparison of the measured activities with the calculated solid curve shows the sample to have been pure to within at least two percent. The initial activity is not proved to be caused by MsTh 1 beta-rays since the same curve would have been obtained with a MsTh 1 sample containing a trace of MsTh 2. Counting of alphas possibly emitted by an equivalent sample of MsTh 1 and 2 showed certainly less than two percent contamination by radium, thorium X, or actinium X.

The ferric hydroxide precipitates containing mesothorium 2 contain also appreciable quantities of mesothorium 1. About eight to ten percent has been found in all such precipitates examined in this work by following the decay of activity with an electroscope. However, if such a sample be dissolved in dilute hydrochloric acid, the hydrogen ion concentration adjusted to about 10^{-4} M by the addition of sodium acetate, and a large excess of sodium dichromate with a trace of barium chloride added, the resulting precipitate removes enough mesothorium 1 so that the ferric hydroxide precipitate which can be prepared from the filtrate will contain mesothorium 2 pure to within 98 percent (see Fig. 3).

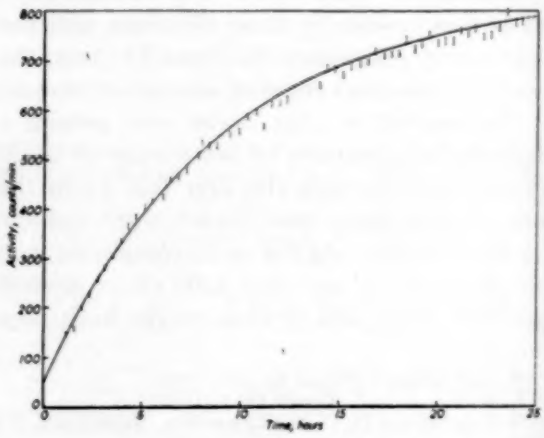

FIG. 2. Growth of mesothorium 1 precipitate.

Samples of radium D and radium E were prepared from the contents of an old radon tube, which was washed in concentrated nitric acid and water, and crushed under about five cc of concentrated HNO_3. After heating and allowing the glass particles to settle, the solution was decanted and diluted by the addition of about three cc of distilled water. Individual preparations were made from one-cc portions of this final solution by the usual methods, i.e., the solution was evaporated twice with excess concentrated HCl, the residue dissolved in about five cc of 0.1*N* HCl, and heated to 90° or 100°C. Then 99 percent of the polonium content was removed by rotating in the solution at about 200 r.p.m. a silver foil (of approximately one cm^2 area) for one hour, and the remaining polonium removed by the same treatment with another silver foil. Radium E was removed similarly on a nickel foil. Such a sample of RaE can be shown by following the decay of activity for 35 days to have been originally free from Po to at least 99.9 percent and to have contained no more than 0.25 percent of RaD. This was done by using the screen wall electroscope to be described later and various aluminum foils in order to distinguish between the beta-rays of RaE and the alphas of Po.

After the above-mentioned removal of RaE, 0.1 cc of a solution containing 10^{-4} gram/cc each of Pb and Bi, as chlorides, were added to prevent the loss of RaE or RaD by occlusion on dust particles, etc. the solution was allowed to stand over night. Then the RaE left by the previous treatment and that produced subsequently by the decay of RaD was removed by rotating in the hot solution a nickel foil of the same size as that used in the previous removal of RaE. The resulting residue was evaporated once again with excess HNO_3, then twice with distilled water, and the final residue digested with five cc of a two percent solution of NH_4NO_3 to insure the solution of the lead content. The $BiONO_3$ residue was filtered off to remove the last traces of RaE. Radium D was removed from the filtrate by precipitating the lead as PbS and found to be radioactively pure to at least 99.8 percent.

Apparatus and Experimental Technique

The counter tubes, voltage supply, amplifier, recorder and magnet used in these magnetic deflection experiments were the same as those described in the preceding article.

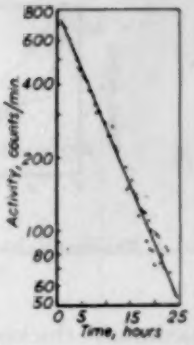

Fig. 3. Decay of mesothorium 2 precipitate.

In determining the absorption of the mesothorium 1 and 2 beta-rays by aluminum, measurements were made with a Lauritsen electroscope having a portion of its cylindrical case cut out and replaced by a piece of copper gauze such as is used for the screen of a screen-wall counter. In order to determine how far an ionizing particle must travel into the space enclosed by this modified case to be detected, measurements were made of the rate of discharge of the electroscope due to the alpha-particles from a Po source placed at various distances from the screened portion. The results showed that any alpha-particle, and presumably any other ionizing radiation which passes into the screen-enclosed space produces ions leading to the discharge of the electroscope.

Corrections for the growth of mesothorium 2 in samples of mesothorium 1 which were used to determine the aluminum absorption and the upper energy limit of the beta-ray spectrum were made in the following manner. The activity observed on the electroscope for the uncovered sample in a standard position was measured first. Then absorbers were added in increasing thicknesses, as measurements of the penetration were made until the absorber thickness reached 7 or 12 mg/cm^2. Following this procedure the absorber thickness was reduced by the same increments until the sample was uncovered. The average of the two readings taken at each absorber thickness automatically gave a value of the activity corrected for growth of mesothorium. This average is nearly the activity which would have been obtained had it been possible to make all measurements simultaneously at the time of the

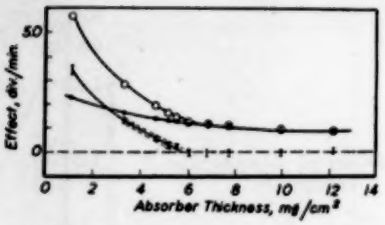

FIG. 4. Aluminum absorption curve for mesothorium 1 and mesothorium 2.

maximum thickness measurement, since the growth of mesothorium 2 is a nearly linear function of time within any period of two hours or less, and the two readings at each thickness are time-symmetrical with respect to the maximum thickness reading. To find the activities caused by mesothorium 1 alone, this curve was compared with the absorption curve for pure mesothorium 2 and the portion of the former curve which was parallel to the latter was extrapolated back. Subtracting the activities on this extrapolated curve from those on the measured curve gives a third curve (see Fig. 4) which is the absorption of the beta-rays of mesothorium 1 in aluminum.

The same technique was used in magnetic deflection experiments on mesothorium. The activities from a pure mesothorium 2 sample were measured at various field strengths and compared with the curve obtained when a sample originally containing only mesothorium 1 was measured at various fields. The field was increased to some maximum strength by predetermined increments, then decreased by the same steps. The difference between the measured curve and the extrapolated mesothorium 2 curve shows the effect of field on the beta-rays of mesothorium 1 alone (see Fig. 5).

In the case of the magnetic deflection experiments on radium D no such corrections were necessary provided the measurements were made within a few hours after preparation of the samples because of the slower growth of radium E.

EXPERIMENTAL RESULTS

The average of two determinations of the mesothorium 1 upper limit by absorption (see Fig. 5) is 57,000±5000 ev, while five magnetic deflection experiments gave an average of 771 ±45 $H\rho$, or 51,000±4700 ev (see Fig. 6). Because of the greater accuracy inherent in the second type of measurement, these values are taken as indicating that the upper limit of the mesothorium 1 spectrum is 53,000±4000 ev. That this is the upper limit of the primary beta-ray spectrum does not necessarily follow, for although no gamma-rays have been observed in the disintegration of mesothorium 1, the present

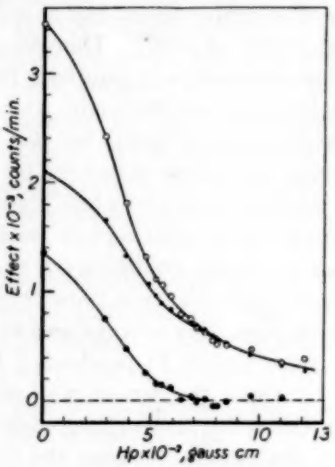

FIG. 5. Magnetic determination of mesothorium 1. Upper limit.

work does not exclude the possibility that soft gamma-rays might exist and their conversion give rise to secondary electrons having energies up to the observed maximum. This might make the observed upper limit somewhat higher than the true value. However, since the total conversion of soft gammas is relatively improbable because it must occur in the L shell in this case, it seems that most of the electrons are of nuclear origin. This point is illustrated in the work on RaD.

Figure 7 shows the activities observed at various magnetic field strengths with a sample of RaD. Curve (I) gives activities due to about one-half of the sample measured at various fields up to 1500 gauss; curve (II) gives the corresponding values for a smaller portion of the same sample. (Electroscope measurements made 19 days later to determine the relative activities of these portions of the sample due to accumulated RaE in each indicated a ratio of 21 to 1.

As the activity of the small portion at zero field is observed to be 1200 counts per minute, that of the large portion must have been over 25,000, a value too large to be recorded by the equipment used.)

Examination of curve (I) reveals an activity which falls off very rapidly with increasing field strength up to an $H\rho$ value of 570 gauss cm, a more gradual slope from that value to 770 gauss cm, and a very gradual slope from 770 to 1500 gauss cm. Curve (II), on the other hand, shows only the steep portion ending at 530±20 gauss cm, which is apparently the upper limit of the primary beta-ray spectrum of RaD, since all the betas from the conversion of the 47,200-ev gamma-rays have larger values of $H\rho$. The gradual slope in curve (I) is, therefore, presumably due to conversion betas, and gives an upper limit of 770±40 gauss cm which is not far from the accepted value,[10] 738 gauss cm for the highest conversion line. The remaining activity in the large sample is undoubtedly due to RaE betas, and perhaps Po alphas, as well as RaD gammas. Similar curves obtained with

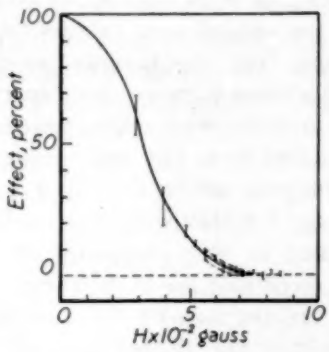

FIG. 6. Average curve for magnetic determination of mesothorium 1. Upper limit.

RaD samples prepared in the same or a slightly different manner, gave the values collected in Table I.

To obtain an independent check on any possible systematic errors in the magnetic depth determinations of such upper limits, measurements were made with a sample of mesothorium 2 and with one of RaE. The observed upper limit for mesothorium 2 was 6880±250 $H\rho$, in excellent agreement with the magnetic spectrographic determination of Yovanovitch and d'Espine.[11] For RaE, the upper limit was 5150±250 $H\rho$, a value entirely concordant with the latest determinations.

[10] L. Meitner, reference 3.

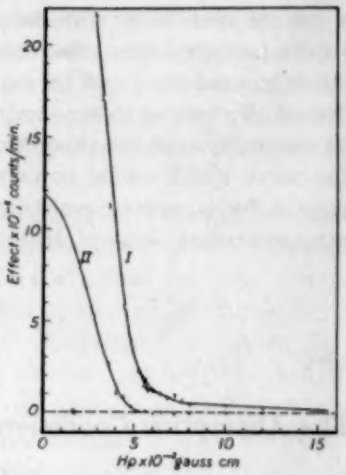

FIG. 7. Magnetic analysis of RaD.

DISCUSSION OF RESULTS

From the data of Table I one is led to conclude that the end point observed with RaD at 546±10 gauss cm, or 25,500±1000 ev, is that of the continuous primary beta-ray spectrum, although it is possible that the conversion of nuclear x-rays, if they exist in this disintegration, might give rise to electrons of energies up to this limit.

The electrons found at $H\rho$ values of 530 to

TABLE I. *Data on* RaD.

TOTAL INTENSITY OF SAMPLE (COUNTS/MIN)	UPPER LIMIT (STEEP PORTION OF CURVE) (GAUSS CM)	HIGHEST CONVERSION LINE (GAUSS CM)
1200	530	Not observed
1500	540	Not observed
1600	540	Not observed
Av. 1433	Av. 537	
15,000	540	Not determined
20,000	570	Not determined
25,000	570	770
35,000	530	760
Av. 23,750	Av. 553	Av. 765

[11] D. K. Yovanovitch and J. d'Espine, Comptes rendus 179, 1162 (1924); J. phys. radium, [6]8, 276 (1927).

770 gauss cm are then to be considered the only observed beta-particles from the conversion of the 47,200 ev gamma-ray; and by extrapolating this portion of the curves to zero magnetic field (under the assumption of the theoretical appearance of the curve which would be expected with this apparatus for a source emitting only the gamma-ray conversion-betas of RaD) one finds about five such conversion electrons per 100 disintegrations. Since this extrapolation is somewhat difficult, it seems entirely possible that there might be as many as ten such conversion betas per 100 disintegrations in which case the calculated L conversion coefficient would be 2.1, very nearly the value calculated by Fisk for the case of dipole radiation.

FEBRUARY 1, 1939 PHYSICAL REVIEW VOLUME 55

The Absorption Coefficient of 5.8-Mev Gamma-Radiation in Aluminum

J. HALPERN AND H. R. CRANE
University of Michigan, Ann Arbor, Michigan

(Received December 7, 1938)

The absorption coefficient of monochromatic 5.8-Mev radiation in aluminum is found to be 0.075 ± 0.009 cm^{-1}. By deducting the theoretical value of the pair absorption coefficient, the Klein-Nishina absorption coefficient is found, which is 0.062 ± 0.009 cm^{-1}. This value is in good agreement with the theoretical value. The experimental method used is such that all quanta which are scattered more than 10 degrees in the aluminum are excluded completely from the data.

SEVERAL measurements[1] of the absorption coefficient of the F+H[1] gamma-radiation have been made by means of the ionization chamber. The experiment to be described gives a result by a different method, which does not involve the assumption that the radiation consists of a single line and which reduces the effect of scattering and geometrical errors to a very small amount. The method was first used by Delsasso, Fowler and Lauritsen[2] for the measurement of the absorption coefficient of the Li+H′ and the F+H[1] radiation in lead.

Our experimental arrangement is shown in Fig. 1. On alternate expansions of the cloud chamber a block of aluminum 10.2 cm thick was placed in the path of the gamma-rays, between the target and the lead collimator. A plot of the number *versus* energy of the recoil electrons ejected from the carbon sheet was made for each of the two cases: with and without the aluminum block in the gamma-ray path. These are shown in Fig. 2. If, in both curves, we consider only tracks in the shaded area (above 4.6 Mev) we can be sure that the gamma-ray quanta responsible for these have not been scattered more than 10 degrees before reaching the carbon sheet. It is calculated from the angle-energy relations in the Compton effect that if a quantum of initial energy 5.8 Mev were scattered more than that amount in the aluminum, it could not produce a recoil electron in the carbon sheet with an energy greater than 4.6 Mev, and hence could not fall within the shaded area of the curve. Similarly, gamma-ray quanta of initial energy less than 4.85 Mev are automatically excluded, because they cannot give rise to recoil electrons of more than 4.6 Mev.

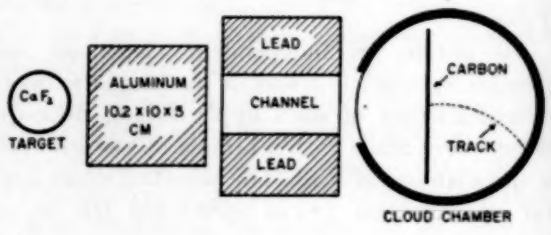

FIG. 1. Experimental arrangement.

[1] E. McMillan, Phys. Rev. **46**, 325 (1934); H. R. Crane, L. A. Delsasso, W. A. Fowler and C. C. Lauritsen, Phys. Rev. **46**, 1109 (1934).
[2] L. A. Delsasso, W. A. Fowler and C. C. Lauritsen, Phys. Rev. **51**, 391 (1937); Phys. Rev. **51**, 527 (1937).

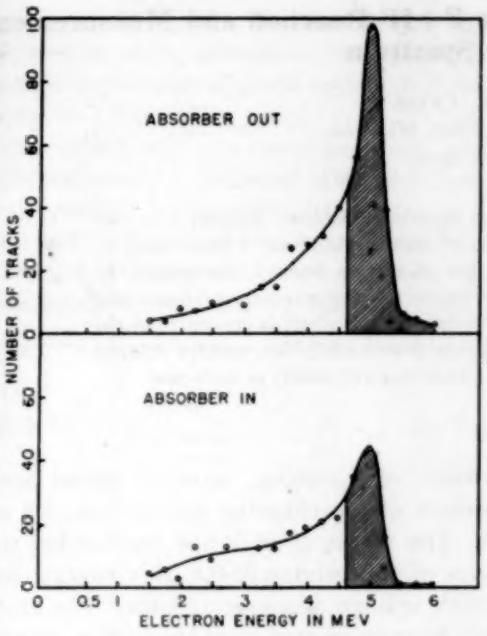

FIG. 2. Energy distribution of recoil electrons ejected from carbon.

By cutting off the distribution in Fig. 2 at a higher energy than that shown, the maximum allowed angle of scattering can be made as small as desired, but on the other hand the uncertainty in the result becomes greater due to the smaller number of tracks included. By cutting off at 4.6 Mev, as is done in this computation, we obtain results which are equivalent, as far as geometry is concerned, to the usual ionization experiment in which the maximum angle subtended at the ionization chamber by the absorber is only 10 degrees.

The numbers of tracks in the two shaded areas are 207 and 98. These give a value $(98\pm6.6)/(207\pm9.6)=0.47\pm0.04$ for the attenuation of the radiation in 10.2 cm of aluminum. The total absorption coefficient is given by writing $0.47\pm0.04=e^{-10.2\mu}$ which gives $\mu=0.075\pm0.009$ cm^{-1}. The pair absorption coefficient is, according to Bethe and Heitler, 0.013 cm^{-1} for aluminum. The photoelectric absorption is negligibly small. The coefficient due to Compton scattering alone (Klein-Nishina absorption coefficient) therefore becomes 0.062 ± 0.009 cm^{-1}. The Klein-Nishina theory gives 0.060 cm^{-1}.

It is interesting to note that there are relatively more low energy electrons in the lower curve than in the upper curve in Fig. 2. This is undoubtedly due to radiation softened by scattering in the aluminum, and it would have vitiated the results, had we been measuring the intensities with an ionization chamber.

The authors are indebted to the Rackham Endowment Fund for the support of this work.

The Pair Internal Conversion Coefficient in the F+H′ Reaction and Measurements on the Gamma-Ray Spectrum

J. HALPERN AND H. R. CRANE
University of Michigan, Ann Arbor, Michigan

(Received December 6, 1938)

The gamma-radiation from F+H′ was studied by the cloud-chamber method and was found to consist of a single line at 5.8 Mev. The group of electrons at about 4 Mev found by Gaerttner and Crane was confirmed, and it is shown that this group probably consists of the negative members of internal conversion pairs. The coefficient for pair internal conversion was measured and found to be about 1 pair per 100 gamma-ray quanta, which is greater than the theoretical value. A search was made for gamma-radiation down to 0.5 Mev, and for delayed emission of electrons by the CaF_2 after bombardment, with negative results in each case.

IT is a well established fact that fluorine bombarded with protons emits a strong gamma-ray line at 5.8 Mev. There has also been some indication of a lower line, at about 3.8 Mev, but the evidence on this point is conflicting. As a result of the experiments to be described here, it has become clear that the coefficient for the internal conversion of the 5.8 Mev gamma-ray into pairs, in the field of the emitting nucleus, is unexpectedly high, and that it was this process which gave rise to electrons which were interpreted as indicating a second gamma-ray line. We shall give the evidence for this and also arrive at a value for the interval conversion coefficient.

Confirmation of Previous Results

The cloud-chamber experiment of Delsasso, Fowler and Lauritsen[1] was repeated with the arrangement shown in Fig. 1, which is essentially the same as theirs. We used a 6″ diameter cloud chamber[2] with a magnetic field of 1850 gauss.

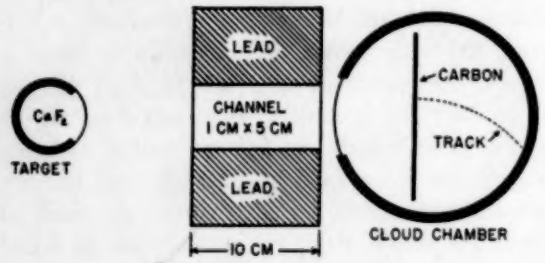

FIG. 1. Experimental arrangement.

The sheet of scattering material placed across the center of the chamber was carbon, 1.5 mm thick. The target (CaF_2) was bombarded with protons of approximately 0.6 Mev energy from the high voltage accelerating tube.[3] The tracks of the electrons ejected from the carbon sheet by the gamma-rays were measured, and the results

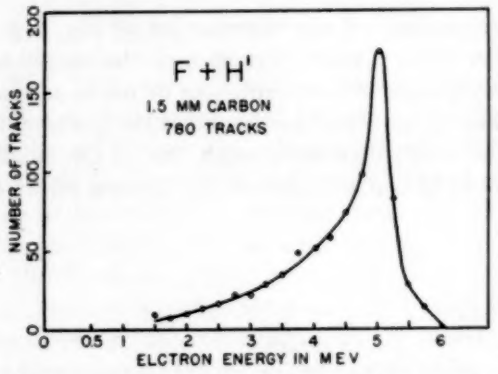

FIG. 2. Energy spectrum of recoil electrons from 1.5 mm carbon, obtained with the arrangement shown in Fig. 1.

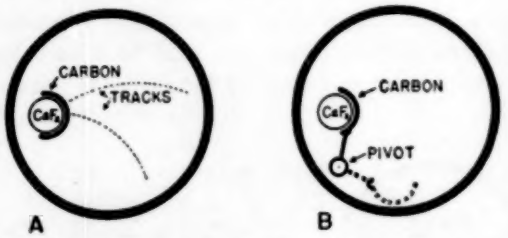

FIG. 3. A Diagram showing the target inside the cloud chamber. The cylindrical piece of carbon, 1.5 mm thick, yields recoil electrons. B The carbon is supported on a shaft which can be rotated from outside the chamber. It is placed in the two positions shown in B on alternate expansions of the chamber.

[1] L. A. Delsasso, W. A. Fowler and C. C. Lauritsen, Phys. Rev. **51**, 527 (1937).
[2] H. R. Crane, Rev. Sci. Inst. **8**, 440 (1937).
[3] H. R. Crane, Phys. Rev. **52**, 11 (1937).

are shown in Fig. 2. The distribution clearly indicates a single gamma-ray line, and is in complete agreement with the results of Delsasso, Fowler and Lauritsen.

The experiment of Gaerttner and Crane,[4] which indicated the presence of a lower line, was next repeated. The experimental set-up is indicated as A in Fig. 3; the essential feature is that the target is inside the cloud chamber, and is immediately surrounded by the scattering ma-

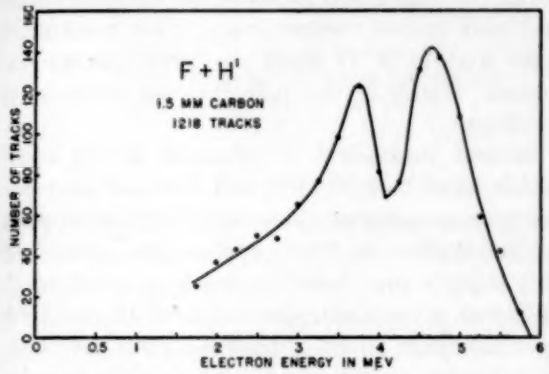

FIG. 4. Energy spectrum of the negative electrons obtained with the arrangement shown in Fig. 3 A.

terial, 1.5 mm of carbon. The distribution of negative electrons found is shown in Fig. 4, and confirms that found by Gaerttner and Crane.

A small number of tracks obtained by Gaerttner and Crane with the arrangement of Fig. 1 seemed also to indicate a second line, but this seems to have been incorrect in view of the distribution shown in Fig. 2, which contains a much greater number of tracks.

NEW EXPERIMENTS

To determine whether the lower energy peak in Fig. 4 is composed of electrons originating in the carbon scatterer or in the CaF_2 target itself, the following experiment was performed. In an arrangement shown as B in Fig. 3, the carbon scatterer was attached to a moveable arm so that it could be placed close to the target on alternate expansions of the cloud chamber, and could be removed on the other expansions. When the carbon was removed, there remained only a thin aluminum wall between the target and the chamber. Both positive and negative electron

[4] E. R. Gaerttner and H. R. Crane, Phys. Rev. **52**, 582 (1937).

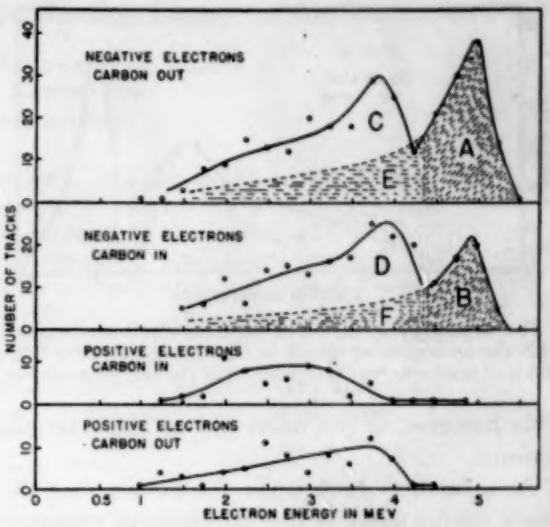

FIG. 5. Positive and negative electrons obtained with the arrangement shown in Fig. 3 B. Equal numbers of photographs were taken with the carbon in the two positions shown.

tracks are recorded in Fig. 5. The higher energy peak in the negative electron distribution is decreased by nearly a factor of two by removal of the carbon. The lower energy peak does not seem to be decreased at all. Our conclusion is that the higher energy peak is composed of Compton recoil electrons and is therefore dependent upon the amount of material surrounding the target; that the lower energy peak is composed of electrons which have originated in the CaF_2 target and have passed *through* the carbon scatterer.

A glance at the plots of positrons will indicate two things: that the number of them is insensitive to the amount of material surrounding the target, and that the plot formed by them is not significantly different from that of the negatives comprising the lower energy peak, *C* or *D*. This approximate equality of positives and negatives makes it unnecessary to postulate any other process than pair formation to account for the effect in question. Gaerttner and Crane have already demonstrated that pair formation by internal conversion takes place in the F+H′ reaction. The only item which does not seem to fit this explanation is the somewhat excessive sharpness of the lower energy peak (especially in the data of Gaerttner and Crane) as compared with that expected from the theoretical distribution of energy between members of pairs.

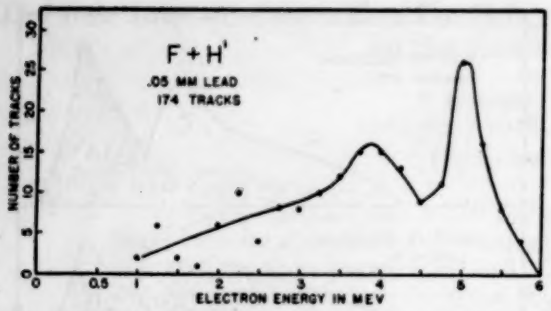

FIG. 6. Energy spectrum of negative electrons obtained with the arrangement shown in Fig. 1, except that a 0.05-mm lead scatterer was used instead of the carbon scatterer.

This however, is too uncertain to cause serious concern.

As a further check upon the notion that the lower energy peak is due to negative members of pairs, a series of photographs were taken under the arrangement of Fig. 1, but using a 0.05-mm lead sheet instead of carbon. The negative electrons appearing in this experiment were a mixture of Compton electron and pair members, but the pairs were formed in the lead instead of in the target as before. The plot of negative electrons, given by Fig. 6, shows that the negative members of pairs give rise to a second peak in the distribution in this case also.

THE COEFFICIENT FOR PAIR INTERNAL CONVERSION

By comparing the curves in Fig. 5 the ratio of the number of pairs to the number of gamma-rays can be determined. The area $E+A$ in Fig. 5 represents approximately those electrons due to Klein-Nishina absorption in the 1.5-mm carbon absorber plus the other material surrounding the gamma-ray source. The difference in areas, $(E+A)$ minus $(F+B)$ gives the absorption in 1.5 mm carbon alone. By using the Klein-Nishina absorption coefficient, the number of gamma-rays emitted by the source (in the interval of time and solid angle determined by the experimental arrangement) is found. The number of pairs emitted under the same conditions should be given by either of the positron plots. It should also be given by either of the areas C or D, since these are thought to be composed of negative members of pairs.

It is desirable to introduce a refinement in the above computation, for the following reason. There is no doubt that many of the electrons and positrons of very low energy are lost in the experiment, due to stopping and scattering in the material surrounding the source. The fact that the positron plots fall off rapidly at low energy is an indication that this is true. Therefore better estimates of the true areas under the curves are obtained by using the areas A, B, and the upper halves (2.25 to 4.5 Mev) of the pair plots, and calculating the total areas from these with the aid of the theoretical forms of the Klein-Nishina and pair curves, respectively. This treatment gives a ratio of 11 pairs per 1000 gamma-ray quanta, which is the pair internal conversion coefficient.

Several theoretical calculations of the coefficient have been made,[5] and indicate that for the fluorine radiation the value should lie between 1.2 and 2 pairs per 1000 gamma-rays, depending only slightly upon whether dipole or quadrupole radiation is assumed. Our value of 11 per 1000 does not seem to be compatible with the theoretical value, on the assumption that the angular momentum change is not greater than 2 units and that either Ne^{20} or O^{16} emits the radiation.

SEARCH FOR LOW ENERGY GAMMA-RADIATION AND FOR DELAYED ACTIVITY

The reaction giving rise to the gamma-radiation remains a mystery. A number of possibilities have been discussed,[6] but none seems to give a satisfactory energy balance. We have searched for gamma-radiation of low energy which might have escaped attention previously, and have found nothing down to 0.5 Mev. We have also tested for delayed emission of electrons or gamma-radiation by placing the CaF_2 inside the cloud chamber about 5 minutes after bombardment. In this case electrons of energy as low as 5 or 10 kev could have been detected. No activity was observed.

The authors are indebted to the Rackham Endowment Fund for the support of this work.

[5] L. Nedelsky and J. R. Oppenheimer, Phys. Rev. **44**, 948 (1933); M. E. Rose and G. E. Uhlenbeck, Phys. Rev. **48**, 211 (1935); J. C. Jager and H. R. Hulme, Proc. Roy. Soc. **148**, 708 (1935).

[6] A complete discussion has recently been given by Professor G. Breit, in a paper published by E. J. Bernet, R. G. Herb and D. B. Parkinson, Phys. Rev. **54**, 398 (1938).

An Independent Determination of the Binding Energy of the Deuteron

F. T. ROGERS, JR., AND MARGUERITE M. ROGERS
The Rice Institute, Houston, Texas

(Received October 4, 1938)

This paper is an account of an experiment designed to determine the binding energy of the deuteron by a method which is relatively insensitive to uncertainties in the energy-range relation for protons of low energy. The protons, produced by the disintegration of Th C'' γ-radiation, were observed in a low pressure cloud chamber in a strong magnetic field. The curvatures of the tracks allowed the calculation of the corresponding kinetic energies. The final value of the binding energy as given by this experiment is

$$V_B = (2.17 \pm 0.05) \times 10^6 \text{ electron volts},$$

which is in reasonable agreement with previous determinations by others. The uncertainty 0.05 Mev is the *maximum* uncertainty to be expected in this value of the binding energy.

I. INTRODUCTION

IN 1935 Chadwick and Goldhaber[1] determined the binding energy V_B of the deuteron from the disintegration of deuterium by Th C'' γ-radiation of high energy. The particles taking part in this disintegration react according to the equation

$$_1H^2 + \gamma \rightarrow {}_1H^1 + {}_0n^1.$$

Chadwick and Goldhaber detected the product protons with a proportional counter and linear amplifier, and estimated the kinetic energies of these protons by the amounts of ionization they produced in the counter. In this way they got

$$V_B = (2.14 \pm 0.16) \times 10^6 \text{ electron volts.}$$

Subsequently Chadwick, Feather, and Bretscher[2] performed with a cloud chamber a more precise experiment designed to measure the ranges of the protons which are liberated when H^2 disintegrates. After converting the observed proton ranges to the corresponding proton kinetic energies by means of the best range-energy data available at that time, they got

$$V_B = (2.25 \pm 0.05) \times 10^6 \text{ ev.}$$

Their data, recalculated by Bethe[3] in the light of more recent data on the energy-range relation for protons, yield, however,

$$V_B = (2.17 \pm 0.04) \times 10^6 \text{ ev.}$$

The discrepancy between these last two values of V_B is caused by previous uncertainties in the energy-range data for protons of low energy.

At about the same time, J. R. Richardson and L. Emo[4] obtained

$$V_B = (2.18 \pm 0.07) \times 10^6 \text{ ev}$$

from the disintegration of H^2 by the high energy γ-radiation from radioactive Na^{24}. This value of V_B also involves the use of the energy-range relation for protons, for Richardson and Emo determined the range of the product protons with a cloud chamber and then got the corresponding kinetic energy by the energy-range relation. They used almost the same relation as that which Bethe[3] used.

Since these previous values of V_B depend upon the somewhat uncertain energy-range relation for protons of low energy (except for the first value quoted above, which is not of high precision), it was thought desirable to determine V_B by a method which yields results that are relatively insensitive to this dependence. An attempt to do this with an ordinary magnetic spectrograph with photographic recording was not successful, probably because the available Th C'' γ-ray source was not sufficiently strong.

It was decided for the present experiment to use a deuterium-filled cloud chamber in which the total pressure was about 8 cm Hg and to place this cloud chamber in a strong magnetic field. Then the observable curvatures of the pro-

[1] J. Chadwick and M. Goldhaber, Proc. Roy. Soc. **A151**, 479 (1935).
[2] J. Chadwick, N. Feather and E. Bretscher, Proc. Roy. Soc. **A163**, 366 (1937).
[3] H. A. Bethe, Phys. Rev. **53**, 313 (1938).
[4] J. R. Richardson and L. Emo, Phys. Rev. **53**, 234 (1938).

ton tracks should enable the kinetic energies of the protons to be determined.

II. Binding Energy in Terms of Proton Energy

In the following derivations we shall not consider either the effects of the relativistic variations of mass or the small difference between the mass of the proton and the neutron.

Let V be the energy in Mev of the Th C'' γ-ray which produces the disintegration of a deuteron; V_B the binding energy of the deuteron in Mev; W the kinetic energy in Mev of the proton liberated by the disintegration of the deuteron; p the ratio of the momentum of the incident γ-ray to the momentum of the product proton (obviously $p=10^4K^{\frac{1}{2}}V/c(2W)^{\frac{1}{2}}$); $K=e/m$ = specific charge of the proton, in e.m.u. per g; θ = angle between the direction of the incident γ-ray and the direction of emission of the product proton.

Then if the equations for the conservation of energy and for the conservation of two perpendicular components of momentum during the collision-disintegration process are properly solved, we have the simple expression

$$V_B=V-2W(1-p\cos\theta+p^2). \tag{1}$$

In this equation we treat V as a known quantity. We determine several pairs of values of θ and W (hence of p also) experimentally by making suitable observations.

III. Theoretical Considerations for Proton Energy

If a product proton were moving in a vacuum in a uniform magnetic field,[5] its trajectory would be a right-circular helix, the axis of which would be parallel to the direction of the magnetic field. Actually, in the present experiment, the protons moved in an almost uniform magnetic field (to within 0.7 percent); but, moving in the cloud chamber, they did not traverse a vacuum. The loss of energy by a proton to the chamber gases thus produces a trajectory which is not at all like the right-circular helix mentioned above. Allowance must be made for this.

[5] See, e.g., J. J. Thomson's *Conduction of Electricity Through Gases* (Cambridge Univ. Press, 1906), p. 106.

Let H be the strength in gauss of the (uniform) magnetic field in which the protons move; π a plane which is perpendicular to the direction of H. Let ψ be the angle between the direction of motion of a proton in H and a π-plane; ψ is of course measured in a plane perpendicular to a π-plane and will be constant (except for the effects of scattering by the chamber gases) over the length of a proton path. Let ρ be the radius of curvature of the π-plane projection of a proton path; ρ will of course decrease as the proton traverses its path. Let ρ' be the value of ρ at the beginning of a proton path; and v the kinetic energy in Mev of a proton when its projected path has a radius of curvature ρ; $v=W$ when $\rho=\rho'$.

Then if for any point on a proton's path we equate the centrifugal force acting on the proton to the force on it due to its motion in H, and if we solve this equation for v, we get

$$v=5\times10^{-15}K(H\rho\sec\psi)^2. \tag{2}$$

Now if we multiply this by dv and integrate from $v=0$ to $v=W$, we get

$$W=10^{-14}K(H\sigma\sec\psi)^2, \tag{3}$$

where

$$\sigma^2=(1/W)\int_0^W\rho^2dv. \tag{4}$$

Eq. (3) gives W in terms of σ, which is a function of the shape of the *entire* proton path, rather than in terms of a radius of curvature (e.g., as ρ') at some one point on the path. The outstanding difficulty in the calculation of W from the "one point" equation,

$$W=5\times10^{-15}K(H\rho'\sec\psi)^2,$$

is the determination of ρ'; in this experiment the accurate determination of ρ' was not possible because the observed proton tracks were: (1) only slightly curved by the magnetic field; (2) often appreciably broadened by diffusion (characteristic of low pressure cloud chamber containing mostly deuterium gas); (3) occasionally scattered through appreciable angles. Eq. (3) allows these three obstacles to radius of curvature measurements to "average themselves out" over the length of a proton track.

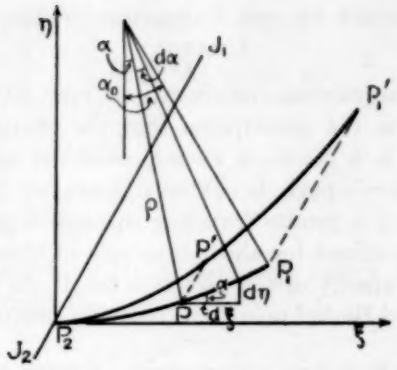

FIG. 1. $P_1'P'P_2$ is an actual proton path. P_1PP_2 is the $\xi\eta$ projection of this path. α is measured from the $P_2\eta$ direction as shown. $J_2P_2J_1$ is the direction perpendicular to the $\xi\eta$ plane. The lengths of the several arcs are: $P'P_2=r'$; $P_1'P'=L'-r'$; $PP_2=r$; $P_1P=L-r$.

IV. APPLICATION OF ENERGY-RANGE RELATION

We now seek a more useful expression for σ. To this end, we shall discuss the equation of a proton's path in the cloud chamber, assuming K to be a constant over the whole path. Suppose we have a proton moving along its path. Since we wish to investigate σ, which contains ρ, consider the projection of this path on a π-plane which passes through the end-point P_2 of the path (see Fig. 1). In this plane establish mutually perpendicular ξ and η axes with origin at P_2, with the ξ axis tangent to the path's projection at P_2. Let P_1 be the $\xi\eta$ projection of the beginning point P_1' of the path, and let P be the $\xi\eta$ projection of any point P' of the path. To be associated with P are the kinetic energy v at P' and the radius of curvature ρ of the projected path at P. Let the range of the proton at P' be r', and let the total length of the path be L'; then let

$$r=r'\cos\psi \quad \text{and} \quad L=L'\cos\psi \tag{5}$$

be the $\xi\eta$ projections of r' and L'. Since the proton loses energy as it traverses the path $P_1'P_2$, the value of ρ decreases, a fact which we indicate by the functional relation

$$\rho^2=g(r). \tag{6}$$

The differential equation of the path in terms of the ξ and η coordinates is the trio of equations:

$$\left.\begin{aligned} d\xi&=dr\cos\alpha, \quad d\eta=dr\sin\alpha,\\ d\alpha&=dr/[g(r)]^{\frac{1}{2}},\end{aligned}\right\} \tag{7}$$

where α is an angle (in the $\xi\eta$ plane) defined adequately by Fig. 1.

Let the chord P_2MP_1, M being the mid-point, be of length $2d$. The perpendicular to this chord erected at M will intersect the projected path P_2PP_1 at some point N; let $MN=h$. Let the radius of the circle through P_2, N, and P_1 be R. Then

$$R=(h^2+d^2)/2h. \tag{8}$$

R, through the measurable h and d of a proton track, will serve as our measure of the radius of curvature of the proton track. We now seek a relation between R and σ.

For the relatively simple case in which ρ^2 is proportional to r', we may take

$$\rho^2=C_1r\sec\psi, \tag{9}$$

where C_1 is a suitable constant. Substituting this into Eq. (7) and integrating, we get for the path of the proton

$$\left.\begin{aligned}\xi&=\tfrac{1}{2}C_1\sec\psi(\cos\alpha+\alpha\sin\alpha-1),\\ \eta&=\tfrac{1}{2}C_1\sec\psi(\sin\alpha-\alpha\cos\alpha),\end{aligned}\right\} \tag{10}$$

which are the equations of the evolute of a circle.[6] If from these equations R^2 is calculated by Eq. (8) for several paths of various lengths (i.e., for various values of α_0 (see Fig. 1)), and if σ^2 is calculated for the same values of α_0, and if then the ratios σ^2/R^2 are formed, we get the values tabulated in Table I. Obviously, for proton tracks formed under the condition that ρ^2 is proportional to r',

$$\left.\begin{aligned}\sigma^2&=(1.23\pm0.03)R^2,\\ 0.2&\leq 2(L'/C_1\sec\psi)^{\frac{1}{2}}\leq 1,\end{aligned}\right\} \tag{11}$$

independently of C_1. (The relation between α_0 and L' comes from Eqs. (7) and (9).)

Now Eqs. (11) cannot be used unless Eq. (9) is known to be valid. Actually, the energy-range relation for protons of low energy is, within five or ten percent of energy, that given in Table II. These energy-range data are those of Livingston and Bethe[7] as revised by them[8] to include the recent experimental data of Parkinson, Herb, Bellamy, and Hudson.[8] It can be seen from this

[6] See, e.g., W. F. Osgood's *Differential and Integral Calculus* (Macmillan, 1927), p. 143.
[7] M. S. Livingston and H. A. Bethe, Rev. Mod. Phys. **9**, 268 (1937).
[8] D. B. Parkinson, R. G. Herb, J. C. Bellamy, and C. M. Hudson, Phys. Rev. **52**, 75 (1937).

table that the strictly linear energy-range relation assumed in Eq. (9) is entirely consistent, for $v \leqslant 0.3$, with the presently accepted relation. Therefore, we should not be in great error in taking Eq. (9) to be true. We must admit, however, that ρ^2 *may* deviate somewhat from the linear relation of Eq. (9).

We can see that even an appreciable deviation from Eq. (9) produces only an insignificant change in the value of σ^2/R^2. To see this, we may work out the case in which ($\psi = 0$ for convenience)

$$g(r) = C_1 r/(a_0 r^{0.4} + a_1 + a_2 r)^2, \tag{12}$$

in which we shall take

$$\begin{aligned} C_1 &= 120, & a_0 &= 0.236, \\ a_1 &= 0.717, & a_2 &= 0.0368. \end{aligned} \tag{13}$$

This form for $g(r)$ is quite similar to that suggested for protons of very low energy by the energy-range graph of Livingston and Bethe.[7] Its average deviation from the function $C_1 r$ is, for proton energies up to 0.3 Mev, of the order of 10 percent. The constants in it are chosen to fit the following case: the stopping power of the gas is 0.075 that of air, and $H = 3520$; the other condition on the constants is that Eqs. (12) and (13) represent (for this case) the data given in Table II.

If we substitute Eqs. (12) and (13) into Eqs. (7) and integrate, and if we then calculate several

TABLE I. σ^2/R^2 vs. α_0.

α_0	σ^2/R^2	α_0	σ^2/R
0.150	1.29	0.600	1.21
0.200	1.26	0.750	1.22
0.300	1.22	0.875	1.23
0.450	1.21	1.000	1.24

values of σ^2/R^2 as a function of L (instead of α_0) as was done to obtain Table I, we find that

$$\left.\begin{aligned} \sigma^2 &= (1.27 \pm 0.05) R^2, \\ 2.5 &\leqslant L < 4. \end{aligned}\right\} \tag{14}$$

Obviously the difference between Eqs. (11) on one hand and Eqs. (14) on the other hand, is essentially a small one relative to the difference between Eq. (9) and Eqs. (12)–(13).

V. Effect of the Variation of Proton's Charge

All our previous considerations, now, have been based on the assumption that the charge on a proton is a constant $e = mK$ over the whole of the proton's path. It is known, however, that the charge of a proton traveling through a gas may be neutralized for short intervals of time if the kinetic energy of the proton is small. As Livingston and Bethe[9] point out, only if a proton has a kinetic energy of 0.1 Mev or more, can one be reasonably safe in taking the charge to be the usual value, $e = 4.8 \times 10^{-10}$ e.s.u. Since the protons which we observed in the present experiment had energies less than 0.1 Mev over almost half their path lengths, we must make an allowance for their reduced charges at low energies if we intend to utilize their entire tracks for calculations. We shall derive a relation analogous to Eqs. (3) and (14) to allow for this variation of charge.

TABLE II. *Energy-range relation for low energy protons.*

Range of Proton in cm in Dry Air at 15°C and 760 mm of Hg	Kinetic Energy of the Proton in Mev
0.0	0.000
0.2	0.202
0.4	0.355
0.6	0.463
0.8	0.550
1.0	0.628

Let E be the kinetic energy in ergs of the proton when liberated by the disintegration of a deuteron; δ the ratio of the true charge on the proton to e (this, of course, varies as the proton traverses its path); i the kinetic energy in ergs of a proton which has a range r'; $i = E$ when $r' = L'$. Now just as Eq. (2) was obtained, we may also find

$$i = (H\delta e\rho \sec\psi)^2/2m;$$

therefore,

$$v = 5 \times 10^{-15} K (H\delta\rho \sec\psi)^2. \tag{15}$$

Note that

$$\rho^2 = C_2 v/\delta^2, \tag{16}$$

where C_2 is a suitable constant. Hence, just as

[9] M. S. Livingston and H. A. Bethe, reference 7, p. 262.

Eq. (3) was obtained,

$$W=10^{-14}K(H\tau\sec\psi)^2, \tag{17}$$

where

$$\tau^2=(1/W)\int_0^W \delta^2\rho^2 dv. \tag{18}$$

Note that for $v\gtrsim 0.18$, $\delta=1$ very nearly and this last reduces to

$$\tau^2=\tfrac{1}{2}\rho'^2, \qquad v\gtrsim 0.18. \tag{19}$$

To evaluate this, we need to know essentially how δ varies with v and how ρ varies with v.

We can get an idea of how δ might be expected to vary with v from the data of Bartels[10] on the variation of charge of positive rays of hydrogen passing through hydrogen. Bartels' data, as given for gas pressures of 1 mm Hg, are summarized in Table III, in which n_+/n_0 is the ratio of the number of protons to the number of neutral hydrogen atoms in a beam of such positive rays. The third column in this table is the ratio $n_+/(n_++n_0)$. These data are the circles in Fig. 2; the (dotted) curve for δ in Fig. 2 is taken, by analogy with the variations of α-particle charges, to pass near the point (0.1, 0.9); its equation will be of the form $\delta=\delta(v)$. This particular variation of δ with v, while of course indicative of the *nature* of the true variation, cannot be expected to give much more than the order of magnitude of the true variation under the very different conditions which existed in the cloud chamber. Here the pressure was 8 cm (80 times as great as the pressure for which the data in Table III are quoted); the gas mixture was only $\frac{3}{4}$ hydrogen (the remainder $H^2{}_2O$ vapor), and the whole was in the presence of moderately intense γ-radiation. We shall see shortly how this variation of δ with v must be replaced by another law for the present experiment.

Continuing with the case (for simplicity) for which $\psi=0$ and for which v is proportional to r:

$$v=C_3 r, \tag{20}$$

where $C_3=0.0713$ (this is appropriate to the example for $H=3520$ and a stopping power of chamber gases of 0.075 that of air, which we have used in Section IV), we have

$$\rho=[g(r)]^{\frac{1}{2}}=41v^{\frac{1}{2}}/\delta(v); \tag{21}$$

$C_2=1687$ from Eq. (16). Substituting this into Eqs. (7) and integrating, we get the path which a proton follows under these conditions. If from the path computed using the dotted-curve variation of δ with v (Fig. 2) we compute for several values of $(r=)L$ the values of R^2, we find that for $2.5\leqslant L\leqslant 4.0$, $R=16.5\pm 0.5$. But the values of R which were found in the present experiment were in the neighborhood of 12 cm. Since the values of R calculated from Eq. (21) are largely independent of C_3, this means that the true variation of δ with v is not the one given by Table III for 1 mm Hg pressure.

The true variation of δ with v must obviously be such that at very small values of v, δ is appreciably greater than is indicated in Table III. Furthermore, the true variation of δ must be such that the values of R calculated from Eq. (21) by means of it, are somewhat smaller than 16.5 cm. An approximation to what must be the true variation of δ with v is given by the solid curve of Fig. 2. With this law for $\delta(v)$ in Eq. (21), the calculated values of R in the neighborhood of 13 cm, are more nearly equal to the observed values of about 12 cm. In view of the necessary experimental uncertainties in the observed values of R, this variation of $\delta(v)$ is probably sufficiently near to the true variation of $\delta(v)$ for the purposes of the present experiment. The values of τ^2/R^2 got

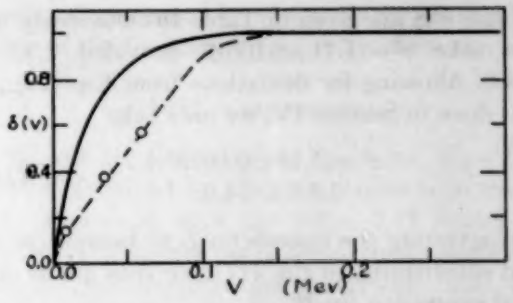

FIG. 2. Values of δ for various values of the kinetic energy v.

TABLE III. *Bartels' data for n_+/n_0 as a function of v at 1 mm Hg pressure.*

v	0.010	0.035	0.060
n_+/n_0	0.16	0.61	1.30
δ	0.14	0.38	0.57

[10] H. Bartels, Ann. d. Physik **13**, 373 (1932).

by this $\delta(v)$ are given in Table IV. Obviously we can take $r^2=(1.11\pm0.09)R^2$ provided $2.5\leqslant L\leqslant 4.0$. Allowing for deviations from Eq. (20) as was done in Section IV, we may take

$$\left.\begin{array}{c} r^2=(1.15\pm0.09)R^2, \\ 2.5\leqslant L\leqslant 4.0. \end{array}\right\} \quad (22)$$

Converting the bounds on L to bounds on W and substituting in Eq. (17), we thus get as our final expression for W,

$$\left.\begin{array}{c} W=(1.15\pm0.09)\times10^{-14}K(HR\sec\psi)^2, \\ 0.175\leqslant W\leqslant 0.275. \end{array}\right\} \quad (23)$$

This expression for W is largely independent of uncertainties in the energy-range relation for protons of low energy, as are Eqs. (11) and (14).

VI. Error Theory

Let ϵ_j, $j=1$ through 7, be the absolute errors which might be present in single determinations of R, ψ, W, V, θ, V_B, and in the mean value $\bar{V}_B$ of n determinations of V_B, respectively. Then it can be shown from Eq. (23), that

$$\epsilon_3\leqq 2W(\Delta k/2k+\epsilon_1/R+\epsilon_2\tan\psi), \quad (24)$$

where k is the coefficient 1.15. In a similar manner,

$$\epsilon_6\leqq\epsilon_4+5\times10^4\epsilon_5+2\epsilon_3. \quad (25)$$

Hence, substituting Eq. (24) into Eq. (25) and noting that in the mean, some of the errors will be reduced by a factor of $n^{\frac{1}{2}}$ (according to the usual theory of errors), we have

$$\epsilon_7\leqq\epsilon_4+2W(\Delta k/k)+[4W(\epsilon_1/R+\epsilon_2\tan\bar{\psi})+5\times10^4\epsilon_5]n^{-\frac{1}{2}}; \quad (26)$$

here $\bar{\psi}$ is the mean of the n values of ψ.

Table IV. r^2/R^2 vs. L.

L	2.5	3.0	3.5	4.0
r^2/R^2	1.02	1.07	1.14	1.20

VII. Observations and Calculated Results

A low pressure (8 cm Hg) cloud chamber was used to observe the protons in this experiment. It was of a depth of about 2.5 cm and an inside diameter of 11 cm. A mixture of H^2_2O vapor and deuterium was used in the chamber, and a γ-ray source (of Ra Th) was placed as close as possible to the glass face of the chamber. The γ-ray activity of the Ra Th was equivalent to about 5 mg of Ra; this source was in a 4-mm thick lead container. In spite of the extreme propinguity of the γ-ray source to the cloud chamber, no great trouble was experienced with the fogging of the chamber by the γ-radiation. This was probably due to the low average atomic weight of the gas in the chamber. The light source was a carbon arc with photographic-flame carbons at 100 amperes d.c. The photographs were taken with a stereoscopic camera having f: 1.9 lenses. The magnetic field at the region of the cloud chamber was measured by the inductive method, with inductances, resistances, and standard cells which had been calibrated at the National Bureau of Standards. Under the conditions which prevailed when the photographs were made, H was found to be 3762 gauss to well within one percent.

In all, about 2300 pictures were made, among which were found fifteen proton tracks which were suited to accurate measurement. The measurement of them was effected as follows:

(1) the tracks were projected on a screen by running the (well illuminated) film back through the camera and moving the screen until the stereoscopic images coincided;

(2) with a Brown and Sharp protractor, ψ and θ for each track was measured (see Table V)—the θ of a track was measured between the line from the center of the γ-ray source to the beginning of the track and the tangent to the track at its beginning point;

(3) the two ends and the mid-point N of each track were carefully recorded on small strips of paper with a very sharp pencil; this was done several times for each track;

(4) the chord (of length 2ω) P_2P_1' (see Fig. 1) was measured and its half-length recorded (see Table V);

(5) the mid-chord perpendicular (length h) from each track to its chord was measured and recorded (see Table V);

(6) from ω, d was calculated and recorded:

$$d=\omega\cos\psi.$$

This method, far from being inaccurate, affords a very reliable method of measuring such curved proton tracks. In fact, it is believed that

TABLE V. *Data on proton tracks.*

TRACK	$\psi(0)$	$\theta(0)$	ω (cm)	h (cm)	d (cm)	V_B (Mev)	$\lvert\bar{V}_B - V_B\rvert$ (Mev)
1	37	137	1.52	0.086	1.215	2.220	0.05
2	30	173	1.25	0.062	1.082	2.197	0.03
3	17	63	1.59	0.096	1.520	2.153	0.02
4	18	134	1.76	0.125	1.681	2.145	0.02
5	35	97	1.61	0.089	1.319	2.166	0.00
6	2	47	1.35	0.069	1.350	2.117	0.05
7	3	38	1.54	0.097	1.540	2.198	0.03
8	42	159	1.33	0.064	0.975	2.261	0.09
9	0	76	1.45	0.086	1.450	2.167	0.00
10	27	131	1.30	0.062	1.160	2.201	0.03
11	12	97	2.00	0.174	1.955	2.198	0.03
12	23	86	2.03	0.151	1.869	2.201	0.03
13	9	0	1.79	0.118	1.769	2.118	0.05
14	7	94	1.20	0.057	1.191	2.123	0.05
15	21	93	1.62	0.112	1.512	2.144	0.03
Mean						2.174	0.03

the determinations of ω are accurate to within one percent and that those of h are accurate to within four percent.

In the seventh column of Table V are the values of V_B calculated by Eqs. (23) and (1) from the data in the earlier columns of the table.[11] In the eighth column are the deviations of the various values of V_B from the mean value $\bar{V}_B$. The mean value of V_B, as seen on the table, is 2.17 Mev. The average deviations of the several V_B's from this mean is 0.03 Mev, corresponding to a "probable error" of 0.02 Mev.

The maximum error ϵ_7 to be expected in this value of $\bar{V}_B$ we get from Eq. (26) taking $\epsilon_1/R=0.05$, $\epsilon_2=0.025$, $\epsilon_4=0.005$, $\epsilon_6=0.02$, $\bar{\psi}=19°$, $\Delta k=0.09$, and $n=15$. Substituting these values and taking $W\leqq 0.2$ Mev, Eq. (26) gives $\epsilon_7=0.05$ Mev. Accordingly, we take as the final value given by this experiment

$$\bar{V}_B=2.17\pm 0.05 \text{ Mev}. \qquad (27)$$

It is to be noted that the uncertainty 0.05 is a conservative value indicating the maximum error to be expected in this value of $\bar{V}_B$; as such, it may be expected to be of the order of two or three times as large as the "probable error" of $\bar{V}_B$. The precision of this experiment thus compares well with the precisions of the previous determinations of the binding energy of the deuteron.

[11] With $V=2.623\pm 0.005$ Mev.

VIII. CONCLUSIONS

It will be noticed that the value $\bar{V}_B=2.17$ Mev determined by this experiment is in excellent agreement with the value 2.17 found by Bethe[3] on recalculation of the data of Chadwick, Feather, and Bretscher,[2] and with the value 2.18 got by Richardson and Emo[4] from the disintegration of H^2 by the high energy γ-radiation from radioactive sodium. This concurrence of values tends to indicate that the presently accepted energy-range relation (used by Bethe and by Richardson and Emo) is correct for protons of energies in the neighborhood of 0.2 Mev. It also tends to fix the mass of the neutron at the presently accepted value of 1.0089 atomic mass units rather than at some higher value.[12] It also tends to indicate very definitely that the variation of protonic charge with energy as the proton traverses a gas such as the presently used $H^2_2O-H^2_2$ mixture, has $\delta(v)$ about twice as great (for $v<0.1$) as the experimental data for pressures of 1 mm Hg would predict—note that this conclusion depends chiefly upon the agreement of calculated values of R with the observed values of R, and is only confirmed by the agreement of $\bar{V}_B$ with the other values of 2.17 and 2.18 Mev.*

Finally, we wish to acknowledge our indebtedness to Dr. H. A. Wilson for his having suggested to one of us that the binding energy of the deuteron be redetermined, and for his having provided us with every desired facility for carrying out the necessary experiment.

We are also grateful to Miss Eby Nell McElrath for assisting in the taking of the necessary photographs, and to Mr. Stanley Heaps for helping with the development of the negatives.

[12] See, e.g., E. Hudspeth and T. W. Bonner, Phys. Rev. **54**, 308 (1938).

* *Note added in proof:* In addition to the values of V_B quoted in the Introduction, G. Stetter and W. Jentschke (Zeits. f. Physik **110**, 214 (1938)) have more recently given the concordant value $V_B=2.189\pm 0.022$ Mev.

Hyperfine Structure of Manganese I and Nuclear Magnetic Moment

RUSSELL A. FISHER AND EDSON R. PECK
Northwestern University, Evanston, Illinois

(Received November 26, 1938)

New measurements of the structure of the green lines of Mn I combined with the data already available make possible a determination of 24 hyperfine interval factors. Interval factor formulas derived by the method of energy sums are in reasonable accord with much of the data. This permits an approximate determination of the nuclear magnetic moment of Mn^{55}, which is found to be 3.0 nuclear magnetons.

INTRODUCTION

MEASUREMENTS on the hyperfine structure of the visible lines in the arc spectrum of manganese were first reported in 1909 by Janicki[1] who measured twenty-one structures using a Lummer Plate. These lines and others have since been remeasured by Wali-Mohammad,[2] by White and Ritchl[3] and by Wali-Mohammad and Sharma.[4] White and Ritchl, whose measurements are the most extensive gave an analysis of the hyperfine structure showing the nuclear spin to be $2\frac{1}{2}$ units. They reported values for the total separations of several of the hypermultiplets and pointed out that the prominent splittings are associated with configurations in which an unbalanced *s* electron occurs. Using the vector model of the atom they developed formulas for the separations expressing the intervals in terms of coupling factors related to the individual electrons of the configuration. Following White and Ritchl's work Wali-Mohammad and Sharma measured many of the lines used by White and Ritchl in their analysis and reported disagreements in some of the measured structures. We have remeasured a number of the lines in the green region concerning whose structure the existing data seemed least conclusive. An analysis of these data along with those of the previous observers yields values for the hyperfine intervals differing in some details from those obtained by White and Ritchl and permits calculations leading to an approximate value for the nuclear magnetic moment.

[1] L. Janicki, Ann. d. Physik **29**, 833 (1909).
[2] Wali-Mohammad, Astrophys. J. **39**, 185 (1914).
[3] H. E. White and R. Ritchl, Phys. Rev. **35**, 1146 (1930).
[4] Wali-Mohammad and P. N. Sharma, Phil. Mag. **18**, 1144 (1934).

EXPERIMENTAL DATA

Table I gives the results of our measurements upon thirteen lines in the green region together with the data of the previous observers. The interval in wave numbers separating each measured component from the strongest line in its pattern is always given. The data of the other observers have been converted to the same units. Since many of the structures are only partially resolved, the measured positions may refer only to points of maximum intensity in the pattern. Components and maxima are designated by numbers specifying their relative intensities in the pattern. When a structure terminates in an unresolved "tail" the terminus is designated by an *e* in the intensity column. White and Ritchl also have indicated the extent of unresolved patterns.

For our observations the manganese was excited in helium in a water-cooled metal hollow cathode discharge tube. Resolution was by means of a ruled Fabry-Perot interferometer[5] and small Hilger glass prism spectrograph. Interferometer spacers of 2.37, 5.28 and 10.03 mm were employed. Three or more spectrograms were taken with each spacer so that each pattern reported in Table I was verified by its appearance under different resolutions and in different intensities, with the exception of the lines λλ5399.5 and 5413.7 which were measurable on only two plates because of their low intensities.

It may be seen (Table I) that in most cases in which the new measurements differ materially from the older the new observations reveal additional components not before resolved. This

[5] R. C. Machler and R. A. Fisher, J. Opt. Soc. Am. **25**, 315 (1935).

is illustrated by the first line of the table, λ5537.8, in which the pair of components at 0.129 and 0.221 cm^{-1}, respectively, were observed as a single component in an intermediate position by Wali-Mohammad and by Wali-Mohammad and Sharma. The same is true of the pair at 0.320 and 0.377 cm^{-1}. White and Ritchl did not resolve structure in this line and so gave only the initial and terminal points of the pattern. The most serious disagreement in data[6] appears in connection with λ5341.4 for which White and Ritchl reported the same pattern as we, but upon a scale some 10 percent larger while Wali-Mohammad and Sharma found a similar pattern on a

[6] The close grouping of lines in the vicinity of 5400A has led to some confusion in their identification in the interferograms. It is evident from Janicki's published spectrograms as well as from his measured separations that the three relatively strong lines identified by him as λλ5394.7, 5399.5 and 5407.4, respectively, are in reality λλ5399.5, 5407.4 and 5420.4, respectively. Wali-Mohammad apparently followed Janicki's example in this identification. We have taken the liberty of shifting these measurements by both Janicki and Wali-Mohammad in the table, thus bringing them into close agreement with those of the later observers.

TABLE I. *Hyperfine structure of green lines of* Mn I *according to different observers.*[*]

λ(A)	Int	Δν(cm⁻¹) New	M&S	W&R	M	J
5537.8	6	0.000	0.000	0.000	0.000	
	3	.129				
			.154		.150	
	3	.221				
	2	.320				
			.346		.340	
	1	.376		.366		
5516.8	6	.000	.000	.000	.000	0.000
	1	.061				
	1	.150				
			.164			
	3	.220				
			.247	.246	.230	.240
	1	.264				
	2	.372		.410	.395	.388
5505.9	5	.000		.000	.000	.000
	3	.149		.152	.154	.154
	2	.270				
				.295	.290	.293
	1	.349				
	e	.408		.392		
5481.4	4	.000	.000	.000	.000	.000
	3	.207	.206	.221	.206	.217
	2	.373	.373	.391	.383	.407
	1	.463				
	e	.516		.512		
5470.7	4	.000		.000	.000	.000
	3	.191		.182	.184	.187
	3	.350		.327	.347	.351
	e	.516		.495		
5432.6	6	.000		.000		
	5	−.106		−.105		
	4	−.195		−.186		
	3	−.266		−.254		
	e	−.310		−.298		
5420.4	5	.000		.000	.000	.000
	4	.190		.197	.185	.195
	3	.341		.356	.356	.359
	2	.440				
				.475		
	1	.510			.503	.492
	e	.59		.627		
5413.7	1	−0.10				
	6	.000		0.000		
	2	.144				
				.171		
	2	.237				
	e	.275				
5407.4	5	.000	0.000	.000	0.000	0.000
	5	.182	.190	.190	.185	.189
	3	.345		.341	.357	.350
	2	.486	.506		.505	.490
				.556		
	e	.623				
5399.5	1	−.114				
	4	.000			.000	.000
	1	.109				
	3	.230			.234	.223
5394.7	8	.000		.000		
	6	−.114		−.112		
	4	−.217		−.210		
	3	−.306		−.289		
	2	−.383		−.357		
	1	−.410		−.395		
5377.6	1	−.098				
	6	.000			.000	.000
	3	.101				
						.121
	2	.130			.130	
5341.1	6	.000	.000	.000	.000	.000
	5	.205	.161	.221	.203	.200
	4	.374	.309	.406	.376	.379
	3	.514	.428	.560	.523	.523
	3	.620	.530	.680		
					.667	.642
	2	.680		.762		

[*] M&S indicates data of Wali-Mohammad and Sharma; W&R indicates data of White and Ritchl; M indicates data of Wali-Mohammad; J indicates data of Janicki.

TABLE II. *Hyperfine structure of violet lines of* Mn I *from measurements of White and Ritchl.**

λ(A)	Δν(cm⁻¹)	λ(A)	Δν(cm⁻¹)
4018.2	0.0000	4048.8	0.0000
	.1188		.0890
	.2147		.1653
	.2946		.2251
	.3565	4055.5	.0000
	.4029*e*		.0742
4030.7	.0000		.1605
	−.0930		.2207
	−.1724		.2633
	−.2352		.2925*e*
	−.2826	4063.5	.0000
	−.3138		.0619
4033.1	.0000		.1426
	−.0873		.2209
	−.1654	4079.2	.0000
	−.2207		.0834
	−.2576		.1494
4034.5	.0000		.1986
	−.0891		.2616*e*
	−.1610	4079.4	.0000
	−.2083		.1182
4035.7	.0000	4082.9	.0000
	.0829		.0672
	.1805		.1218
	.2462		.1638
	.3113*e*	4083.6	.0000
4041.4	.0000		.0654
	.1010		.1956*e*
	.1867		
	.2577		
	.3146		
	.3513		

* White and Ritchl gave intervals between successive components in cm⁻¹. These intervals have been added to give positions with respect to the strongest component of the pattern. *e* following a position indicates the end of the pattern rather than a component.

scale 17 percent smaller. The new measurements on this line are, however, in close agreement with those of Janicki and of Wali-Mohammad.

Other data of use in this analysis are the excellent measurements of White and Ritchl upon the group of lines in the vicinity of 4000A listed in Table II. The measurements of other observers in this region are too fragmentary for inclusion in the table. White and Ritchl have also given microphotometer curves depicting the complex unresolved patterns found for λλ4754.1, 4783.4 and 4823.5 with a wave-length scale.

ANALYSIS OF HYPERFINE STRUCTURE

The term classification of the Mn I lines[7] here of interest is shown by Table III. The wave-lengths of the lines appear within the rectangles and the terms from which they originate along the margins; even terms are above and odd terms to the left.

All of the information now available is in complete accord with White and Ritchl's assigned value for the nuclear spin, $I=2\frac{1}{2}$. Accepting the value of I as established and assuming that the interval rule for hypermultiplets is obeyed within the limits of observation, we may proceed to apply the graphical method of hyperfine structure analysis described by Fisher and Goudsmit.[8] The scheme employed throughout the analysis of the twenty-nine hyperfine structures has been to construct for each pattern what may be called a "pattern graph" representing the observed positions of components on a varying scale by means of properly spaced diverging pencil lines. This pattern graph which is on semi-transparent paper is then laid over the appropriate analysis graph and shifted about until the position is found at which the corresponding lines of the two graphs coincide. This determines the ratio between the interval factors of the two hypermultiplets. The relation of the two graphs for λ5537.8 is illustrated in Fig. 1.

TABLE III. *Classification of* Mn I *lines.*

	J	$3d^5\,4s\,{}^6D$ $4\frac{1}{2}$	$3\frac{1}{2}$	$2\frac{1}{2}$	$1\frac{1}{2}$	$\frac{1}{2}$
$3d^5\,4s(^5S)4p\,{}^6P^0$	$1\frac{1}{2}$			5481.4	5516.8	5537.8
	$2\frac{1}{2}$		5420.4	5470.7	5505.9	
	$3\frac{1}{2}$	5341.1	5407.1			
$3d^5\,4p\,{}^6D^0$	$4\frac{1}{2}$	4041.4	4079.2			
	$3\frac{1}{2}$	4018.2	4055.5	4083.6		
	$2\frac{1}{2}$		4035.7	4063.5	4082.9	
	$1\frac{1}{2}$			4048.8		4079.4

	J	$3d^5\,4s^2\,{}^6S_{2\frac{1}{2}}$	$3d^5\,4s\,5s\,{}^8S_{3\frac{1}{2}}$
$3d^5\,4s\,4p\,{}^8P^0$	$2\frac{1}{2}$	5432.6	4754.1
	$3\frac{1}{2}$	5394.7	4783.4
	$4\frac{1}{2}$		4823.5
$3d^5\,4s(^7S)4p\,{}^6P^0$	$1\frac{1}{2}$	4034.5	
	$2\frac{1}{2}$	4033.1	
	$3\frac{1}{2}$	4030.7	

	J	$3d^5\,4s\,5s\,{}^4S_{1\frac{1}{2}}$
$3d^5\,4s\,4p\,{}^4P^0$	$2\frac{1}{2}$	5377.6
	$1\frac{1}{2}$	5399.5
	$\frac{1}{2}$	5413.7

[7] See R. Bacher and S. Goudsmit, *Atomic Energy States* (McGraw-Hill Book Company), for references.

[8] R. A. Fisher and S. Goudsmit, Phys. Rev. **37**, 1057 (1931).

The indicated ratio of interval factors is $A(^6D_4)/A(^6P_{1\frac{1}{2}}^0) = -0.87$. From the measured spacings we then get $A(^6D_4) = 0.028$ cm^{-1} and $A(^6P_{1\frac{1}{2}}^0) = -0.032$ cm^{-1}.

The pattern of λ5537.8 is the most completely resolved of the observed structures, since five of the expected six components are measurable. Using this line as key we have carried through the analysis and obtained values for the interval factors of all states involved. These interval factors appear in Table IV. Since most of the patterns are less completely resolved than λ5537, an unambiguous determination of the interval factors cannot always be made from a single structure. However, the requirement of consistency in the interpretation of related patterns provides in every case more conditions than are necessary for a unique assignment of values to the interval factors. It is to be recognized that the interferograms contain significant information having to do with the contours of the patterns which cannot conveniently be tabulated, but which nevertheless can be used to advantage in the graphical method of analysis when the plates are available for study. Aside from the number of significant figures with which they are expressed the interval factor data cannot all be given equal weights because of the varying element of judgment which is represented in the interpretation of the patterns. We have indicated the degree of our confidence in the data of Table IV by grading them *A*, *B* and *C*, *A* indicating that we regard the figure as comparatively reliable, *C* that we regard it as somewhat dubious.

TABLE IV. *Hyperfine interval factors*, Mn I.

STATE	J	INTERVAL FACTOR (CM^{-1})	
$3d^5\,4s^2\,{}^6S$	$2\frac{1}{2}$	0.000	*B*
$3d^5\,4s\,{}^6D$	$\frac{1}{2}$	0.0278	±0.0005, *A*
	$1\frac{1}{2}$	.0165	
	$2\frac{1}{2}$	.0145	
	$3\frac{1}{2}$	.0135	
	$4\frac{1}{2}$	.0145	
$3d^5\,4s\,4p\,{}^6P^0$	$2\frac{1}{2}$	.0222	± .001, *A*
	$3\frac{1}{2}$	.0205	
	$4\frac{1}{2}$	.018	
$3d^5\,4s\,4p\,{}^4P^0$	$\frac{1}{2}$	−.056	± .001, *A*
	$1\frac{1}{2}$	−.023	
	$2\frac{1}{2}$	−.020	
$3d^5\,4s(^7S)4p\,{}^6P^0$	$1\frac{1}{2}$	.0230	± .001, *A*
	$2\frac{1}{2}$	.0185	
	$3\frac{1}{2}$	.0160	
$3d^5\,4s(^5S)4p\,{}^6P^0$	$1\frac{1}{2}$	−.0315	± .001, *A*
	$2\frac{1}{2}$	−.0215	
	$3\frac{1}{2}$	−.0170	
$3d^5\,4p\,{}^6D^0$	$1\frac{1}{2}$	−.005	*C*
	$2\frac{1}{2}$	−.002	
	$3\frac{1}{2}$	.002	
	$4\frac{1}{2}$	.001	
$3d^5\,4s\,5s\,{}^8S$	$3\frac{1}{2}$	.0265	± .0005, *A*
$3d^5\,4s\,5s\,{}^4S$	$1\frac{1}{2}$	−.049	± .001, *B*

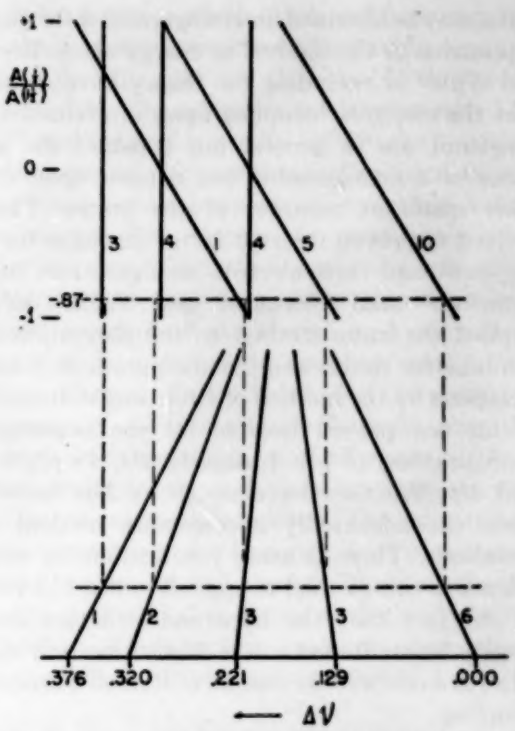

FIG. 1. Graphical analysis of λ5537.8 of Mn I. Above: Analysis graph showing theoretical line distribution for transition $J = \frac{1}{2} \rightarrow J = 1\frac{1}{2}$ with varying interval factor ratio, $A(\frac{1}{2})/A(1\frac{1}{2})$. Theoretical relative intensity of each component is indicated. Below: Pattern graph showing observed pattern on varying scale. Estimated relative intensity of each component is indicated. Coincidence between the two graphs occurs at $A(\frac{1}{2})/A(1\frac{1}{2}) = -0.87$.

NUCLEAR MAGNETIC MOMENT

In order that the nuclear magnetic moment may be found from hyperfine structure data it is necessary that formulas expressing the observed interval factors in terms of the coupling between the nucleus and the individual electrons be available. Goudsmit[9] has shown how such for-

[9] S. Goudsmit, Phys. Rev. **37**, 663 (1931).

mulas may be obtained for configurations through application of the method of energy sums. Breit and Wills[10] in extending the theory have shown that the electron "coupling constants" used by Goudsmit are in general not constant for all states of a configuration but depend upon the inner quantum numbers of the states. They derived improved interval factor formulas for a few two- and three-electron configurations and Crawford[11] and Crawford and Wills[12] have applied the same method to the derivation of formulas for the d^2s and p^3s configurations. Computations by the method of Breit and Wills have so far not proved feasible for the important configurations of Mn I, namely d^6s, $d^5s\,p$, $d^5s\cdot s$ and d^6p. We then have no choice but to rely upon the admittedly approximate method of Goudsmit. There is some justification for confidence in this method as applied to Mn I in view of the fact that the hyperfine structure may largely be attributed to the 4s electron and that Mn I is a celebrated example of Russell-Saunders coupling.

The method of energy sums depends upon the assumption that an externally applied magnetic field may remove some couplings completely and leave others entirely undisturbed. Thus explicit expressions may be written for the various interactions in each stage of decoupling. It is assumed that the interactions between the individual electrons and the nucleus may be expressed by coupling factors associated with individual electrons. These factors are assumed to be constant within a given configuration but may vary from configuration to configuration. Without giving in detail the rather laborious algebraic steps leading to the interval factor formulas we will mention briefly the stages of decoupling which it has been necessary to consider in order to obtain each set of formulas appearing in Table V.

$3d^6(^5D)4s\ ^6D$. Here it is necessary to consider two stages of decoupling. The first is that in which merely the coupling between the nuclear magnetism and the total electron configuration is broken, the configuration itself being coupled as before. The second stage assumed is that in which the 4s electron is broken away from the configuration leaving the strongly coupled $3d^6(^5D)$ group acting as an entity having the quantum numbers characteristic of a ^5D state.

$3d^5(^6S)4s\ 4p\ ^8P^0$. Here also two stages must be considered, i.e., (1) the nuclear spin decoupled from the configuration which retains the properties of an ^8P, and (2) both the 4s and 4p electrons decoupled from the $3d^5(^6S)$ group which retains the properties of a ^6S.

$3d^5(^6S)4s\ 4p\ ^6P^0(\alpha)$ and $^6P^0(\beta)$. Two $^6P^0$ states arise in this configuration. The symbols α and β will be used to designate the ^6P states of lower and of higher absolute energy respectively. One,

TABLE V. *Interval factor formulas derived by method of energy sums.*

$d^5(^5D)s\ ^6D$

$$A(\tfrac{1}{2}) = (7/15)a(s) - (4/3)a(d^5) - (4/3)b(d^5)$$
$$A(1\tfrac{1}{2}) = (13/75)a(s) + (2/15)a(d^5) + (74/105)b(d^5)$$
$$A(2\tfrac{1}{2}) = (23/175)a(s) + (12/35)a(d^5) + (164/245)b(d^5)$$
$$A(3\tfrac{1}{2}) = (37/315)a(s) + (26/63)a(d^5) + (122/441)b(d^5)$$
$$A(4\tfrac{1}{2}) = (1/9)a(s) + (4/9)a(d^5) - (20/63)b(d^5)$$
$$\Sigma A = a(s)$$

$d^5(^6S)sp\ ^8P^0$

$$A(2\tfrac{1}{2}) = (9/49)a(s) - (88/245)a(p)$$
$$A(3\tfrac{1}{2}) = (59/441)a(s) + (80/441)a(p)$$
$$A(4\tfrac{1}{2}) = (1/9)a(s) + (8/45)a(p)$$
$$\Sigma A = (3/7)a(s)$$

$d^5(^6S)sp\ ^4P^0$

$$A(\tfrac{1}{2}) = -\tfrac{1}{3}a(s) - (8/15)a(p)$$
$$A(1\tfrac{1}{2}) = -(11/75)a(s) + (32/375)a(p)$$
$$A(2\tfrac{1}{2}) = -(3/25)a(s) + (56/125)a(p)$$
$$\Sigma A = -\tfrac{1}{3}a(s)$$

$d^5(^6S)sp\ \alpha\ ^6P^0$ and $\beta\ ^6P^0$

$$\alpha A(1\tfrac{1}{2}) + \beta A(1\tfrac{1}{2}) = (2/25)a(s) - (104/125)a(p)$$
$$\alpha A(2\tfrac{1}{2}) + \beta A(2\tfrac{1}{2}) = (62/1225)a(s) + (1696/6125)a(p)$$
$$\alpha A(3\tfrac{1}{2}) + \beta A(3\tfrac{1}{2}) = (2/49)a(s) + (136/245)a(p)$$
$$\Sigma(\alpha A + \beta A) = (6/35)a(s)$$

$\alpha\ ^6P^0$

$$A(1\tfrac{1}{2}) = (4/15)a(s) - (8/25)a(p)$$
$$A(2\tfrac{1}{2}) = (124/735)a(s) - (8/1225)a(p)$$
$$A(3\tfrac{1}{2}) = (20/147)a(s) + (16/49)a(p)$$
$$\Sigma A = (4/7)a(s)$$

$\beta\ ^6P^0$

$$A(1\tfrac{1}{2}) = -(14/75)a(s) - (44/75)a(p)$$
$$A(2\tfrac{1}{2}) = -(62/525)a(s) + (248/875)a(p)$$
$$A(3\tfrac{1}{2}) = -(2/21)a(s) + (8/35)a(p)$$
$$\Sigma A = -\tfrac{2}{3}a(s)$$

$d^5(^5D)p\ ^6D^0$

$$A(\tfrac{1}{2}) = -(8/225)a(p) - (10/9)a(d^5) - (8/15)b(d^5)$$
$$A(1\tfrac{1}{2}) = -(86/1125)a(p) + (1/9)a(d^5) + (148/525)b(d^5)$$
$$A(2\tfrac{1}{2}) = -(32/875)a(p) + (2/7)a(d^5) + (327/1225)b(d^5)$$
$$A(3\tfrac{1}{2}) = (142/4725)a(p) + (65/189)a(d^5) + (244/2205)b(d^5)$$
$$A(4\tfrac{1}{2}) = (16/135)a(p) + (10/27)a(d^5) - (8/63)b(d^5)$$
$$\Sigma A = 0$$

[10] G. Breit and L. A. Wills, Phys. Rev. **44**, 470 (1933).
[11] M. F. Crawford, Phys. Rev. **47**, 768 (1935).
[12] M. F. Crawford and L. A. Wills, Phys. Rev. **48**, 69 (1935).

the lower in energy, may be described as $d^5(^6S)s$ $(^7S)p$ $^6P^0$, the other as $d^5(^6S)s$ $(^5S)p$ $^6P^0$. While these designations are useful as a means of distinguishing the states they cannot be regarded as an accurate statement of the manner in which the states are built up since each $^6P^0$ must be thought of as built in part upon the ^7S and in part upon the ^5S of the ion by addition of the p electron. If we are to obtain interval factor formulas for these states and avoid this ambiguity we may consider only the sums of the interval factors of states having the same J value in the two multiplets. These formulas for the sums of interval factors may be obtained by considering the same stages of decoupling as in treating the $^8P^0$.

In Mn I the two states $^6P^0(\alpha)$ and $^6P^0(\beta)$ are found to be some 11,000 cm^{-1} apart. This suggests that the designation mentioned above may be fairly accurate. Proceeding on this assumption we may obtain interval factor formulas for the two multiplets separately. For this purpose it is necessary to consider an intermediate stage in which the $4p$ electron is decoupled from the $3d^5$ $4s$ (^7S) or (^5S) group as the case may be. While this is admittedly a questionable procedure it leads to relations which seem to have some significance when compared with the experimental data. A variation calculation too involved for inclusion here indicates that values for the coupling factors obtained by introduction of the experimental interval factors into formulas for α^6P^0 and β^6P^0 will represent lower and upper limits, respectively, for the "correct" value.

$4d^5(^6S)4s$ $4p$ $^4P^0$. The same considerations as applied to the $^8P^0$ of this configuration lead to the formulas.

$3d^6(^5D)4p$ $^6D^0$. Since several states arise from this configuration the formulas can be obtained only by making a further assumption not used in deriving the other formulas, i.e., that the sums of energies of all states characterized by the same values of M_L and M_S are independent of the degree of decoupling.

In the formulas of Table V the interval factors of the hypermultiplets are designated by A followed by the inner quantum number of the particular state in parentheses. Each electron coupling factor is designated by a followed by parentheses indicating the particular electron or electron group to which it refers. The interaction of the d^6 group is expressed by two factors, one relating to the spin and the other to the orbital interaction. The orbital factor is represented by $a(d^6)$ and the spin factor by $b(d^6)$ in the formulas.

Introducing the experimental interval factors into these formulas we obtain numerical values for the coupling factors. In most cases more relations exist than there are constants to be determined so that consistency provides a test of the accuracy of the formulas. A convenient means of determining the coupling constant for the s electron is provided by the common property of all formulas of Table V, that the sum of the interval factors of all states within a given multiplet depends only upon the contributions of unpaired s electrons. The values given below are those found to give best consistency within a given set of formulas. These results are graded A, B and C in accord with their relative reliability. The coupling constants determined for the different states are as follows:

$3d^6$ $4s$ ^6D

$a(4s)=0.0863$ cm^{-1}
$a(3d^6)=0.0094$ "
$b(3d^6)<0.0001$ "
} A

$3d^5$ $4s$ $4p$ $^8P^0$

$a(4s)=0.143$ cm^{-1}, A
$a(4p)=0.009$ " , B

$3d^5$ $4s$ $4p$ $^4P^0$

$a(4s)=0.162$ cm^{-1}, A
$a(4p)=0.006$ " , C

$3d^5$ $4s$ $4p$ α $^6P^0$

$a(4s)=0.095$ cm^{-1}, B
$a(4p)$, small, values inconsistent.

β $^6P^0$

$a(4s)=0.175$ cm^{-1}, B
$a(4p)$, small, values inconsistent.

As an example of the relative consistency within a set of formulas we may consider the $3d^6$ $4s$ ^6D terms, for which the experimental interval factors are rather accurately known. Substituting the values, $a(s)=0.0863$ cm^{-1}, $a(d^6)=0.0094$ cm^{-1}, $b(d^6)=0$, into the five formulas, we obtain for the interval factors $A(\frac{1}{2})$ to $A(4\frac{1}{2})$, respectively, 0.0278, 0.0162, 0.0145, 0.0140 and 0.0138 cm^{-1}. These are to be compared with the experimental values of Table IV.

The only coupling factor that adapts itself to a calculation of the nuclear magnetic moment is that of the $4s$ electron. In addition to the fact that our formulas are probably less reliable in reference to a p electron, the smallness of the indicated values for $a(4p)$ makes them extremely sensitive to errors in measurement. The value of $a(4s)$ obtained from the $3d^6\ 4s\ {}^6D$ state is probably the most reliable. The values for the same factor determined from the $3d^5\ 4s\ 4p\ {}^8P^0$ and ${}^4P^0$ are considerably larger and in only moderate agreement with one another. That they should be larger is expected, since the screening of a $4p$ electron must be rather less than that of a $3d$ electron. The interval factor formulas for the two ${}^6P^0$ states are the least satisfactory when applied to the observed interval factors. However, if the values of $a(4s)$ obtained from these two multiplets are regarded merely as an upper and a lower limit for the correct value as mentioned above, then these values are in accord with those obtained from the ${}^8P^0$ and ${}^4P^0$ of the same configuration. The observed interval factors from the $3d^5\ 4s\ 5s\ {}^8S$ and ${}^4S$ terms are not useful because formulas derived by the method of energy sums do not distinguish between the contributions of the two s electrons.

Goudsmit's relation[13] expressing the nuclear g factor in terms of the coupling between an s electron and the nucleus may be written in the form,

$$g(I)=\tfrac{3}{8}a(s)\frac{R^{\frac{1}{2}}Z_0 1838}{\alpha^2 Z_i W^{\frac{1}{2}} K(\frac{1}{2}, Z_i)}.$$

Here W represents the energy in cm^{-1} necessary to remove the s electron from the atom in that stage of ionization in which it is the only outer electron. The other symbols have their conventional meanings. The computation must be made for each configuration since $a(s)$, Z_0 and W are different for different configurations.

Considering the state $3d^6\ 4s\ {}^6D$ we have, $a(4s)=0.0863\ \text{cm}^{-1}$, $W=53{,}500\ \text{cm}^{-1}$, $Z_0=1$, $Z_i=25$, $K=1.06$. W is the approximate energy necessary to remove the $4s$ electron from an atom in the above state leaving the ion in the state $3d^6\ {}^5D$, the centers of gravity of both states being taken into account.[7] Putting these numerical values into the formula we obtain

$$g(I)=1.13.$$

Considering the configuration $3d^5\ 4s\ 4p$ we have two indicated values of $a(4s)$, i.e., 0.143 and $0.162\ \text{cm}^{-1}$. Since the larger one is to be favored in such cases[13] we suppose that the value of $0.160\ \text{cm}^{-1}$ is satisfactory for use in computation. Here W is the energy needed to remove the $4s$ electron from the configuration $3d^5\ 4s$ of Mn II leaving the configuration $3d^5$ of Mn III. If centers of gravity are taken into account, $W=123{,}000\ \text{cm}^{-1}$, approximately. Also $Z_0=2$. We now obtain from the formula,

$$g(I)=1.20.$$

In view of the comparative agreement between these two independent calculations we believe that the value 1.2 may be assigned as the nuclear g factor of Mn^{55} until more precise means for its determination are available. Multiplying by the value of I, we obtain a nuclear magnetic moment of 3.0 nuclear magnetons.

[13] S. Goudsmit, Phys. Rev. **43**, 636 (1933).

On the Absence of Polarization in Electron Scattering

M. E. Rose and H. A. Bethe
Cornell University, Ithaca, New York

(Received December 16, 1938)

In an attempt to explain the discrepancy between Mott's theory and the observational results on the polarization of electrons in the double scattering experiment, we have investigated the depolarizing effect of (1) multiple elastic scattering, (2) inelastic scattering with spin change of the incident electron and (3) exchange scattering in which the exchanged electrons have opposite spins. Although multiple scattering actually takes place in the Au foils used in the experiments, the depolarization caused by such scattering is negligible. For a screened Coulomb field and electrons of 100 kv the depolarization in a 2.5×10^{-5} cm Au foil is only 2.2 percent whereas a 90–100 percent depolarization is needed to reconcile theory and experiment. The depolarization caused by inelastic scattering is about 100 times smaller than that caused by elastic scattering. The small depolarization in these two cases is due to the fact that while there are many elastic and inelastic collisions, most of these collisions take place with small scattering angle ϑ and for small angles the depolarization per collision is small (of order ϑ^2). The main contribution to the depolarization by inelastic collisions comes then from large scattering angles at which inelastic scattering is relatively infrequent. The exchange scattering contributes practically no depolarization ($\sim10^{-12}$). While the depolarization per collision in each exchange process is relatively complete, the number of exchange processes is extremely small due to interference ($\sim10^{-14}$ times the number of elastic collisions). Therefore the absence of polarization in electron scattering cannot be explained on the basis of the processes considered here.

A discussion of the validity of the first Born approximation is given (Appendix §2). It is shown that in the case that the Born expansion parameter $e^2Z/\hbar v$ is of order unity, the first Born approximation gives a result for the scattered intensity which is accurate to within 20 percent or better. The depolarization is given with an accuracy of 18 percent or better.

I. Introduction

ONE of the important consequences of the Dirac theory of the electron is the prediction that an initially unpolarized beam of electrons will become partially polarized as the result of an elastic scattering process. If this partially polarized beam of electrons is made to undergo a second scattering, the intensity of the twice scattered beam, according to the theory, should be asymmetrical in the azimuth about the direction of incidence on the second target. In fact, the calculated scattering consists of two parts: The first, independent of the azimuth, is the product of the relativistic Rutherford intensities corresponding to the scattering angles at the two targets. The second part arises from spin-orbit interaction in the scattering field; it depends on the orientation of the magnetic moment with respect to the second scattering plane, that is, it is azimuth dependent. Obviously this term yields a nonvanishing contribution to the scattering only after the spin axes have been given a preferential direction.

The quantitative theory of the polarization of electrons by double scattering has been given by Mott.[1] According to his exact treatment of the scattering in a Coulomb field the expected azimuthal asymmetry is large enough to be observed experimentally if the following conditions are fulfilled: (1) only single scattering should take place in the two targets,[2] (2) the atomic number of the scattering atoms of both targets should be large ($Z/137$ comparable with unity), (3) both scattering angles should be large (of order $\pi/2$), and (4) the energy of the incident electrons should not be too small.[3]

The intensity of the doubly scattered beam is proportional to J where

$$J=1+\delta(\vartheta_1,\vartheta_2)\cos\varphi. \tag{1}$$

Here ϑ_1 and ϑ_2 are the two scattering angles, φ is the azimuthal angle and δ is a function of the two scattering angles which has been calculated by Mott. The asymmetry, that is, the quantity given in the experiments is

$$2\delta=(J_0-J_\pi)/J_{av}, \tag{2}$$

[1] N. F. Mott, Proc. Roy. Soc. **135**, 429 (1932).
[2] As will be seen in the following, this condition is perhaps too stringent.
[3] For Au the theoretical asymmetry is negligible below 30 kv, attains a (rather flat) maximum at 130 kv and then very slowly approaches zero for infinite energy.

where the subscripts refer to the azimuthal angle. For $\vartheta_1=\vartheta_2=\pi/2$, the scattering in Au of electrons of 90 to 160 kv should be characterized by an asymmetry of 12 to 16 percent.

Very careful experiments for the purpose of observing the asymmetry have been carried out by Dymond.[4] With electrons of 90, 125 and 160 kv energy scattered through angles $\pi/2$ at two Au foil targets the asymmetry observed was of the same magnitude as the experimental error of one percent. That is, *if there is any asymmetry at all*, it is small enough to be completely masked by the one percent experimental error due to the small deviations from ideal geometry, etc.

In the attempt to reconcile the theoretical results of Mott and Dymond's experiments we may first inquire whether all the conditions mentioned above were fulfilled. The only condition the fulfillment of which may be open to question is that of single scattering. It can be shown (Appendix §3) that an appreciable amount of multiple scattering (about 50 collisions) takes place even in the thin foils used by Dymond (2.5×10^{-5} to 5×10^{-6} cm thickness). It is evident that multiple scattering will result in some depolarization of the beam but just how much remains to be seen.

In addition to multiple scattering we have investigated the depolarizing effect of other processes. These are: (1) inelastic scattering with change of spin of the incident electron and (2) exchange scattering in which the exchanged electrons are of opposite spin.

The result of these considerations may be stated very briefly. Unfortunately, none of the effects considered produces any appreciable depolarization of the electrons and the discrepancy between theory and experiment remains—perhaps more glaring than before.

II. The Theory of Polarization

Before discussing the depolarizing effect of multiple scattering it will be most convenient to recapitulate some of the general theory of double scattering.[1] We consider an electron with wave number k incident along the z axis and scattered elastically in the direction ϑ, φ by some field of force. The wave function describing the electron is asymptotically

$$\psi_\nu\sim s_\nu e^{ikz}+u_\nu(\vartheta,\varphi)e^{ikr}/r, \quad \nu=1\cdots4, \tag{3}$$

where s_ν are the components of the amplitude of the Dirac plane wave. In particular we have

$$s_3=A, \quad s_4=B, \tag{4}$$

where A and B are constants related to the direction of the spin axis (χ_0, ω_0) in the incident beam.

$$-B/A=\cot(\chi_0/2)e^{i\omega_0}. \tag{5}$$

We may further impose the normalizing condition

$$|A|^2+|B|^2=1. \tag{6}$$

The differential cross section for scattering into the solid angle $d\Omega$ is then given by

$$\Phi_0 d\Omega=(|u_3|^2+|u_4|^2)d\Omega. \tag{7}$$

The general solution of the scattering problem may be obtained by a superposition of the two waves corresponding to $A=1$, $B=0$ and $A=0$, $B=1$. Mott has shown that in these two cases the asymptotic forms of the wave functions ψ_3 and ψ_4 are given by:

$A=1$, $B=0$:

$$\begin{aligned}\psi_3&\sim e^{ikz}+f(\vartheta)e^{ikr}/r\\ \psi_4&\sim g(\vartheta)e^{i\varphi}e^{ikr}/r,\end{aligned} \tag{8a}$$

$A=0$, $B=1$:

$$\begin{aligned}\psi_3&\sim -g(\vartheta)e^{-i\varphi}e^{ikr}/r\\ \psi_4&\sim e^{ikz}+f(\vartheta)e^{ikr}/r,\end{aligned} \tag{8b}$$

where f and g are independent of φ and are the same functions in (8a) as in (8b). By superposition we find for the scattered beam

$$u_3=Af-Bge^{-i\varphi}, \quad u_4=Bf+Age^{i\varphi}. \tag{9}$$

For the scattered electron the direction of the spin axis χ, ω is given by (cf. Eq. (5))

$$-u_4/u_3=\cot(\chi/2)e^{i\omega}. \tag{10}$$

[4] E. G. Dymond, Proc. Roy. Soc. **136**, 638 (1932), **145**, 657 (1934). For further references and a critical survey of the experimental work see H. Richter, Ann. d. Physik **28**, 533 (1937).

The scattering of an initially unpolarized beam may be described by considering the beam to be composed of two equally intense completely polarized beams with opposing directions of polarization. This direction is arbitrary and it is convenient to choose it so that the *direction* of polarization in each beam is the same after one scattering as before. That is, from (5) and (10)

$$u_4/u_3=B/A. \tag{11}$$

From (9) we find

$$B/A=\pm ie^{i\varphi}. \tag{11a}$$

Choosing the scattering plane as the plane $\varphi=0$, we have

$$B/A=\pm i, \tag{11b}$$

which means that the direction of polarization is normal to the scattering plane. The two polarized beams may now be considered separately.

The amplitude of the once scattered beam is then

$$u_3/A=u_4/B=f\mp ig \tag{12}$$

and the intensities for the two scattered beams are given by

$$\Phi_\pm=|f|^2+|g|^2\mp i(f^*g-fg^*). \tag{12a}$$

Thus after one scattering the beam is polarized with a polarization given by

$$\delta^1=i(fg^*-f^*g)/(|f|^2+|g|^2). \tag{12b}$$

The existence of a polarization therefore depends not only on the existence of g but also on a difference in phase between f and g.

The scattered intensity averaged over the spin directions is from (12a)

$$\Phi_0(\vartheta)=|f|^2+|g|^2. \tag{12c}$$

Since the two beams are treated independently the intensity for the double scattering is obviously equal to (compare (1))

$$\Phi_0(\vartheta_1)\Phi_0(\vartheta_2)[1+(\delta(\vartheta_1)\delta(\vartheta_2))^1\cos\varphi]. \tag{12d}$$

III. Depolarization by Multiple Elastic Scattering

We consider that the scattering in each target consists of many small angle scatterings (multiple scattering) plus one large angle scattering so that the total deflection is $\pi/2$. The small angle scatterings taking place before the first large deflection do not polarize the initial beam and, of course, we are not interested in the depolarizing effect of the small angle scattering after the second large deflection. Therefore our problem is to determine the depolarization of the beam between the two large deflections after it has been polarized by the first of these large deflections.

We define the polarization p in terms of the probability amplitudes for the two spin directions:

$$p=|A|^2-|B|^2. \tag{13}$$

Then the change of polarization per collision is

$$\delta p=(|u_3|^2-|u_4|^2)/(|u_3|^2+|u_4|^2)-p. \tag{14}$$

From (13), (9), (7) and (12c) we find for the change in polarization averaged over the azimuth[5]

$$\delta p=-2p|g|^2/(|f|^2+|g|^2). \tag{15}$$

Multiplying by the number of collisions with scattering angle ϑ which take place in a distance x_1 in the first target and a distance x_2 in the second target, which from (12c) is $2\pi N(x_1+x_2)(|f|^2+|g|^2)\sin\vartheta d\vartheta$, we find for the net polarization

$$P(x_1, x_2)$$

$$=\exp\left[-4\pi N(x_1+x_2)\int_0^\pi |g|^2\sin\vartheta d\vartheta\right], \tag{16}$$

if the polarization is complete initially. Here N is the number of scattering atoms per unit volume. Averaging over the effective thickness of each target for 45° incidence (and emergence) we have

$$P=\frac{1}{2d^2}\int_0^{\sqrt{2}d} dx_1\int_0^{\sqrt{2}d} dx_2 P(x_1, x_2), \tag{17}$$

where d is the actual thickness of the target. Thus we find for the degree of polarization

$$P=\left(\frac{1-e^{-\gamma d}}{\gamma d}\right)^2, \tag{18}$$

[5] There is no correlation between the direction of the spin axis and the azimuth of the scattering plane.

where

$$\gamma = 4\sqrt{2}\pi N \int_0^\pi |g|^2 \sin\vartheta d\vartheta. \quad (18a)$$

From the above treatment it is apparent that P represents the ratio of the polarization of the beam just before the second large deflection to that just after the first large deflection. Therefore the asymmetry is now given by

$$2\delta = P 2\delta_{\text{Mott}}. \quad (19)$$

In the following we shall refer to $1-P$ as the degree of depolarization.

Calculation of degree of depolarization

The calculation of g may be carried out by formulating the scattering problem in terms of the phases of the scattered (partial) waves at infinity. We denote the radial wave functions of the third and fourth components of the Dirac wave function by $G_\varkappa$. For the two types of solutions of the wave equation, that is, for the total angular momentum quantum number $j=l+\frac{1}{2}$ and $l-\frac{1}{2}$, $\varkappa$ is given by

$$\begin{aligned} \varkappa &= l \quad \text{for} \quad j=l+\tfrac{1}{2} \\ \varkappa &= -l-1 \quad \text{for} \quad j=l-\tfrac{1}{2}. \end{aligned} \quad (20)$$

At large distances r from the scattering atom $G_\varkappa$ has the asymptotic form

$$G_\varkappa \sim 1/r \cos(kr-(l+1/2)\pi+\eta_\varkappa). \quad (21)$$

Defined in this manner, the phase $\eta_\varkappa$ vanishes for the free particle.[6]

Mott[1] has shown that superpositions of the partial waves, $G_\varkappa$ multiplied by a suitable spherical harmonic, may be found which have the asymptotic form (8) with $g(\vartheta)$ given by

$$g(\vartheta) = i/2k \sum_0^\infty P_l^1(\cos\vartheta)[e^{2i\eta_l} - e^{2i\eta_{-l-1}}], \quad (22)$$

where

$$P_l^1(\cos\vartheta) = \sin\vartheta (d/d\cos\vartheta) P_l(\cos\vartheta) \quad (22a)$$

and P_l is the ordinary Legendre polynomial. With this expression for g the integral occurring in (18a) becomes

$$\int_0^\pi |g|^2 \sin\vartheta d\vartheta = 2/k^2 \sum_1^\infty (l(l+1)/(2l+1)) \sin^2 \delta\eta_l, \quad (23)$$

where

$$\delta\eta_l = \eta_l - \eta_{-l-1}. \quad (24)$$

To determine the phase difference $\delta\eta_l$ we consider the differential equation obtained for $G_\varkappa$ by eliminating the radial function of the first and second Dirac components from the well-known pair of simultaneous first-order equations.[7] The equation obtained may be written in the form

$$d^2G'/dr^2 + Q(r)G' = 0, \quad (25)$$

$$G = (2mc^2+E-V)^{-1}G'/r. \quad (25a)$$

E is the kinetic energy of the electrons and V is the scattering potential.

$$Q(r) = k^2 - \frac{\varkappa(\varkappa+1)}{r^2} - \frac{2V(E+mc^2)}{\hbar^2c^2} + \frac{\varkappa+1}{r}\frac{dV/dr}{2mc^2+E-V} + \frac{1}{4}\frac{(dV/dr)^2+2(2mc^2+E-V)d^2V/dr^2}{(2mc^2+E-V)^2}. \quad (26)$$

For the scattering potential V we must use a screened Coulomb field since at the small angles in which we are interested, the scattering by the atomic electrons is just as important as the nuclear scattering. We shall take

$$V = -(e^2Z/r)e^{-r/b}, \quad (27)$$

where b is the screening length (see Eq. (39) below).

We may solve (25) by the W. K. B. method. If r_1 is the (largest) root of $Q(r)$ we have for $r>r_1$,

$$G_\varkappa = \frac{\text{const.}}{rQ^{\frac{1}{4}}}(2mc^2+E-V)^{-\frac{1}{4}} \times \cos\left[\int_{r_1}^r Q^{\frac{1}{2}}dr - \pi/4\right]. \quad (28)$$

[6] For the free particle $G_\varkappa \sim r^{-1}J_{|\varkappa+\frac{1}{2}|}(kr)$, where J is the Bessel function

[7] Cf. e.g., H. A. Bethe, *Handbuch der Physik*, Vol. 24/1, p. 311.

In order to evaluate the integral in (28) we note first of all that the last two terms in (26) are small compared to the third term. As is evident from (26) the relative magnitude of the small terms will be largest for small r. In this case we have

$$dV/dr\sim V/r, \qquad d^2V/dr^2\sim 2V/r^2. \tag{29}$$

Then in the last term the important part is that involving d^2V/dr^2, *viz.*:

$$(dV/dr)^2/4mc^2d^2V/dr^2\sim V/8mc^2 \lesssim (Z/137)(k\hbar/mc)1/8l\ll 1, \tag{29a}$$

since for 100 kv $k\hbar/mc\sim 1$. In (29a) we have evaluated V at the minimum r, i.e., $r_1\sim l/k$. (See Eqs. (33a) and (34a) below.) The ratio of the fifth to the third term is

$$\tfrac{1}{4}(\hbar/mcr)^2\lesssim \tfrac{1}{4}(k\hbar/mc)^2 1/l^2<1/l^2. \tag{29b}$$

Similarly, the ratio of the fourth term to the third is less than $1/l$ which is also small compared to one.

The third term is therefore the leading term of those involving the potential V. This term will be comparable with the free particle terms $\sim k^2$ only for the smallest values of l, *viz.*:

$$\frac{\text{third term}}{\text{first term}}\lesssim\frac{2Ze^2}{r_1}\frac{m}{\hbar^2k^2}e^{-l/kb}\sim\frac{2}{l}\left(\frac{E_K}{E}\right)^{\frac{1}{2}}e^{-l/kb}, \tag{29c}$$

where E_K is the ionization potential for the K shell; $E_K\approx 40$ kv for Au.

We may now expand Q in powers of the small terms. We set

$$Q=q+q', \tag{30}$$

where

$$q=k^2-\varkappa(\varkappa+1)/r^2+2k_0e^{-r/b}/r, \tag{30a}$$

$$k_0=e^2Z(E+mc^2)/\hbar^2c^2. \tag{30b}$$

Then

$$\delta\eta_l=\int_{r_1}^{\infty}(Q_l^{\frac{1}{2}}-Q_{-l-1}^{\frac{1}{2}})dr \cong\tfrac{1}{2}\int_{r_1}^{\infty}q^{-\frac{1}{2}}(q'_l-q'_{-l-1})dr \tag{31}$$

$$=\frac{l+\frac{1}{2}}{E+2mc^2}\int_{r_1}^{\infty}q^{-\frac{1}{2}}(dV/dr)dr/r,$$

since q is the same for both values of $\varkappa$.

Denoting the integrand in (31) by I we use the identity

$$\int_{r_1}^{\infty}Idr=\int_{r_0}^{\infty}I_0dr+\left(\int_{r_1}^{\infty}Idr-\int_{r_0}^{\infty}I_0dr\right), \tag{31a}$$

where $I_0=I(k_0=0)$ and $r_0=r_1(k_0=0)$ is the root of q for $k_0=0$. We denote the contribution of the first integral to the phase difference by $\delta\eta_l^{(0)}$ and that of the last two integrals by $\delta\eta_l^{(1)}$; the latter will be important only for small l (cf. above). When the last two integrals are considered together, the difference between the integrands is appreciable only when the term $2k_0e^{-r/b}/r$ is important compared to the free particle terms in (30a). This is the case for $r\sim r_1\sim r_0$. Then, since we consider l small, in $I-I_0$ we may set the exponential $e^{-r/b}=1$ and neglect the term $1/b$ in dV/dr since these two neglections partially compensate each other and the error thus induced is $\sim(r_0/b)^2\sim(l/kb)^2$ $(l/20)^2$ for energies of the order 100 kv, (cf. (33a) below).

With

$$\delta\eta_l=\delta\eta_l^{(0)}+\delta\eta_l^{(1)}, \tag{32}$$

we have

$$\delta\eta_l^{(0)}=\frac{l+\frac{1}{2}}{E+2mc^2}\frac{e^2Z}{k}\int_{r_0}^{\infty}\frac{dr}{r}\left(\frac{1}{r}+\frac{1}{b}\right)\frac{e^{-r/b}}{(r^2-r_0^2)^{\frac{1}{2}}}. \tag{33}$$

In the following we shall replace $\varkappa(\varkappa+1)$ by $(l+\frac{1}{2})^2$ for both values of $\varkappa$, this procedure being appropriate for the W. K. B. solutions. Then

$$r_0=(l+\tfrac{1}{2})/k. \tag{33a}$$

The contribution to the phase difference $\delta\eta_l^{(1)}$ is given by

$$\delta\eta_l^{(1)}=\frac{l+\frac{1}{2}}{E+2mc^2}e^2Z\left[\int_{r_1}^{\infty}\frac{dr}{r^2}q^{-\frac{1}{2}}(k_0) -\int_{r_0}^{\infty}\frac{dr}{r^2}q^{-\frac{1}{2}}(k_0=0)\right]_{b=\infty}. \tag{34}$$

It may be noted that r_1 differs very little from r_0:

$$r_1\approx r_0(1-k_0/k^2r_0)\approx r_0[1-(Z/137l)k\hbar/mc]. \tag{34a}$$

The integration in (33) is carried out in the following manner. With the substitution $r=r_0\cosh x$ the integral in (33) becomes

$$\frac{1}{r_0^2}\int_0^{\infty}\operatorname{sech}^2 x(1+\lambda\cosh x)e^{-\lambda\cosh x}dx,$$

where $\lambda=r_0/b=(l+\frac{1}{2})/kb$. Integrating the first term by parts we find

$$\delta\eta_l^{(0)}=\frac{\lambda k}{l+\frac{1}{2}}\frac{e^2Z}{E+2mc^2}\int_0^{\infty}\cosh x e^{-\lambda\cosh x}dx. \tag{33b}$$

From Heine's integral representation of the Hankel function,[8] the integral in (33b) is equal to $-\pi/2H_1^{(1)}(i\lambda)$. Then we obtain

$$\delta\eta_l^{(0)}=-\frac{\pi}{2}\frac{e^2Z}{b}\frac{H_1^{(1)}(i\lambda)}{E+2mc^2}. \tag{35}$$

The integral (34) may be evaluated in terms of elementary functions. We find

$$\delta\eta_l^{(1)}=\frac{1}{(l+\frac{1}{2})^2}\left(\frac{e^2Z}{\hbar c}\right)^2\frac{E+mc^2}{E+2mc^2}\Theta \tag{36}$$

$$\tan\Theta=-(l+\tfrac{1}{2})k/k_0,\quad \pi/2<\Theta<\pi. \tag{36a}$$

From (35) and (36) we note that the phase difference $\delta\eta_l$ is small for all l. Since both $\delta\eta_l^{(0)}$ and $\delta\eta_l^{(1)}$ decrease monotonically with increasing l, the largest $\delta\eta_l$ will be $\delta\eta_1$. For energies of the order 100 kv and for any reasonable screening length b the argument of the Hankel function in (35) is small for small l.

$$\delta\eta_l^{(0)}=\frac{e^2Z}{\hbar c}\left(\frac{E}{E+2mc^2}\right)^{\frac{1}{2}}\frac{1}{l+\frac{1}{2}}. \quad \text{(small } l\text{)} \tag{37}$$

For $l=1$ and $E=100$ kv (37) and (36) give $\delta\eta_1^{(0)}=0.116$ and $\delta\eta_1^{(1)}=0.176$ so that $\delta\eta_1=0.29$. Therefore we may replace $\sin\delta\eta_l$ in (23) by $\delta\eta_l$ for all l. For very large l, $l\gg kb$ the phase difference behaves like $e^{-l/kb}$. For small l, $l\ll kb$ the summand in (23) is comparatively small because of the factor $l(l+1)/(2l+1)$. For the important values of l, $l\sim kb$ the summand varies very slowly and we may replace summation by integration.

For the quantity γ occurring in the polarization factor P (compare (18)) we find from (18a), (23), (35) and (36):

$$\gamma=4\sqrt{2}\pi N\left(\frac{e^2Z}{E+2mc^2}\right)^2 \times(\log 2kb-C-\tfrac{1}{2}+2\zeta S_1+\zeta^2S_2), \tag{38}$$

where C is Euler's constant $=0.577$ and

$$\zeta=\frac{e^2Z}{\hbar c}\frac{E+mc^2}{E^{\frac{1}{2}}(E+2mc^2)^{\frac{1}{2}}}, \tag{38a}$$

$$S_1=-\frac{\pi}{2}\sum_1^\infty\frac{\lambda H_1^{(1)}(i\lambda)}{(l+\frac{1}{2})^2}\Theta, \tag{38b}$$

$$S_2=\sum_1^\infty\Theta^2(l+\tfrac{1}{2})^{-3}. \tag{38c}$$

The sums S_1 and S_2 may be evaluated numerically. For b we use the Thomas-Fermi atomic radius

$$b=\hbar^2/me^2Z^{\frac{1}{3}}=1.23\times10^{-9}\text{ cm for Au.} \tag{39}$$

Then for $E=100$ kv we have $kb=21$, $\zeta=1.05$, $S_1=1.98$ and $S_2=1.76$. Then

$$\gamma=890\text{ cm}^{-1}. \tag{40}$$

For the thickest foil used by Dymond, $d=2.5\times10^{-5}$ cm and

$$\gamma d=2.2\times10^{-2}. \tag{41}$$

Since the main contribution to the sum S_1 (and to S_2 as well) arises from small[9] l where $H_1^{(1)}(i\lambda)\sim2/\pi\lambda$, it follows that S_1 and therefore γ is practically independent of the screening length b. In addition, for the energies of interest, γ is insensitive with energy and *in general γd will be of the order* 10^{-2}. For such small values of γd the degree of depolarization $1-P$ (Eq. (18)) is just γd. Hence multiple elastic scattering produces a negligible depolarization of the electron beam. To resolve the discrepancy between theory and experiment a degree of depolarization of about 95 percent or more is necessary, i.e., γd should be $\gtrsim4$. It is very unlikely that the approximations made in the above derivation can introduce an error of more than a factor two or three, certainly not a factor 100.

The explanation of the small depolarization we have found lies in the fact that while several small angle collisions occur the depolarization in each collision is too small to give an appreciable total depolarization. (Compare further Appendix §1).

IV. Inelastic Scattering

In this section we shall investigate the effect of inelastic scattering on the azimuthal asym-

[8] Jahnke-Emde, *Tables of Functions*, p. 218.

[9] In the sum S_1 the first term contributes about half and the first five terms about 90 percent of the total value of the sum. In S_2 the contribution of the first term is 75 percent and of the first five terms about 99 percent of the total value of the sum.

metry of the doubly scattered electron beam. Inelastic scattering may reduce the asymmetry in two ways: (1) a simple reduction of the energy before the large deflections take place and (2) depolarization caused by change of spin of the incident electron in the inelastic collision.

The first effect would reduce the asymmetry since the large deflections would then occur at lower energies at which the polarization is indeed smaller (cf. reference 3). However, the rate of energy loss[10] in Au is two Mev per g/cm² and with Dymond's foils the total energy loss is only one kv. Therefore this reduction in the asymmetry is entirely negligible.

We consider now the inelastic scattering in which the incident electron changes its spin. If we denote the differential cross section for this process by $\Phi_n' \sin\vartheta d\vartheta$, the depolarization per collision is $2\Phi_n'/\Phi_n$ where Φ_n is the total scattering cross section for excitation of the nth atomic state. In a manner similar to that used in the derivation of (18) we have for the degree of depolarization

$$1-P=1-\left(\frac{1-e^{-\gamma d}}{\gamma d}\right)^2, \tag{42}$$

where now

$$\gamma=4\sqrt{2}\pi N\sum_n\int_0^\pi \Phi_n'(\vartheta)\sin\vartheta d\vartheta. \tag{42a}$$

The summation in (42a) is to be taken over all excitations.

To calculate the differential cross section we may use the Born approximation. That this procedure will yield a sufficiently good result may be concluded from the fact that the values of the angular momentum of the incident electron for which the inelastic scattering is important are larger than the corresponding momenta for elastic scattering. Since larger angular momentum implies smaller phases of the scattered partial waves, it follows that the Born approximation is better for the inelastic scattering than for the elastic scattering—and for the latter the Born approximation is quite accurate even for the values of atomic number and energy with which we are concerned (see Appendix §2).

[10] See e.g., H. A. Bethe, reference 7, p. 522.

The differential cross section (per solid angle) in Born approximation is given by[11]

$$\Phi_n'=\frac{4e^4}{[(\mathbf{k}-\mathbf{k}')^2+(E-E'/\hbar c)^2]^2}\times\left(\frac{E+mc^2}{\hbar^2c^2}\right)^2|M_n|^2, \tag{43}$$

$$M_n=\int d\tau u_n^*\sum_j \exp(i\mathbf{q}\cdot\mathbf{r}_j)(a_0+\mathbf{a}\cdot\boldsymbol{\alpha}_j)u_m, \tag{43a}$$

$$a_0=s(\mathbf{k})s^*(\mathbf{k}'),\quad \mathbf{a}=-s^*(\mathbf{k}')\boldsymbol{\alpha}s(\mathbf{k}) \tag{43b}$$

and $$\mathbf{q}=\mathbf{k}-\mathbf{k}',\qquad q=2k\sin\vartheta/2. \tag{43c}$$

Here E, $\mathbf{k}$ and E', $\mathbf{k}'$ are the energies and wave vectors before and after the scattering; $s(\mathbf{k})$ and $s(\mathbf{k}')$ are the amplitudes of the Dirac plane waves for positive and negative spin, respectively; u_m and u_n are atomic wave functions for the initial and final state, respectively, the components being Schrödinger-like wave functions since very little energy is given to the atom; the Dirac operator $\boldsymbol{\alpha}_j$ acts on the spin coordinate of the jth electron. In (43) and (43c) we have used the fact that the energy loss is small: $k\approx k'$, $E\approx E'$.

In §4 of the appendix it will be shown that the second term of (44a) is much smaller than the first term over practically the entire range of integration over ϑ. Then the retardation term in the denominator of (43) may be neglected and the matrix element (43b) becomes

$$M_n=a_0F_n, \tag{44}$$

where F_n is the "generalized form factor"

$$F_n=\int d\tau u_n^*\sum_j \exp(i\mathbf{q}\cdot\mathbf{r}_j)u_m. \tag{44a}$$

With $$a_0=-\frac{1}{2}\frac{E}{E+mc^2}\sin\vartheta e^{i\varphi} \tag{45}$$

the differential cross section (43) becomes

$$\Phi_n'=\frac{1}{4}\left(\frac{e^2}{E+2mc^2}\right)^2\cot^2(\vartheta/2)|F_n|^2. \tag{46}$$

[11] H. A. Bethe, reference 7, p. 495.

Summing over all excitations we have, using the Hartree model[12]

$$\sum_{n\neq m}|F_n|^2=\sum_m(1-|F_m|^2), \tag{47}$$

where F_m is the atomic form factor for the mth electronic state

$$F_m=\int d\tau\exp(i\mathbf{q}\cdot\mathbf{r})|\psi_m(\mathbf{r})|^2, \tag{47a}$$

wherein ψ_m is the wave function of a single atomic electron in the mth state. The integration in (47a) is now to be taken over the coordinates of a single electron. The summation on the right-hand side of (47) is to be taken over all occupied states.

For large q the atomic form factor F_m is negligible due to interference. We may set

$$F_m=0 \quad \text{for} \quad q>1/b_m, \tag{48}$$

where b_m is the radius of the mth electron shell. For smaller q we may expand the exponential in (47a) and obtain

$$F_m=1-\tfrac{1}{2}q^2\int d\tau\, r_q^2|\psi_m|^2, \quad q<1/b_m \tag{48a}$$

where r_q is the component of $\mathbf{r}$ in the direction of $\mathbf{q}$. The term linear in r_q vanishes from symmetry. The matrix element of r_q^2 may be set equal to b_m^2. Thus we have

$$1-|F_m|^2=\begin{cases}q^2b_m^2 & q<1/b_m\\ 1 & q>1/b_m\end{cases}. \tag{49}$$

Actually $1-|F_m|^2$ is less than the smaller of the two values on the right-hand side of (49).

For the evaluation of the total cross section for excitation of the atomic electron in initial state m we have

$$\int_0^\pi\Phi_n'\sin\vartheta d\vartheta=\tfrac{1}{4}\left(\frac{e^2}{E+2mc^2}\right)^2\sum_m(I_0+I_1), \tag{50}$$

where

$$I_0=b_m^2\int_0^{\vartheta_m}\cot^2(\vartheta/2)q^2\sin\vartheta d\vartheta \tag{50a}$$

is the contribution to the scattering from small angles and

$$\sin\vartheta_m/2=1/(2kb_m). \tag{50b}$$

The contribution from the large angle scattering is

$$I_1=\int_{\vartheta_m}^\pi\cot^2\vartheta/2\sin\vartheta d\vartheta. \tag{50c}$$

Carrying out the integrations in (50a) and (50c) we find

$$I_0+I_1=4\log 2kb_m. \tag{50d}$$

In carrying out the summation over m occurring in (50) we obtain the geometric mean of the shell radii b_m which we may replace for order of magnitude purposes by b, the screening length introduced in Section III (cf. Eq. (39)). That is,

$$\sum_m(I_0+I_1)=4Z\log 2kb. \tag{50e}$$

For the quantity γ we obtain from (42a)

$$\gamma=4\sqrt{2}\pi NZ(e^2/E+2mc^2)^2\log 2kb. \tag{51}$$

For $E=100$ kv and the foil thickness $d=2.5\times10^{-5}$ cm we find

$$\gamma=5.0\text{ cm}^{-1}, \quad \gamma d=1.3\times10^{-4}. \tag{52}$$

We see then that the depolarization by inelastic collisions is negligible. We observe that the depolarization caused by inelastic scattering is smaller than that caused by elastic scattering by about a factor $1/Z$ (cf. Eqs. (38) and (51)). This can be understood from the fact that the small angle scattering gives a small contribution (cf. Eqs. (50a), (50c)) to the depolarization. At large scattering angles, it is well known that the total elastic scattering is about Z times larger than the inelastic, and the depolarization in *one* scattering process is the same for elastic and inelastic collisions at a given scattering angle, (see Appendix, Eqs. (107), (107a)).

V. Exchange Scattering

A change in the polarization of an electron beam can take place as a result of exchange scattering only if the exchanged electrons have opposite spins. Since the spin forces are weak for

[12] The transitions which are forbidden by the exclusion principle (state n initially occupied) have not been subtracted. Therefore the cross section is *overestimated*.

the atomic electrons the spin of each electron will not change in the capture and emission processes. This also has the important consequence, that such exchange processes as we are considering can take place only with atomic electrons in incomplete shells. Exchange between the incident electron and an atomic electron of opposite spin in a closed shell will result in two atomic electrons having the same set of quantum numbers and this is forbidden by the Pauli exclusion principle. Thus in Au only the 6*s* valence electron can participate in the type of exchange scattering which leads to depolarization.

In contrast to the case of depolarization by elastic and inelastic scattering, the depolarization *per collision* due to exchange scattering will not be small but the *net depolarization* will be extremely small because very few exchange collisions of the type considered will take place. This is due essentially to the strong interference between the wave functions for the valence state and the continuum.

To obtain a quantitative estimate of the importance of exchange scattering we make the following (necessarily) rough calculation of the exchange cross section. The differential cross section is given by[13]

$$\Phi_{ex}(\vartheta)\sin\vartheta d\vartheta=(8\pi^2a_0^2)^{-1}|M_{ex}|^2\sin\vartheta d\vartheta, \quad (53)$$

where $a_0=\hbar^2/me^2$ is the Bohr radius. A factor $\frac{1}{2}$ has been inserted in (53) because the spin of the incident electron must be opposed to that of the valence electron and this is true in half the cases.

The matrix element for exchange is essentially given by

$$M_{ex}=\int d\tau_r d\tau_Z\psi_Z^*(\mathbf{r})\chi_{\mathbf{k}'}^*(\mathbf{r}_Z)\times|\mathbf{r}-\mathbf{r}_Z|^{-1}\psi_Z(\mathbf{r}_Z)\chi_{\mathbf{k}}(\mathbf{r}), \quad (54)$$

where $\mathbf{r}$, $\mathbf{r}_Z$ denote the coordinates of the electrons initially in the continuum and valence state, respectively. ψ_Z is the wave function for a single electron in the valence state and moving in the field of the rest of the atom. $\chi_{\mathbf{k}}$ and $\chi_{\mathbf{k}'}$ are the wave functions of the incident and outgoing electrons, respectively. We take

$$\chi_{\mathbf{k}}(\mathbf{r})=\exp(i\mathbf{k}\cdot\mathbf{r}), \quad \chi_{\mathbf{k}'}(\mathbf{r}_Z)=\exp(i\mathbf{k}'\cdot\mathbf{r}_Z), \quad (55)$$

$\mathbf{k}$ and $\mathbf{k}'$ representing the initial and final wave vectors.

Because of the rapid oscillation of χ the contribution to the matrix element will be small in the region where ψ_Z is slowly varying, but will be appreciable near the nucleus where ψ_Z also varies rapidly. We therefore represent the valence state wave function by

$$\psi_Z(r)=\psi_Z(0)e^{-\beta r}, \quad \beta=Z/a_0. \quad (56)$$

With the wave functions (55) and (56) the matrix element (54) may be evaluated to give approximately

$$M_{ex}\approx\frac{32\pi^2}{k^2}|\psi_Z(0)|^2\frac{\beta}{(\beta^2+q^2)^2}, \quad (57)$$

where $\mathbf{q}=\mathbf{k}-\mathbf{k}'$ (cf. Eq. (43c)).

The value of the 6*s* wave function ψ_Z at the nucleus may be obtained from considerations of the type used in the theory of hyperfine structure.[14] For *s* electrons we find

$$\psi_Z^2(0)=\frac{Z_i(1+z)^3\kappa(\frac{1}{2},Z_i)}{\pi a_0^3n^{*3}}=\frac{\beta^3\kappa}{\pi Z^2n^{*3}}, \quad (58)$$

where z is the degree of ionization (here $=0$), Z_i the effective nuclear charge (here $=Z$), n^* is the effective quantum number and $\kappa(\frac{1}{2},Z)$ is a relativistic correction factor given in Eq. (246) of reference 14. For the 6*s* state of Au, $n^*=1.21$ and $\kappa=2.0$.

From (53), (57) and (58) we find for the differential cross section

$$\Phi_{ex}(\vartheta)=128\frac{\kappa^2}{Z^4n^{*6}}\left(\frac{R_y}{E}\right)^2\frac{a_0^2}{(1+\xi^2)^4}, \quad (59)$$

where $\xi=(2ka_0/Z)\sin\vartheta/2$ and $R_y=e^4m/2\hbar^2$ is the Rydberg energy.

From (59) we obtain for the total cross section

$$\Phi_{ex}^{tot}=\frac{32\pi}{3}\frac{\kappa^2}{n^{*6}}\left(\frac{R_y}{E}\right)^3\left(\frac{a_0}{Z}\right)^2\times[1-(1+4k^2/\beta^2)^{-2}]. \quad (60)$$

[13] See e.g., H. A. Bethe, Ann. d. Physik **5**, 325 (1929).

[14] See e.g., H. A. Bethe and R. F. Bacher, Rev. Mod. Phys. **8**, 82 (1936), Chapter VIII.

For energies of order 100 kv, $k/\beta \approx 1$ and the square bracket in (60) is practically equal to one.

For the degree of depolarization we have (compare (42a))

$$\gamma d = 2\sqrt{2} N d \Phi_{ex}^{tot} = \frac{64\sqrt{2}\pi}{3} \frac{\kappa^2}{n^{*6}} \left(\frac{R_y}{E}\right)^3 \left(\frac{a_0}{Z}\right)^2 Nd. \quad (61)$$

For $E=100$ kv, $d=2.5\times10^{-5}$ cm we find $\gamma d = 2\times10^{-12}$, an entirely negligible depolarization. This result is due to the rarity of exchange collisions. Since most of the collisions are elastic we see by comparison of (60) and the total cross section for elastic collisions (Appendix, Eq. (112)) that the fraction of collisions which are of the exchange type is

$$\frac{\Phi_{ex}^{tot}}{\Phi_{el}^{tot}} = \frac{8}{3} \frac{\kappa^2}{n^{*6}} \left(\frac{R_y}{E}\right)^3 \left(\frac{\hbar v}{e^2 Z}\right)^2 Z^{-4/3}. \quad (62)$$

Thus for $E=100$ kv only one in 4×10^{13} collisions is of the exchange type.

Appendix

§1. Depolarization per collision at small angles

In order to see that in each elastic collision only a small depolarization occurs, it is advantageous to consider the angular dependence of the depolarization. The depolarization in a deflection at angle ϑ was given in Eq. (15) as

$$-\delta p/p = 2|g|^2/(|f|^2+|g|^2). \quad (101)$$

The function g is given by (22). The Faxen-Holtzmark expression for f is

$$f(\vartheta) = i/2k \sum_0^\infty P_l(\cos\vartheta) \times [(l+1)(e^{2i\eta_l}-1)+l(e^{2i\eta_{-l-1}}-1)]. \quad (102)$$

From (21) and (28) the phase η_κ is given by

$$\eta_\kappa = \operatorname*{Lim}_{r\to\infty} \left(\int_{r_1}^{r} Q^{\frac{1}{2}} dr - \int_{r_0}^{r} Q_0^{\frac{1}{2}} dr \right), \quad (103)$$

where the subscript 0 refers to $Z=0$. We can expand the integrand in terms of the most important potential term and find for both values of κ (compare (30))[15]

$$\eta_\kappa = k_0 \int_{r_0}^{\infty} \frac{dr}{r} e^{-r/b} Q_0^{\frac{1}{2}} = \frac{e^2 Z}{\hbar v} \frac{\pi i}{2} H_0^{(1)}(i\lambda). \quad (103a)$$

For the sake of simplicity we first eliminate η_{-l-1}. We can see very easily that the phase difference $\eta_l - \eta_{-l-1} = \delta\eta_l$ is small compared to η_l for all l. The ratio $\delta\eta_l/\eta_l$ is largest for $l=1$. From (103a) and ((37) *et seq*) we find for the usual values of the constants, $\delta\eta_1/\eta_1 = 0.10$. Therefore in (102) and (22) we expand $e^{2i\delta\eta_l}$ and f and g become

$$f = (i/2k) \sum_0^\infty (2l+1) P_l(\cos\vartheta)(e^{2i\eta_l}-1), \quad (104)$$

$$g = -(1/k) \sum_0^\infty P_l^1(\cos\vartheta) \delta\eta_l e^{2i\eta_l}. \quad (104a)$$

Now since most of the collisions take place for small scattering angles we are interested in the values of f and g for ϑ small. Making the appropriate expansions we have from (22a)

$$f = (i/2k) \sum_0^\infty (2l+1)(e^{2i\eta_l}-1), \quad (105)$$

$$g = (\vartheta/2k) \sum_0^\infty l(l+1) \delta\eta_l e^{2i\eta_l}. \quad (105a)$$

Since η_l and $\delta\eta_l$ behave like $e^{-l/kb}$ for large l, the series (105a) converge and we find from (101) that at small scattering angles the depolarization per collision is small of order ϑ^2. This result is, therefore, true for any scattering field for which the scattered intensity is finite for small angles. For scattering in a pure Coulomb field, the series (105a) will, of course, diverge. In this case, for small ϑ,[16]

$$|f| = (2e^2 Z/\hbar v)(1/\vartheta^2 k), \quad (106)$$

$$|g| = (e^2 Z/\hbar v)(E/E+mc^2)(1/\vartheta k), \quad (106a)$$

[15] The error incurred by this expansion is small for the important values of $l(\sim kb)$. The error is greatest for $l=1$; with $E=100$ kv the phase η_l from (103a) is 2.62 whereas a numerical integration of (103) gives the exact value $\eta_l = 2.87$. The difference between the exact value of η_κ and the value given by (103a) decreases rapidly with increasing l.

[16] Reference 1, Eq. (6.8).

so that the depolarization per collision for small deflections is of order ϑ^2 for all scattering fields.

For the numerical value of the depolarization in one elastic collision we find for 100 kv (see Eqs. (109) and (109a) below)

$$2|g/f|^2=0.013\vartheta^2. \quad (107)$$

For inelastic collisions we have, of course, the same result. The depolarization per inelastic collision is from Section IV (cf. (45) and remarks preceding Eq. (42)),

$$2\Phi_n'/\Phi_n=2|a_0|^2=\tfrac{1}{2}(E/E+mc^2)^2\sin^2\vartheta \approx 0.013\vartheta^2. \quad (107a)$$

The small depolarization found in the foregoing may now be understood as follows. The depolarization depends on the product of the scattering cross section and the depolarization per scattering (101). The former is large only for small ϑ and just in this region the latter is small.

§2. Validity of the Born approximation

In the foregoing the statement has been made that the Born approximation is accurate for the elastic scattering even though the Born expansion parameter $e^2Z/\hbar v\approx 1$ for the energies and atomic number in which we are interested. We shall now show that this is so not only for the scattered intensity $|f|^2+|g|^2$ but also for the depolarization $\sim|g|^2$. For large scattering angles the Born approximation is known to give a result for the scattered intensity which is in agreement with the exact formula of Mott (nuclear scattering).

In the Born approximation the phases η_l and $\delta\eta_l$ are assumed small and for f and g we have from (105) and (105a)

$$f_B=-(2/k)\sum_0^\infty(l+\tfrac{1}{2})\eta_l, \quad (108)$$

$$g_B\cong(\vartheta/2k)\sum_0^\infty(l+\tfrac{1}{2})^2\delta\eta_l. \quad (108a)$$

Replacing sums by integrals and using (103a) and (35) we find[17]

$$f_B=-\pi ikb^2(e^2Z/\hbar v)\int_{1/kb}^\infty \lambda H_0^{(1)}(i\lambda)d\lambda = -\pi(e^2Z/\hbar v)bH_1^{(1)}(i/kb) \approx 2(e^2Z/\hbar v)kb^2, \quad (109)$$

since $kb\gg 1$;

$$g_B=-\frac{\pi}{4}kb^2\frac{e^2Z}{\hbar c}\left(\frac{E}{E+2mc^2}\right)^{\frac{1}{2}}\vartheta\int_{1/kb}^\infty\lambda^2H_1^{(1)}(i\lambda)d\lambda = -\frac{\pi i}{4}\frac{e^2Z}{\hbar c}\left(\frac{E}{E+2mc^2}\right)^{\frac{1}{2}}\frac{\vartheta}{k}H_2^{(1)}(i/kb) \approx(e^2Z/\hbar c)(E/E+2mc^2)^{\frac{1}{2}}kb^2\vartheta. \quad (109a)$$

Of course g_B and f_B depend on the screening length b, but their ratio is essentially independent of the screening and in agreement with (106) and (106a) as it should be, cf. Sauter.[18]

In order to test the Born approximation for our problem, the exact value of the sums occurring in (104a) were found numerically.[19] For $kb=100$ and $e^2Z/\hbar v=1$ corresponding to E about 100 kv we find

$$|f|=1.81\times10^4/k, \quad |g|=0.167\times10^4\vartheta/k. \quad (110)$$

The Born approximation yields

$$f_B=2.0\times10^4/k, \quad g_B=0.182\times10^4\vartheta/k. \quad (110a)$$

The use of the Born approximation therefore overestimates f by only ten percent and g by 9 percent. For the scattering the error is 21 percent and for the depolarization 18 percent. The screening radius b has been taken rather large in the above example. For smaller screening lengths the phases for a given l are smaller and the Born approximation better.

This result is perhaps not surprising insofar as it is well known that the condition for the validity of the Born approximation $e^2Z/\hbar v\ll 1$ is

[17] It is obviously consequent in the first Born approximation to use for the phase and phase difference the limiting forms for small scattering potential, hence $\delta\eta_l=\delta\eta_l^{(0)}$.

[18] F. Sauter, Ann. d. Physik **18**, 61 (1933).

[19] For the calculation of these sums the part $\delta\eta_l^{(1)}$ of the phase difference may be neglected since this part of $\delta\eta_l$ contributes to g the amount

$$g_1\sim\frac{1}{2}\left(\frac{e^2Z}{\hbar c}\right)^2\frac{E+mc^2}{E+2mc^2}\frac{\vartheta}{k}\sum_1^{kb}\Theta e^{2i\eta_l}.$$

The absolute value of the sum is of order or less than πkb and for the numerical case considered in (110) $g_1\lesssim 30\vartheta/k$ as compared to $g\sim 1700\vartheta/k$ from $\delta\eta_l^{(0)}$.

a sufficient but not a necessary condition. In the problem considered here it is possible to see qualitatively the reason for the fair agreement between (110) and (110a). In (104) and (104a) the main contribution to each of the sums arises from those values of l for which the phase η_l is $\pi/2$ or smaller and in this region the assumption of small phases is sufficiently well fulfilled.

It may be pointed out that the Born approximation is not accurate for the calculation of the polarization of the electrons, but only for the depolarization (or scattered intensity). The polarization as was mentioned in the foregoing, depends on the relative phase of f and g whereas the depolarization depends on the value of g itself. The relative phase of f and g is in fact zero in the first Born approximation[20] (in contrast to the value of g itself) and at least the second approximation is necessary for the calculation of the asymmetry.

§3. Total number of collisions

a. Elastic collisions.—The average number of elastic collisions taking place in a foil of thickness d is

$$n_e = 2\sqrt{2}\pi N d \int_0^\pi \Phi_{el}(\vartheta) \sin\vartheta d\vartheta, \qquad (111)$$

where a factor $\sqrt{2}$ has been inserted because of the obliquity of the path. With $\Phi \leqq |f|^2$ and f given by (104) we have in the Born approximation

$$\Phi_{el}{}^{tot} = 2\pi \int_0^\pi \Phi_{el}(\vartheta) \sin\vartheta d\vartheta = 4\pi(e^2Z/\hbar v)^2 b^2. \qquad (112)$$

With $d = 2.5\times10^{-5}$ cm and $b = \hbar^2/me^2Z^{\frac{1}{3}}$ we find that on the average 40 elastic collisions take place in each foil.

b. Inelastic collisions.—The total number of inelastic collisions in each foil is[13]

$$n_i = 2\sqrt{2}\pi N d \frac{e^4}{mv^2} \sum_n \frac{\nu_n}{A_n} \log\frac{2mv^2}{A_n}, \qquad (113)$$

where A_n is an energy of the order of magnitude of the ionization potential and ν_n the number of electrons in the nth shell. For Au we may take

$A_n =$ 6 volts for the $6s$ shell
$= 20$ " " " $5d$ "
$= 100$ " " " $5s$, $5p$ and $4f$ shells.

The contributions to the sum in (113) from the $6s$, $5d$ and the $5s$, $5p$ and $4f$ shells are 1.85, 4.95 and 1.7 reciprocal volts, respectively. The contribution from the remaining shells will be about 0.5. The total number of inelastic collisions is then $n_i \sim 16$. This number may be in error by a factor 3 or so in either direction but in any case it is indicative of the fact that several collisions can take place in the foils under consideration.

§4. Relative magnitude of transition "current" and "density" terms

In Section IV it was stated that the current term in (43a), *viz:*

$$\mathbf{a}\cdot\mathbf{J} = \mathbf{a}\cdot\int d\tau u_n^* \sum_j \exp(i\mathbf{q}\cdot\mathbf{r}_j)\boldsymbol{\alpha}_j u_m \qquad (114)$$

makes a contribution to the inelastic scattering which is much smaller than that due to the density term a_0F_n (cf. (44), (44a)). Since the relative magnitude of the current term is largest for small scattering angles we may expand the exponential and obtain

$$F_n = i\mathbf{q}\cdot\mathbf{r}_n, \qquad (115)$$

where

$$\mathbf{r}_n = \int \sum_j \mathbf{r}_j u_n^* u_m d\tau \qquad (115a)$$

is the dipole moment corresponding to the transition $u_m \to u_n$. For the current term we have, with $\boldsymbol{\alpha}_j = -\mathbf{t}_j/c$

$$\mathbf{J} = i(\Delta E/\hbar c)\mathbf{r}_n, \qquad (116)$$

where ΔE is the energy loss. Therefore the ratio of the current to density term is

$$\frac{\mathbf{a}\cdot\mathbf{J}}{a_0F_n} = \frac{\Delta E}{\hbar c a_0}\frac{\mathbf{a}\cdot\mathbf{r}_n}{\mathbf{q}\cdot\mathbf{r}_n} = \frac{\Delta E}{\hbar c a_0}\frac{|\mathbf{a}|}{q}, \qquad (117)$$

[20] N. F. Mott, Proc. Roy. Soc. **124**, 425 (1929). Also F. Sauter, reference 18.

since the direction of $\mathbf{r}_n$ is not significant. From (43b) we find

$$|\mathbf{a}| = \hbar c[q^2-(\Delta E/\hbar c)^2]^{\frac{1}{2}}/2(E+mc^2). \quad (118)$$

With a_0 given by (45) we find

$$\frac{\mathbf{a}\cdot\mathbf{J}}{a_0F_n} < \rho = \frac{\Delta E}{E\sin\vartheta}. \quad (117a)$$

The right-hand side of (117a) is appreciable only for

$$\vartheta \lesssim \Delta E/E \sim \vartheta_m^2, \quad (118)$$

where ϑ_m is the angle introduced in (50b). In the average $\vartheta_m \sim 1/kb$ so that $\rho \sim 1$ for

$$\vartheta \sim 1/400 = 0.14°.$$

For scattering angles $\vartheta > \vartheta_m^2$, $\mathbf{a}\cdot\mathbf{J} \ll a_0F_n$. Therefore over practically the entire range of integration over ϑ the current term need not be considered at all.

FEBRUARY 1, 1939 PHYSICAL REVIEW VOLUME 55

The Interaction Between Rotation and Oscillation in Deutero-Formaldehyde

HARALD H. NIELSEN
Mendenhall Laboratory of Physics, Ohio State University, Columbus, Ohio

(Received December 17, 1938)

The unsymmetrical broadening of the Q branch toward higher frequencies in the parallel type bands near 1100 cm^{-1} in the absorption spectrum of deutero-formaldehyde is taken as a manifestation of convergence toward lower frequencies rather than, as is usual, in the case of infra-red bands, toward higher frequencies. This phenomenon is accounted for by taking into account an interaction between rotation and oscillation of the Coriolis type arising from the accidental degeneracy of the three vibration frequencies, belonging to three different symmetry classes, falling near 900 cm^{-1}, 1000 cm^{-1} and 1100 cm^{-1}.

I. INTRODUCTION

THE absorption spectrum near 10μ in the deutero-formaldehyde spectrum consists of three bands which badly overlap. Two of these are characteristic of oscillations of the electric moment normal to the axis of symmetry of the molecule, while the third is characteristic of a vibration parallel to the axis of symmetry. The first two of these consist essentially of a group of prominent lines protruding above a background which at present cannot be resolved spectroscopically, and the third contains P, Q and R branches. It has already been pointed out elsewhere[1] that the spacings between the prominent lines in the perpendicular bands in this region are noticeably greater than the spacings between the lines in a similar band near 4.6μ and it has been suggested that the explanation for this is undoubtedly the same as that for the similar effect observed in two overlapping perpendicular bands in the spectrum of ordinary formaldehyde near 8.0μ.[2] The effect is here quite satisfactorily explained by taking account in the energy of a Coriolis interaction between the two frequencies. In the third of the above bands referred to in the spectrum of deutero-formaldehyde the convergence is in the direction of lower frequencies

[1] E. S. Ebers and H. H. Nielsen, J. Chem. Phys. **6**, 311 (1938).

[2] H. H. Nielsen, J. Chem. Phys. **5**, 818 (1937). The type of interaction between rotation and oscillation discussed recently by W. H. J. Childs and H. A. Jahn (Nature **141**, 916 (1938)) in connection with the methane spectrum is entirely similar to the one discussed in this work relative to H_2CO. The formaldehyde case is especially interesting in that both perturbing frequencies are optically active so that the convergence in opposite directions in the two bands, described by C. and J., can here actually be observed. In the case of the methane molecule the perturbing frequencies are two- and three-fold degenerate, respectively, while in this case they are nondegenerate. The importance of such terms in the interpretation of spectra was already emphasized by E. B. Wilson, Jr., in one of his early papers on this subject.

rather than in the direction of higher frequencies as is usually the case for bands in the infra-red. Although the P and R branches are too incompletely resolved to satisfactorily study the convergence it may be established that this is true by observing that the Q branch is unsymmetrically broadened toward higher frequencies. For this to be so, what corresponds to the classical moment of inertia of the molecule must be smaller in the upper state than it is in the ground state. An explanation suggests itself when one reviews the case of ordinary formaldehyde. Here, due to Coriolis forces, the two nearly coincident frequencies which, however, belong to different symmetry classes, suffer perturbations to their accompanying rotational levels in such a manner that the band of lesser frequency is strongly convergent toward higher frequencies while the other band is strongly convergent toward lower frequencies. In this case we have, not two, but three different oscillations of nearly coincident frequencies, and belonging, here also, to *three* different symmetry classes. We shall investigate in this note what the nature of the interactions may be here between rotation and oscillation to see whether or not they may give rise to effects in the spectrum such that the Q branch of the parallel type band will be unsymmetrically broadened toward higher frequencies and at the same time the type of convergence retained which is characteristic of the overlapping perpendicular type bands in the spectrum of ordinary formaldehyde.

II. Solution to the Quantum Mechanical Problem

The three oscillations which give rise to the three bands in question are the following ones given in the order of ascending frequencies: the deformation frequency of the molecule in and out of its own plane; the frequency caused by the deformation in the plane of the molecule of the O−C−D bond angle and the frequency caused by the deformation in the plane of the molecule of the CD_2 bond angle. The first two of these will give rise to changes in the electric moment perpendicular to the axis of symmetry, while the third will produce an alteration of the electric moment parallel to this axis. As a simplified

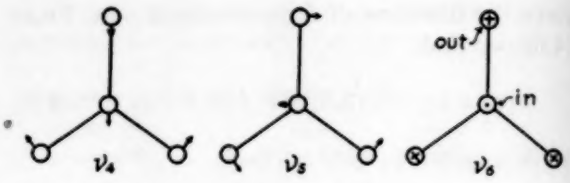

FIG. 1. The three modes of oscillation which the molecular model may execute.

model of the molecule which will approximate to the actual case when it is oscillating in these three modes we shall adopt one where the C and O atoms and the C and D atoms, respectively, are rigidly joined together, an assumption which is justified when further we adopt force fields of the valence force type, bearing in mind that the frequencies in which we are interested are all deformation frequencies where no changes in the interatomic distances take place. This simplification is in reality tantamount to suppressing the other three modes of oscillation of the molecule. The xz plane has been taken as the plane of the molecule, the z axis having been made to lie along the axis of symmetry and the origin of the system to coincide with the center of gravity of the molecule. In this system the coordinates of the C, O and D particles when they are at rest, will be respectively, $(0, 0, z_3^0)$, $(0, 0, z_4^0)$, and $(x_1^0, 0, z_1^0)$ and $(x_2^0, 0, z_2^0)$ where $x_1^0 = -x_2^0$ and $z_1^0 = z_2^0$. The three modes of oscillation which this model may execute are described in Fig. 1 and are respectively identified with the frequencies of the molecule, ν_4, ν_5 and ν_6 where $\nu_4 > \nu_5 > \nu_6$.

The quantum mechanical equation for this molecular model, oscillating harmonically in these three modes and rotating, has been developed with the neglect, however, of all terms in the moments of inertia which arise from deformation of the molecule. This can be justified on the basis that these will almost certainly contribute amounts to the energy small in comparison with the interaction terms in which we are interested, namely those arising from the Coriolis forces. The derivation of the quantum mechanical equation will be omitted here since the method is a perfectly straightforward one. The equation which is obtained may be divided into zeroth and higher order terms of which only the two first sets will here be set down:

$$(H_0-E_0)\psi_0=(h\nu/2)\{2E_0/h\nu+(\nu_5/\nu)(\partial^2/\partial\eta^2-\eta^2)$$
$$+(\nu_4/\nu)(\partial^2/\partial\zeta^2-\zeta^2)+(\nu_6/\nu)(\partial^2/\partial\xi^2-\xi^2)$$
$$+u^2(2\pi/h)^2[(P_x^2+P_y^2)+(2\pi/h)^2(A_0/C_0)P_z^2]$$
$$-2\lambda_3u^2(A_0/C_0)[(\nu_6/\nu_5)^{\frac{1}{2}}\eta\partial/\partial\xi$$
$$-(\nu_5/\nu_6)^{\frac{1}{2}}\xi\partial/\partial\eta](2\pi i/h)P_z\}\psi_0=0, \quad (1a)$$

$$H_1=-u^2h\nu\{\lambda_1[(\nu_4/\nu_6)^{\frac{1}{2}}\xi\partial/\partial\zeta$$
$$-(\nu_6/\nu_4)^{\frac{1}{2}}\zeta\partial/\partial\xi(2\pi i/h)]P_x+\lambda_2[(\nu_5/\nu_4)^{\frac{1}{2}}\zeta\partial/\partial\eta$$
$$-(\nu_4/\nu_5)^{\frac{1}{2}}\eta\partial/\partial\zeta](2\pi i/h)P_y\}. \quad (1b)$$

In the above $u^2=(h/4\pi^2A_0\nu)$,

$$\lambda_1=[2m(M_c+M_0)\tan\alpha$$
$$+4m(M_c\sigma-M_0\rho)\tan\alpha][(M_c+M_0)\mu_2^{\frac{1}{2}}\mu_3^{\frac{1}{2}}]^{-1},$$
$$\lambda_2=[-4m(M_c+M_0)\epsilon\tan\alpha$$
$$+4m(M_c\epsilon-M_0\delta)\tan\alpha][(M_c+M_0)\mu_1^{\frac{1}{2}}\mu_2^{\frac{1}{2}}]^{-1},$$
$$\lambda_3=(2m+4M_c\epsilon\sigma+4M_0\delta\rho)(\mu_1^{\frac{1}{2}}\mu_3^{\frac{1}{2}})^{-1},$$

P_x, P_y and P_z are the usual angular momentum operators[3] (functions of the eulerean angles θ, φ and ψ) conjugate to the x, y and z axes, A_0, B_0 and C_0 are the principal moments of inertia. In the above m, M_c and M_0 are respectively the masses of the deuterium, carbon and oxygen atoms, σ, ρ, ϵ and δ are constants defined as follows:

$$(mz_4^0-m(z_1^0-z_3^0))(M_c(z_4^0-z_3^0)+2m(z_1^0-z_3^0))^{-1}$$
$$(m/M_0)(M_cz_3^0-(M_c+2m)(z_1^0-z_3^0))$$
$$\times(M_c(z_4^0-z_3^0)+2m(z_1^0-z_3^0))^{-1}$$
$$m(z_4^0-(z_1^0-z_3^0+x_1^0\tan\alpha))(M_c(z_4^0-z_3^0)$$
$$+2m(z_1^0-z_3^0+x_1^0\tan\alpha))^{-1}$$
$$(m/M_0)(M_cz_3^0-(M_c+2m)(z_1^0-z_3^0+x_1^0\tan\alpha))$$
$$\times(M_c(z_4^0-z_3^0)+2m(z_1^0-z_3^0+x_1^0\tan\alpha))^{-1}.$$

The variables η, ξ and ζ are related to the displacements of the D, C and O atoms from equilibrium in the x, y and z coordinates in the following manner:

$$\eta=(4\pi^2\mu_1\nu_5/36h)^{\frac{1}{2}}(x_1+x_2-(x_3/\epsilon)+(x_4/\delta)),$$
$$\xi=(4\pi^2\mu_3\nu_6/36h)^{\frac{1}{2}}(y_1+y_2-(y_3/\sigma)+(y_4/\rho)),$$
$$\zeta=(4\pi^2\mu_2\nu_4/4h)^{\frac{1}{2}}(z_1+z_2)\cot\alpha,$$

where:

$$\mu_1=((2m+4M_c\epsilon^2+4M_0\delta^2)$$
$$+2m(1+4\epsilon+4\epsilon^2)\tan^2\alpha),$$
$$\mu_2=(2m(M_c+M_0)(1+\tan^2\alpha)$$
$$+4m^2\tan^2\alpha)(M_c+M_0)^{-1},$$
$$\mu_3=(2m+4M_c\sigma^2+4M_0\rho^2)$$

and may be regarded as reduced masses respectively to be associated with one of the three modes.

The last term in (1a) is an interaction term between rotation and oscillation. Normally it would be retained as a part of (1b) with the other similar terms. Because of its coefficient (A_0/C_0), which for D_2CO is of the order six, this term will, however, be considerably larger than the other interaction terms so that for values of the rotational quantum numbers up to about ten it will be actually of the same order of magnitude as the rotational energy. It is therefore included as a part of H_0. The second-order terms of H_1 which are not given here, consist of terms which are essentially the squares of the oscillational angular momentum components along the x, y and z axes. Their contributions to the energy of the molecule will be entirely independent of the rotational quantum numbers. Since they are therefore not an interaction energy we shall not compute their value.

Following the procedure suggested in the earlier work referred to herein we take as a solution to the zeroth-order Hamiltonian for the ground and first excited states ν_4, ν_5 and ν_6, the functions:

$$\psi(0)=\{(64\pi^3\mu_1\mu_2\mu_3\nu_4\nu_5\nu_6/h^3)^{\frac{1}{2}}$$
$$\times\exp-(\eta^2+\xi^2+\zeta^2)/2\}\Theta(\theta,J,K,M)$$
$$\times\exp(iK\varphi+iM\psi), \quad (2a)$$

$$\psi(\nu_5)=N(\nu_5)\{-ih[(\nu_6-\nu_5)/2$$
$$+((\nu_6-\nu_5)^2/4+(K\lambda_3h/4\pi^2C_0)^2)^{\frac{1}{2}}]$$
$$\times(2\xi\exp-(\eta^2+\xi^2+\zeta^2)/2)$$
$$+(K\lambda_3h^2/4\pi^2C_0)(\nu_5/\nu_6)^{\frac{1}{2}}$$
$$\times(2\eta\exp-(\eta^2+\xi^2+\zeta^2)/2)\}$$
$$\times\Theta(\theta,J,K,M)\exp(iK\varphi+iM\psi), \quad (2b)$$

[3] E. C. Kemble, *Fundamental Principles of Quantum Mechanics* (McGraw-Hill Co., 1937), p. 232.

$$\psi(\nu_6)=N(\nu_6)\{(iK\lambda_3h^2/4\pi^2C_0)(\nu_6/\nu_5)^{\frac{1}{2}}$$
$$\times(2\xi\exp-(\eta^2+\xi^2+\eta^2)/2)+h[(\nu_6-\nu_5)/2$$
$$+((\nu_6-\nu_5)^2/4+(K\lambda_3h/4\pi^2C_0)^2)^{\frac{1}{2}}]$$
$$\times(2\eta\exp-(\eta^2+\xi^2+\zeta^2)/2)\}$$
$$\times\Theta(\theta,J,K,M)\exp(iK\varphi+iM\varphi),\quad(2c)$$

where

$$N_k^2=\{(K\lambda_3h^2/4\pi^2C_0)^2(\nu_k/\nu_j)+h^2[(\nu_6-\nu_5)^2/4$$
$$+(K\lambda_3h/4\pi^2C_0)^2)^{\frac{1}{2}}]^2\}^{-1}(16\pi^3\mu_1\mu_2\mu_3\nu_4\nu_5\nu_6/h^3)^{\frac{1}{2}}$$

j and k taking the values 6 and 5 and 5 and 6, respectively.

$$\psi(\nu_4)=\{(16\pi^3\mu_1\mu_2\mu_3\nu_4\nu_5\nu_6/h^3)^{\frac{1}{2}}$$
$$\times(2\zeta\exp-(\eta^2+\xi^2+\zeta^2)/2)\}$$
$$\times\Theta(\theta,J,K,M)\exp(iK\varphi+iM\psi).\quad(2d)$$

$\Theta(\theta,J,K,M)\exp(iK\varphi+iM\psi)$ in the above functions is the normalized eigenfunction for the symmetric rotator problem; K and M are integers less than, or equal in the limiting case, to J. The functions (2) give the energies of H_0 as diagonal matrices except for a small contribution arising from $(\Delta\nu/\nu)$ which may be regarded as a left over from the term representing the Coriolis interaction. This term may actually be included as a part of H_1 and its contribution to the energy taken into account at a later point if this is desirable.

The zeroth-order energies for the molecules in the corresponding states are readily found to be:

$$\begin{aligned}
E(0)&=(h/2)(\nu_5+\nu_4+\nu_6)+(J(J+1)-K^2)\\
&\quad\times(h^2/8\pi^2A_0)+K^2h^2/8\pi^2C_0\\
E(\nu_4)&=(h/2)(\nu_5+3\nu_4+\nu_6)+(J(J+1)-K^2)\\
&\quad\times(h^2/8\pi^2A_0(1-\alpha-\beta))+K^2h^2/8\pi^2C_0\\
E(\nu_5)&=h(\nu_5+\nu_4/2+\nu_6)+h((\nu_6-\nu_5)^2/4\\
&\quad+(K\lambda_3h/4\pi^2C_0)^2)^{\frac{1}{2}}+(J(J+1)-K^2)\\
&\quad\times(h^2/8\pi^2A_0(1+\beta))+K^2h^2/8\pi^2C_0\\
E(\nu_6)&=h(\nu_5+\nu_4/2+\nu_6)+h((\nu_6-\nu_5)^2/4\\
&\quad+(K\lambda_3h/4\pi^2C_0)^2)^{\frac{1}{2}}+(J(J+1)-K^2)\\
&\quad\times(h^2/8\pi^2A_0(1+\alpha))+K^2h^2/8\pi^2C_0,
\end{aligned}\quad(3)$$

where α and β may be regarded as correction terms to A_0 which to this approximation are, however, both equal to zero.

To evaluate the corrections to the energy contributed by H_1 we may without hesitation make use of the nondegenerate perturbation theory and proceed in the usual straightforward manner to evaluate E_1 and E_2, the first of which vanishes. We shall include in E_2 only the second-order contributions from H_1 as already suggested, and of these we may actually neglect all the terms except those where the frequency differences $(\nu_4-\nu_5)$ and $(\nu_4-\nu_6)$ occur in the denominators, since all others will be small when compared to these. The term $(\Delta\nu/\nu)\eta\xi$ of which we have already made mention will contribute an amount entirely too small to justify its evaluation and it also will be omitted. The remaining terms of E_2 when computed and added to E_0 change the expression (3) only in this respect that now α and β are no longer zero but take the values:

$$\alpha=(h/8\pi^2A_0)\{\lambda_1^2(K\lambda_3h^2\nu_5/4\pi^2C_0\nu_6)$$
$$\times((\nu_4+\nu_6)/\nu_4^{\frac{1}{2}}\nu_6^{\frac{1}{2}})^2+\lambda_2^2h^2[(\nu_6-\nu_5)/2$$
$$+((\nu_6-\nu_5)^2/4+(K\lambda_3h/4\pi^2C_0)^2)^{\frac{1}{2}}]^2$$
$$\times((\nu_4+\nu_5)/\nu_4^{\frac{1}{2}}\nu_5^{\frac{1}{2}})^2\}\{(\nu_4-\nu_5)(h^2[(\nu_6-\nu_5)/2$$
$$+((\nu_6-\nu_5)^2/4+(K\lambda_3h/4\pi^2C_0)^2)^{\frac{1}{2}}]^2$$
$$+(K\lambda_3h^2/4\pi^2C_0)(\nu_6/\nu_5))\}^{-1}$$

and

$$\beta=(h/8\pi^2A_0)\{\lambda_1^2h^2[(\nu_6-\nu_5)/2+((\nu_6-\nu_5)^2/4$$
$$+(K\lambda_3h/4\pi^2C_0)^2)^{\frac{1}{2}}]((\nu_6+\nu_4)/\nu_4^{\frac{1}{2}}\nu_6^{\frac{1}{2}})^2$$
$$+\lambda_2^2(K\lambda_3h^2/4\pi^2C_0)(\nu_6/\nu_5)((\nu_4+\nu_5)/\nu_4^{\frac{1}{2}}\nu_5^{\frac{1}{2}})^2\}$$
$$\times\{(h^2[(\nu_6-\nu_5)/2+((\nu_6-\nu_5)^2/4$$
$$+(K\lambda_3h/4\pi^2C_0)^2)^{\frac{1}{2}}]^2$$
$$+(K\lambda_3h^2/4\pi^2C_0)^2(\nu_6/\nu_4))(\nu_4-\nu_6)\}^{-1},$$

both of which are quantities greater than zero.

We shall not here consider it necessary to obtain the selection rules, these having been discussed elsewhere, but shall be content with stating what these are. The transitions which may take place and which are of interest to us in this discussion are the following ones: from the ground state to the states ν_5 and ν_6, with $\Delta J=\pm1, 0$ and $\Delta K=\pm1$; from the ground state to the state ν_4 with $\Delta J=\pm1, 0$ and $\Delta K=0$.

III. The Effect of the Interaction on the Spectrum

We are now in a position to inquire into what will be the effect on the spectrum caused by these interaction terms. We may accomplish this by obtaining expressions for the frequency positions of lines in the spectrum using the above energy relations and selection rules. For the frequencies ν_5 and ν_6 only those lines arising from the transitions $\Delta J=0$, $\Delta K=\pm 1$ are of interest, the other lines being at present spectroscopically unresolved. The frequency positions of these lines in the two bands are given by:

$$\nu=(\nu_5+\nu_6)/2-(h/8\pi^2)(1/C_0-1/A_0)$$
$$\pm[(\nu_6-\nu_5)^2/4+(K\lambda_3 h/4\pi^2 C_0)^2]^{\frac{1}{2}}$$
$$+(J(J+1)-K^2)\alpha h/8\pi^2 A_0$$
$$\pm(Kh/4\pi^2)(1/C_0-1/A_0), \quad (5)$$

a relation which, except for the presence of a small term $\alpha h^2/8\pi^2 A_0$, confirms the one used by Ebers and Nielsen in their work on ordinary formaldehyde.

For the frequency ν_4 we obtain as frequency positions of the permitted lines, according as $\Delta J=\pm 1$, $\Delta K=0$ and as $\Delta J=0$, $\Delta K=0$, respectively, the two expressions:

$$\nu=\nu_4\pm(Jh/8\pi^2 A_0)(2+\alpha+\beta)$$
$$+(J^2-K^2)(\alpha+\beta)h/8\pi^2 A_0$$

and $$\nu=\nu_4+(J(J+1)-K^2)(\alpha+\beta)h/8\pi^2 A_0. \quad (6)$$

Equation (5) has already been used by Ebers and Nielsen to explain the structure of the two bands ν_5 and ν_6 in the spectrum of formaldehyde, and as we have pointed out, a structure analagous to this is found in the corresponding two bands in deutero-formaldehyde. Our endeavor from the outset was, however, to account for the unsymmetrical broadening toward higher frequencies of the Q branch of the parallel band in this region. We are therefore particularly interested in the second of Eqs. (6) which sets forth the components comprising the Q branch. Since α and β are both positive quantities it becomes clear at once that, consistent with measurement, the Q branch must spread out toward higher frequencies. The lines of Eq. (6) have been plotted with their relative intensities for comparison with the branch as actually observed. This diagram is not reproduced here, but is in reasonably good agreement with experiment both in shape and in breadth.

In determining the values of the moments of inertia of the formaldehyde molecules, it has always been assumed that the spacings of the perpendicular C−H and C−D vibrations near 2875 cm^{-1} and 2160 cm^{-1} are the correct ones to use, an assumption which has been justified principally on the basis that this vibration is a single perpendicular oscillation. While this is indeed true, it may be pointed out that the other CH and CD vibrations, parallel to the axis of symmetry, and therefore normal to the first ones, lie near 2780 cm^{-1} and 2056 cm^{-1}, respectively. One may then advance the argument that these frequencies might interact so as to perturb the accompanying rotation levels to such extent that also these spacings are unsuitable directly for determining the values of the moments of inertia. The extent of this perturbation can be determined by referring to Eqs. (3). Since there is only one perpendicular frequency in this region, any other perpendicular frequencies which the molecule may have must lie so far away that the difference $\nu_6-\nu_5$ will be large compared to $(K\lambda_3 h/8\pi^2 C_0)$. The term under the radical may therefore be expanded and $E(\nu_6)$ takes the form:

$$E(\nu_6)=(h/2)(\nu_4+\nu_5+3\nu_6)+(J(J+1)$$
$$-K^2)h^2/8\pi^2 A_0(1+\alpha)+K^2h^2/8\pi^2 C_0(1+\gamma), \quad (7)$$

where γ is equal to $\lambda^2 3h/8\pi^2 C_0(\nu_5-\nu_6)$. γ will under these conditions be small and we have already seen that α is not large. To a fair approximation then A_0 and C_0 remain unchanged as the molecule makes a transition from the ground state to this excited state so that these spacings may safely be used in making numerical determinations of the moments of inertia of the molecule.

The Temperature Distribution in the High Pressure Mercury Discharge Tube

W. ELENBAAS
Natuurkundig Laboratorium der N. V. Philips' Gloeilampenfabrieken, Eindhoven, Holland
(Received July 6, 1938)

Several arguments are given which support the view that the temperature distribution of the vapor in the high pressure mercury discharge tube is not that given by Adams and Barnes (line A_g of Fig. 1) but has a shape as indicated by the line B_g of Fig. 1.

IN TWO recent articles Barnes and Adams[1] have concluded that the temperature distribution of the vapor in the high pressure mercury arc is as indicated by the line A_g in Fig. 1, in contradiction with the distribution B_g which I proposed some years ago.[2] A_g indicates that the temperature of the vapor is substantially constant over the whole cross section except in the boundary layer which is about 0.8 mm thick (in analogy to the stationary film of Langmuir).[3] The curve B_g was found[2] from the condition that

$$\int_0^R \frac{2\pi r dr}{T(r)}$$

must have a given value (pressure and mean density were known) and from a plausible assumption on the dependence of the coefficient of heat-conduction on temperature (the absolute value was not used in the calculation). As the convection current in the vertical mercury tube is substantially laminar and vertical, it has only little influence on the horizontal temperature distribution (we do not consider the case that the convection is turbulent).[4]

The distribution A_g agrees with the first condition as well. By assuming a constant temperature over the total cross section one finds from the same data which led to the distribution B_g, a temperature of $555/0.223 = 2500°K$,[2] which is in agreement with the ditribution A_g of Barnes and Adams. The difference between the two curves thus arises from the second condition according to which I used the equation of heat-conduction (energy streaming through a cylinder one cm high is $2\pi r\lambda dT/dr$) whereas Adams and Barnes use the theory of Langmuir. Furthermore, the distribution of the electron temperature, according to Barnes and Adams, is as substantially indicated by the line A_e, whereas I supposed the electron temperature (curve B_e) to be only slightly higher than the gas temperature, so that calculations can be made on the assumption that a temperature equilibrium between the gas molecules and the electrons exists in the arc.

The difference between the two conceptions is so considerable that we wish to state the following objections against that of Adams and Barnes:

(a) Barnes and Adams find the intensity ratio for a number of spectral lines to be the same in the axis and 8 mm aside (inner tube diameter 36 mm); from this fact they conclude the temperature to be the same in both points. However, this does not agree with my own measurements[5] and with more extensive recent measurements of Fischer and König,[6] who find that the intensity of a line drops more rapidly if its initial level is higher. This indicates that the excitation temperature is a maximum in the axis. As the points through which Barnes and Adams have to draw a straight line, whose slope determines the temperature, scatter much, it is possible that the temperature difference between the axis and 8 mm aside, has escaped their attention.

(b) Even if the temperature in the arc path were uniform, we may not conclude that the temperature over the total cross section (except the boundary layer) is constant (diameter of measured portion 16 mm and PQ about 34 mm).

(c) Langmuir's theory of the film of stationary gas around a heated wire cannot be applied to the

[1] B. T. Barnes and E. Q. Adams, Phys. Rev. **53**, 545 (1938); E. Q. Adams and B. T. Barnes, Phys. Rev. **53**, 556 (1938).
[2] W. Elenbaas, Physica **1**, 211 (1934).
[3] I. Langmuir, Phys. Rev. **34**, 401 (1912).
[4] W. Elenbaas, Physica **3**, 484 (1936). C. Kenty, J. App. Phys. **9**, 53 (1938).
[5] W. Elenbaas, Revue d'optique **15**, 343 (1936).
[6] E. Fischer und H. König, Physik. Zeits. **39**, 313 (1938).

high pressure arc, where the energy is conducted to the surrounding solid part (tube wall) instead of from the solid body (the wire) to the surrounding gas, as in the case studied by Langmuir. This is caused by the fact, that in the case of the wire there can exist a practically uniform temperature field (namely room temperature or temperature of the bulb) beyond the stationary film (by the upward stream of the cold convection gas), but inside the mercury tube there must be a temperature gradient when energy flows to the walls (unless the gas is in a rapid and irregular motion in the part PQ (Fig. 1)); this is, however, not the case as stated under (d). The temperature distribution A_g would therefore only be possible if no energy were transformed into heat in the region between P and Q, but only on the edge PQ. This is very unlikely, as the arc burns in the central part of the tube.

(d) Convection is observable on small particles which are moving along with the vapor.[4] They indicate a chiefly laminar streaming which goes upwards in the central part of the discharge and downwards in the surrounding part. The convection cannot cause a uniform temperature across the diameter PQ, as for that purpose only radial components, which practically do not exist, would be useful. If the temperature distribution were as indicated by A_g the convection would be upward in the whole part PQ. Actually the particles are moving downward at a much greater distance from the wall. This phenomenon cannot be caused by electrical forces, as it is the same with alternating and direct current.

(e) For the energy which is conducted to the wall, Barnes and Adams calculate from the Langmuir theory 32 watts per cm of length. The total radiation according to Barnes and Adams is therefore as a maximum $40-32=8$ watt or 20 percent of the input. The total radiation in the above case, however, is greater. For the total radiation S per cm of length of the high pressure mercury discharge in a quartz tube we found in a wide range of diameters and pressures:[7]

$$S=0.7(L-10) \text{ watt}, \qquad (1)$$

where L is the input per cm of length. Applying this to the tube of 20 mm diameter, mentioned by Barnes and Adams, on which I did the measurements,[2] we find $S=0.7(40-10)=21$ watt ($L=40$ and not 43.8 as stated in reference 2, where the energy losses at the electrodes had not been taken into account). Therefore, at most only 19 watts could be conducted to the wall. The interpretation given of Eq. (1) leads even to a smaller amount of energy which is conducted to the wall, namely 10 watts per cm of length (we supposed that of the input L, 10 watts are conducted to the wall and $L-10$ watts are radiated, of this radiation only 70 percent passes the quartz wall). This energy of 10 watts is in agreement with measurements on the influence of noble gases on the mercury arc[8] and with the behavior of the gradient as a function of L at a given mean vapor density.[9] If we put this energy of conduction in the formulas of reference 2, we find for the coefficient of heat conduction λ for mercury vapor $2.1\times10^{-7}T^{3/4}$. Extrapolating to 476° (203°C) we find a value of 21×10^{-6} for λ, whereas a value of 18.5×10^{-6} has been measured

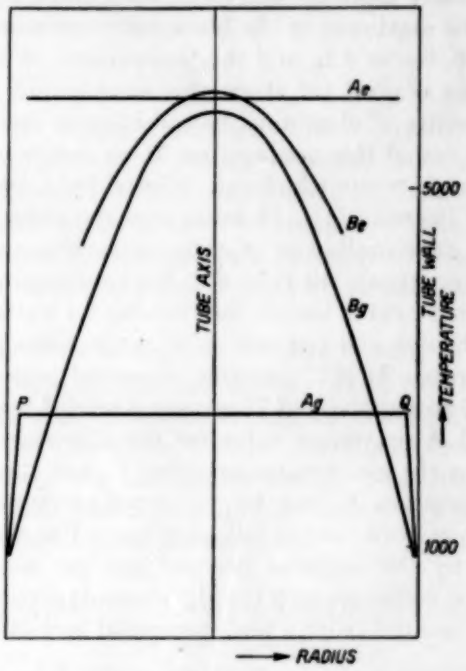

FIG. 1. Gas temperature A_g and electron temperature A_e as functions of the distance to the axis according to Barnes and Adams. B_g and B_e are the corresponding temperatures according to the author.

[7] W. Elenbaas, Physica **4**, 413 (1937).

[8] W. Elenbaas, Physica **3**, 219 (1936).

[9] W. Elenbaas, Physica **2**, 757 (1935).

by Schleiermacher.[10] Thus the loss of 10 watts by conduction *is in agreement with the slope of curve* B_g. As the convection currents in this tube were laminar, the energy loss by convection may be neglected (only at the first part from the bottom there appears an additional loss caused by the heating up of the colder convection gas).

(f) According to Adams and Barnes the energy of 32 watts, which is conducted to the wall per cm of length, can be dissipated just at a temperature of 900°K (outer diameter of the tube 22 mm). With a temperature of 900° they calculate a loss of 5.3 watts by conduction and convection and a loss of 25.6 watts by radiation. They obviously treat the glass wall as a black body. As the maximum of the black body radiation of 900°K lies at 3.2μ and the transmission of most glasses is good till about this wave-length, the emissivity of glass must be considerably smaller than one at this temperature. If we assume that of the 21 watts which are radiated by a quartz tube (formula (1)), 18 watts pass the glass wall (the tube wall was of thin, ultraviolet-transmitting glass), the tube wall has to dissipate 22 watts per cm of length. Subtracting 5.3 watts for conduction and convection, 17 watts remain for radiation. At 875° (actually measured temperature) an emissivity of 75 percent is needed hereto.

(g) A maximum value for the difference between the electron temperature T_e and the gas temperature T_g may be calculated according to Druyvesteyn[11] in the following way: The energy lost by the electrons per cm³ and per sec. by elastic collisions with the Hg atoms, is according to Cravath[12] (with a few immaterial neglections)

$$Q=8n_e n_a \sigma^2 kT_e\left(\frac{2\pi kT_e}{m}\right)^{\frac{1}{2}}\frac{m}{M}\left(1-\frac{T_g}{T_e}\right). \quad (2)$$

n_e and n_a are the number of electrons and Hg atoms per cm³, σ the radius of the Hg atoms and m and M the mass of the electron and the Hg atom. We can find n_e from the mobility equation:

$$i=\frac{3n_e e^2 G}{8\sigma^2 n_a(2\pi mkT_e)^{\frac{1}{2}}}, \quad (3)$$

where i is the current density and G the gradient.

Substituting (3) in (2) and putting $n_a=n_0(273/T_g)$, if n_0 is the number of atoms per cm³ at a pressure of one atmos. and at 0°C (the pressure in the above-mentioned tube was one atmos.), we find as $Q<iG$

$$\left(\frac{T_e}{T_g}\right)^2-\left(\frac{T_e}{T_g}\right)<\frac{3e^2G^2M}{128\pi(273)^2\sigma^4k^2n_0^2m}. \quad (4)$$

If we take for $\pi\sigma^2$ the value 5×10^{-15} and for $G=8$ volt/cm (measured value), we find 0.17 for the right side of Eq. (4). This gives $(T_e/T_g)<1.15$. As only a fraction of the input will be transferred to the atoms by elastic collisions, the real difference between electron temperature and gas temperature will be smaller than 15 percent. The only uncertain quantity in (4) is σ. The value 5×10^{-15} for $\pi\sigma^2$ may be wrong to a factor 3.[13] Taking $\pi\sigma^2$ three times smaller we find $(T_e/T_g)<1.83$, whereas Barnes and Adams need at least a value of 2.4 (6000/2500). If, however, the electron temperature is 6000° and the vapor temperature 2500°, the total excitation is practically caused by the electrons, so that the energy transferred to the atoms by elastic collisions, will be smaller than $\frac{1}{2}iG$ (the measured total radiation is 50 percent of the input, Eq. (1)). A ratio of 2.4 for T_e/T_g, therefore corresponds to a value of $\pi\sigma^2<0.8\times10^{-15}$, which seems to be a very improbable value.

For all these reasons we believe that it is much more likely that the temperature distribution is as indicated by the line B_g than as indicated by the line A_g.

[10] A. Schleiermacher, Wied. Ann. **36**, 346 (1889).
[11] Unpublished. See also R. Mannkopff, Zeits. f. Physik **86**, 161 (1933).
[12] A. M. Cravath, Phys. Rev. **36**, 248 (1930).
[13] W. Elenbaas, Physica **5**, 573 (1938).

A Study of Beta-Brass in Single Crystal Form

WAYNE WEBB
Department of Physics, University of Iowa, Iowa City, Iowa

(Received September 21, 1938)

The resistances of twenty single crystals of brass in the beta-phase have been measured as a function of temperature from room temperature to about 550°C for the purpose of studying the order-disorder phenomenon. The results obtained are compared with the theory of Bragg and Williams. The resistivities at 25°C as a function of composition place the limits of the beta-phase at 51.3 and 55.5 atomic percent copper. A study of the thermal e.m.f. of the crystals against copper shows only a slight discontinuity in the second derivative of the e.m.f.-temperature curve at the temperature of complete disorder. The e.m.f. curves themselves are quite smooth. Young's modulus, E, for ten of the crystals, measured at room temperature, gives the elastic constant S_{11}, (44.8×10^{-13} cm²/dyne) and the combination of constants, $2S_{12}+S_{44}$, (0.028×10^{-13} cm²/dyne). A graph of $1/E$ against the orientation function, $(l^2m^2+m^2n^2+n^2l^2)$ is linear. From it the ratio of the maximum to minimum E is found to be 8.94. Below the elastic limit the stress-strain relation is linear with no permanent set nor hysteresis.

INTRODUCTION

RESEARCHES on the properties of metal alloys capable of forming superlattices have been stimulated, particularly in this country and England, by the recent theoretical developments of Bragg and Williams,[1] and Bethe.[2] Improvements in details of the theory have been made by a number of workers.[3] On the experimental side specific heat and electrical resistance have been determined as functions of temperature and have been correlated with the state of order existing.[4] An excellent review of both theory and experiment has been given recently by Nix and Shockley.[5]

Beta-brass is one of the simplest of alloys showing the order-disorder phenomenon. It is the beta-phase of the copper-zinc system, with a composition in the neighborhood of the one-to-one ratio of atoms. The crystal structure is body-centered cubic. In the disordered state the two kinds of atoms have equal probabilities of being at any lattice point. In the ordered condition the zinc atoms occupy the cube centers and the copper atoms the cube corners or vice versa. This fact, though surmised from other data, was definitely established by Jones and Sykes in an x-ray study in which they were able to obtain superlattice lines for the ordered alloy[6] by a judicious selection of the x-ray wave-length used.

The present research includes a study of certain properties of single crystals of this beta-brass in the ordered condition (at room temperature), and of the order-disorder transformation by following the changes in certain properties as the temperature is gradually raised to a point above the critical temperature.

PREPARATION OF CRYSTALS AND DETERMINATION OF ORIENTATION

The beta-brass from which the crystals were grown was prepared from very pure commercial materials. The copper was cathode copper from Anaconda Copper Company and was stated by the Company to be 99.95 percent copper. The zinc was Bunker Hill from Platt Brothers and Company and contained not more than 0.01 percent impurity.[7]

[1] W. L. Bragg and E. J. Williams, Proc. Roy. Soc. **A144**, 340 (1934).
[2] H. A. Bethe, Proc. Roy. Soc. **A150**, 552 (1935).
[3] R. Peierls, Proc. Roy. Soc. **A154**, 207 (1936); N. F. Mott, Proc. Phys. Soc. **49**, 258 (1937); T. S. Chang, Proc. Roy. Soc. London **A161**, 546 (1937); E. E. Easthope, Proc. Camb. Phil. Soc. **33**, 502 (1937).
[4] C. Sykes and F. W. Jones, Proc. Roy. Soc. **A157**, 213 (1936).
[5] F. C. Nix and W. Shockley, Rev. Mod. Phys. **10**, 1 (1938).
[6] F. W. Jones and C. Sykes, Proc. Roy. Soc. **A161**, 440 (1937).
[7] An estimate of the impurities present in this brand of zinc is given by H. E. Way, Phys. Rev. **50**, 1181 (1936). Actually the writer's material was all taken from a slab which showed distinctly less lead than Way's, but other impurities in the same amount. See Way's footnote 14, which refers to the slab used by the writer.

The crystals were grown from the molten state in a horizontal mold by the method employed for some time in this laboratory.[8] The preliminary polycrystalline casting was prepared by melting together in a crucible[9] suitable proportions of copper and zinc and pouring the molten metal into the crystal mold. This was done in a furnace in which a nitrogen atmosphere was maintained throughout. The crystal was grown in a second furnace also in nitrogen. The orientation of the crystal was not predetermined by the use of a nuclear crystal, since it was found that, by making the end of the casting pointed, a single crystal would start. There seemed to be no particularly preferred orientation, so that thus a suitable variety of orientations was assured.[10] The crystals were of a trapezoidal (nearly square) cross section, about 0.7 cm^2 in area, and 14 cm long. All the crystals were grown with a temperature gradient of about 6°C/cm and a rate of growth of approximately 6 cm/hr.

During the cooling following the formation of the crystals the temperature was checked at 600°C for twenty-four hours and then allowed to fall slowly to room temperature. The purpose of this anneal was to secure homogeneity of composition throughout the crystal.

After completion of the measurements the crystals were analyzed for copper content by the standard method of electrolytic deposition from a sulfate solution. In most cases the sample analyzed was about 3 g, 1.5 g from each end of the crystal. In three cases separate analyses were also made for the two ends. None of these showed a difference between the two ends greater than 0.1 percent of copper content. The compositions obtained extended throughout the beta-brass phase and somewhat beyond at room temperature as can be seen from Table II.

The crystals, as removed from the mold and without further treatment, showed in a very marked manner the phenomenon of strong light reflection in definite directions, precisely as described by Bridgman[11] for a number of metal crystals. These reflections could be improved in some cases by heating the crystals from two to three hours in a hydrogen atmosphere. Etching the surfaces damaged the reflections and made them more diffuse.

These reflections were used to determine the orientation of the length of the specimen relative to the space lattice by a slight variation of Bridgman's method. The general idea of the method is to locate the normal to each reflecting plane by causing a fixed beam of incident light to be reflected back on itself. When the normals to a number of planes have been located, the angles between the planes are then easily computed. To identify the planes it is then necessary to see whether each plane can be assigned a set of Miller indices so that measured and computed angles between every possible combination of pairs of planes form a completely consistent scheme. Table I shows the degree of consistency

[8] C. A. Cinnamon, Rev. Sci. Inst. **5**, 187 (1934).

[9] The crucible and molds were made from lava obtained from the American Lava Company. The writer is indebted to the company for furnishing the unfired material and later firing the molds, etc., after they were made.

[10] It is doubtful if a seed crystal could be fused to the casting with a flame since attempts to fuse two pieces of beta-brass together resulted in evaporating so much zinc that the joint became alpha-brass.

[11] P. W. Bridgman, Proc. Am. Acad. Arts and Sci. **60**, 305 (1925).

TABLE I. *Orientation of crystal lattice, measured angles.*

1	2	3	4	5	6	7	8		Reflected Beam No.
{111}	{110}	{110}	{111}	{110}	{111}	{110}	{110}	Assumed Plane	
	35° 8′	35° 25′	70° 45′	89° 59′	70° 26′	89° 53′	89° 50′	{111}	1
		60° 3′	35° 36′	59° 44′	89° 52′	58° 54′	89° 35′	{110}	2
			89° 54′	60° 16′	35° 7′	89° 59′	60° 3′	{110}	3
theoretical angles				34° 56′	70° 19′	35° 7′	89° 56′	{111}	4
{111} with {111} 0°, 70° 32′					35° 25′	59° 41′	60° 11′	{110}	5
{111} with {110} 35° 16′, 90°						89° 58′	35° 36′	{111}	6
{110} with {110} 0°, 60°, 90°.							60° 9′	{110}	7
								{110}	8

obtained for eight of the reflections from one of the crystals. The numbers across the top and down the side refer to arbitrary numbers assigned to the reflections. In parentheses are the Miller indices which give the type of plane. The angles in the body of the table are those observed between the normals to the planes in the corresponding column and row. It can be seen that rarely do the observed angles disagree by more than one degree with one of the geometrically possible angles given in the table. More complete tables involving all observed reflections, were fully as consistent. Besides the two types of planes shown in the table, planes of type {112} were frequently observed.

The above measurements were made by use of an especially constructed goniometer, which need not be described in detail. It permitted one to obtain a particular reflection from the whole of the crystal length without disturbing the angle setting. Only specimens for which the direction of the reflection remained constant the full length were considered to be single crystals and satisfactory for use in subsequent measurements.

Naturally, once the positions and types of several lattice planes are determined, it is merely a matter of geometry to compute the orientation. The orientations so obtained are given in Table II by stating the two larger of the three direction cosines of the long axis of the specimen with reference to the three principal crystal axes (cube edges). While it has been stated that the angles between the lattice planes did not involve an error greater than one degree the error involved in the orientation angles may be as great as three degrees. This difference is caused by inability to set the specimen in a precise manner on the goniometer.

TABLE II. *Resistance characteristics of the crystals. Limits of the beta-phase are indicated by the arrows. T' and T'' represent the temperatures between which the resistance-temperature curves were nonlinear.*

Atomic Percent Copper	$\alpha \times 10^6$ per °C	$\rho''' - \rho'' \times 10^6$ ohm-cm	T'(°C)	T''(°C)	Two Largest Direction Cosines	
					l	m
50.22	3.54	4.40	193	490	0.806	0.560
50.70	3.85	4.31	250	480	.807	.562
50.81	3.47	4.41	200	490	.622	.561
50.89	3.41	4.37	165	485	.868	.396
51.25	3.61	4.46	207	490	.914	.294
51.63	3.50	3.62	240	480	.693	.656
52.13	3.43	3.76	250	475	.986	.097
52.16	3.53	4.03	205	487	.908	.357
53.20	3.02	3.76	160	475	.788	.488
53.34	3.32	4.35	160	485	.876	.439
53.65	2.96	3.46	175	490	.914	.334
53.77	3.16	3.04	185	490	.801	.435
53.81	2.42	4.30	150	480	.813	.583
54.25	2.87	2.68	212	480	.717	.633
54.26	3.07	3.09	210	480	.716	.716
54.60	3.12	2.57	240	465	.739	.584
54.89	3.08	3.34	150	475	.900	.453
55.50	2.96	2.99	200	485	.779	.624
55.85	3.00	2.67	200	490	.933	.291

Resistivity and Resistance

Two sets of resistance measurements were made on each crystal; one to obtain an accurate value of the resistivity at room temperature, and the other to study the temperature dependence of resistance. A potentiometer method employing a Leeds & Northrup, Type K2, potentiometer was used to make both sets of measurements.

For the resistivity measurements needle points were used as potential contacts which made possible a precise measurement of the length. The average cross-sectional area between the potential contacts was determined by finding the volume of this portion of the crystal. This was done by sawing out this section, at the completion of the work, and getting its mass and density.

To measure the resistance as a function of temperature the crystal was placed in a furnace in a holder equipped with three thermocouples, one near the middle and one near each end of the crystal. The potential and current leads were spot-welded to the crystal. Readings were taken as the temperature of the furnace was raised at a rate which varied from a degree per minute for the lower temperature range to about one-fourth degree per minute at the higher temperatures.[12] Readings were also taken with the temperature decreasing gradually to 400°C, and a final reading at room temperature. There was a slight temperature gradient along the crystal of such

[12] These runs were made at this slow rate to eliminate any lag between the temperature indicated by the thermocouples and the actual temperature of the crystal. The agreement for rising and falling temperatures shows that this was accomplished. It shows further no lag between order and temperature; such a lag was not expected, however, since it is known that the relaxation time for this alloy is very short.

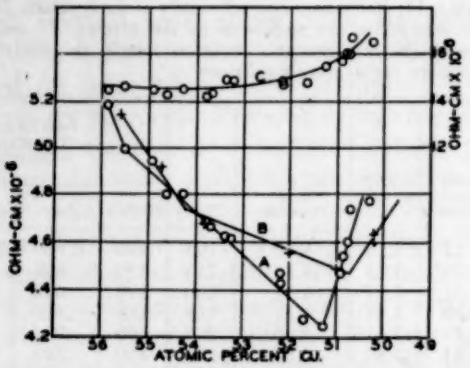

FIG. 1. Resistivity as a function of composition. Curve A at 25°C; curve C at 500°C. Curve B, Haughton and Griffiths' curve; they state their values are for room temperature. The ordinate scale for C is on the right.

amount that the temperatures at the potential contacts usually differed by about three degrees, never, however, exceeding ten degrees. Thermal e.m.f.'s caused by this difference were corrected for by taking potential readings with the current through the crystal both direct and reversed; also, with no current.

In curve A, Fig. 1, the resistivity at 25°C is shown as a function of composition. Curve B, given for comparison, represents the data of Haughton and Griffiths[13] for polycrystalline material at "room temperature." The two curves are seen to agree in a general way. Some of the difference is undoubtedly caused by difference in purity of materials and to the mechanical treatment given the samples of Haughton and Griffiths.

The boundaries of the beta-phase occur at the end points of the middle straight section of the resistivity-composition curve. The writer's data (curve A) indicate 51.3 and 55.5[14] atomic percent copper whereas Haughton and Griffiths estimate 50.7 and 54.2 atomic percent copper from their data. Values given by metallurgists, obtained usually by thermal and micrographic analyses, vary considerably among themselves. The exact limits of the beta-phase at room temperature are extremely difficult to determine, since, while an alloy may be examined at room temperature, the structure observed may be typical of a higher temperature if the cooling to room temperature has been too fast, or perhaps at any finite rate. Some typical values for the beta-phase limits in atomic percent copper are: Gayler:[15] 55.0−51.0; Hansen:[16] 55.6−51.0; Saldau and Schmidt:[17] 54.4−49.8; *International Critical Tables:* 54.7−51.2. Sykes and Wilkinson[18] obtained phase boundaries by measurement of the energy difference of the ordered and disordered state as a function of composition. Their limits are: 55.3 and 51.1 atomic percent copper, in very good agreement with the writer's.

It is interesting to note that practically all determinations of the beta-phase of brass just fail to include the ideal, equiatomic ratio. It is only for such a ratio that perfect order, or a perfect superlattice can exist. Other compositions in the beta-phase may have a maximum order, but never perfect order since the number of copper atoms is always too large. Sykes and Wilkinson in order to find the transformation energy for the ideal CuZn, extrapolated their data to the one-to-one ratio. The writer's resistivity data may be treated in the same way by extending the straight middle portion of curve A, Fig. 1, to 50 atomic percent copper. The value of the resistivity so found is 4.02×10^{-6} ohm-cm. This is very near the mean value of the resistivities of the constituent metals, which is 3.93×10^{-6}, derived from Way's[19] value for Bunker Hill zinc, and the *International Critical Tables* value for pure copper. This shows that the completely ordered structure behaves in resistivity like a pure metal, with value intermediate between those of the constituents, and does not show the enhanced resistivity characteristics of an ordinary, or random, solid solution. The temperature coefficient, as will be seen later, is also about that of a pure metal. This simple relation seems to be approximately satis-

[13] J. S. Haughton and W. T. Griffiths, J. Inst. Met. **34**, 245 (1925).

[14] This boundary is not closely established by the data. The break in the curve might well come anywhere between 54.5 and 55.5 percent Cu with an equally good fit of the curve to the observed points.

[15] M. L. V. Gayler, J. Inst. Met. **34**, 235 (1925).

[16] M. Hansen, *Der Aufbau der Zweistofflegierungen* (Julius Springer, Berlin, 1936).

[17] P. Saldau and I. Schmidt, J. Inst. Met. **34**, 258 (1925). The specimens of Saldau and Schmidt were annealed 84 days at 440°C.

[18] C. Sykes and H. Wilkinson, J. Inst. Met. **61**, 223 (1937). These authors give a good discussion of the uncertainties of these boundaries.

[19] Reference 10. An average value for random orientation is given by $\frac{2}{3}\rho_{90}$ and $\frac{1}{3}\rho_0$. The value so obtained is reduced to 25°C, and gives the value in the text.

fied in other similar cases[20] but in this case is really surprising in view of the very different lattice structures of the alloy and either constituent (alloy, b.c.c.; copper, f.c.c.; and zinc, hex.).

Curve C of Fig. 1 gives the resistivity at 500°C. These data are taken from the resistivity at room temperature combined with the resistance temperature results, to be described later. It is seen that the phase boundaries are no longer defined by this curve. All the crystals were within the beta-phase at this temperature. This curve is similar to those for continuous solid solutions, such as shown by Mott and Jones.[21]

The very regular variation of the resistivity with composition shown by curves A and C, Fig. 1, indicates that there is certainly no very large dependence of resistivity on orientation. In view of the fact that the lattice structure is cubic it is almost certain that no such variation should be expected.

The curves of Fig. 2 show typical resistivity-temperature relations. Both curves are for crystals inside the β-phase, one, A, near the boundary on the copper rich side, and one, B, near the other boundary and very close to the ideal equiatomic ratio. These curves have the following features: a straight portion at lower temperatures followed by a portion of rapidly increasing slope, a short "tail" of decreasing slope, and finally another linear portion extending to higher temperatures. The curves for all the other crystals were similar to these two. Without presenting all these curves, the differences between crystals may be indicated as follows. If the straight line portions are extended (curve B), the point T' at which the curve departs from the lower tangent marks the onset of detectable disorder, while T'' marks the completion of the principal disordering process. Furthermore, the difference, $\rho'''-\rho''$, is the contribution of disorder to the resistivity under the assumption that the temperature dependence of resistivity, aside from disorder, may be linearly extrapolated. Values for such quantities taken from corresponding curves for all the crystals are given in Table II. This table includes also the composition and temperature coefficient of resistivity of the ordered state taken from the resistance-temperature curves.

It is seen from this table that the total contribution of the disorder to the resistivity is roughly greater the closer the crystals are to the ideal equiatomic ratio. There are, however, easily noted exceptions to this general behavior. These arise largely because of the irregularity of occurrence of the temperature T', which is seen to range from 150° to 250°C. When it comes at a high temperature, less resistance change is attributed to disorder, than when it comes low. However, for want of a better criterion it seems fair to consider the "disordering" as starting in a noticeable fashion at T' as chosen. The general trend to lower values of $\rho'''-\rho''$ for increasing copper content seems reasonable because the greater the excess of copper (above equiatomic proportions) the less the completeness of the order which must be destroyed at the high temperature. The alloys beyond the beta-phase, at the top and bottom of the table, behave quite similarly to alloys just within. These alloys in the two-phase field are quite interesting in that the disordering process is accompanied by change of the alpha- or gamma-brass present to the

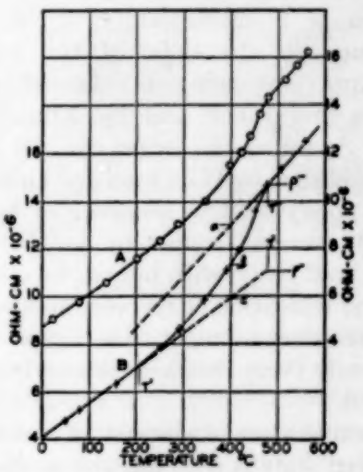

FIG. 2. Resistivity-temperature. Curve A for crystal of 55.50 atomic percent copper. Curve B for one of 51.25 atomic percent copper. The ordinate scale for curve A is on the right.

[20] See F. C. Nix and W. Shockley for CuAu and CuPd systems.

[21] N. F. Mott and F. W. Jones, *The Theory of Properties of Metals and Alloys* (Clarendon Press, Oxford, 1936), Fig. 103, page 299 and Fig. 104, page 300.

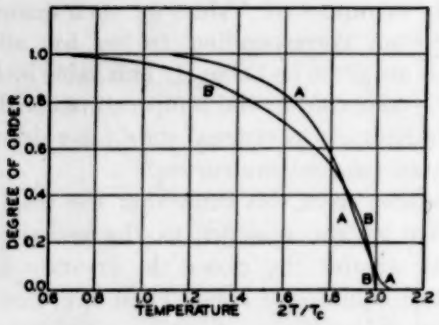

FIG. 3. Order *versus* temperature. Curve A, experimental curve for crystal 51.25 atomic percent copper. Curve B, Bragg-Williams theoretical curve for equiatomic ratio.

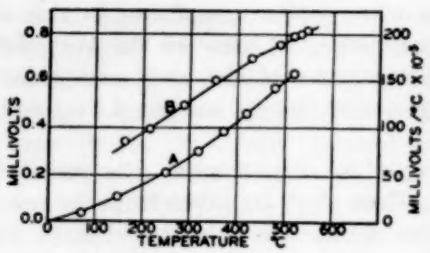

FIG. 4. Curve A, ordinate scale on left, shows a typical thermal e.m.f.-temperature relation. Curve B, ordinate scale on right, thermoelectric power-temperature.

beta-phase as the resistance-temperature measurements are made.

The completion of disorder is far more definite than the onset, as shown by the smaller range of values of T'', 475°C to 500°C. The existence of the "tail" at the upper portion of the curves is quite definite and was shown by all the crystals. Points on it could be repeated on different runs, on the same run for heating and cooling, as well as by holding a constant temperature at a particular point. Only a small part of this "tail" is caused by the slight temperature gradient along the crystal since the width due to this cause should not exceed the difference in temperature between the points of contact, which was in most instances certainly less than 5°C with an observed "tail" of the order of 15°C wide. Thus in no case was there any indication of a discontinuity at the critical temperature in the slope of the resistivity-temperature curve such as is indicated for Cu_3Au by Sykes and Jones[4] and by Kurnakow and Ageew.[22] As far as the writer can tell from the figures published by Haughton and Griffiths[23] for a single polycrystalline specimen of brass containing 47 percent copper by weight, no pronounced "tail" is present, but on the other hand, there is no indication of the very sudden upturn of the resistance-temperature curve and the consequently very marked discontinuity just mentioned.

The temperature coefficient of resistivity of the ordered state is seen likewise to decrease in general as the composition varies from the neighborhood of the equiatomic ratio toward the copper-rich side of the phase. This is to be expected because the behavior should depart from that of an ordered alloy and approach that of a disordered solid solution. From the curves of Fig. 2 it is seen that the slopes of the upper linear portions are greater than those of the lower. This tendency was general, the difference in the slopes being greater the greater the copper content of the crystals. There seems to be no obvious explanation for this unless perhaps it be attributed to a gradual disappearance of local order after the main disordering process is complete.

A very rough estimate of the dependence of resistivity on order has been made by Bragg and Williams.[1] They assumed essentially that the amount of added resistance was proportional to the disorder present. This may be illustrated from curve B of Fig. 2 in which the order at any temperature is given by the ratio of the ordinate segments, ab/ac. Curve A, Fig. 3, is a plot of the order obtained in this way, for the crystal of 51.25 atomic percent copper. For abscissae a reduced temperature, $2T/T_c$, is used, in which T is the absolute temperature and T_c is the critical temperature at which long range order disappears. As the critical temperature for this composition the writer has adopted the carefully determined value of Sykes and Wilkinson,[18] 741°K (468°C). For comparison the Bragg and Williams[1] curve for long range order and for equiatomic proportions is shown, curve B, Fig. 3. The general agreement is fairly good. The assumption that has been made throughout that order is complete at room temperature naturally causes the experimental curve to lie above the

[22] N. S. Kurnakow and N. W. Ageew, J. Inst. Met. **46**, 481 (1931).
[23] Reference 13, Figs. 2 and 3, pp. 248–249.

Bragg and Williams curve in the high order region.[24] The order shown beyond the critical temperature is largely due to the "tail" of the resistance-temperature curves, a possible explanation for which has already been suggested. Similar curves for the other crystals are somewhat as follows: (1) crystals near the equiatomic ratio agree very well with curve A; (2) crystals of high copper content differ from curve A, and lie about ten percent or less above or below it in regions of order greater than 0.5, and distinctly to the right in the region of rapidly decreasing order, below 0.5; (3) crystals with copper less than the equiatomic proportion lie very close to curve A for high order and either close or slightly to the left in the region of lower order.

The theory of T. Muto[25] leads to a connection between order and resistivity given by:

$$\rho = \rho_1 + \rho_2 S + \rho_3 S^2.$$

A comparison of the above experimental results with this expression is not possible because of the inability to evaluate the quantities ρ_1, ρ_2 and ρ_3 which are themselves temperature dependent. The Bragg and Williams approximation is equivalent to the first two terms of Muto's expression.

Thermal e.m.f. and Thermoelectric Power

The thermal e.m.f. of the crystals against copper was measured from room temperature up to 550°C. The curves obtained for e.m.f.-temperature difference were quite smooth, with no noticeable effect in the region of disordering. A typical result is given in Fig. 4, curve A. The e.m.f. values for all the crystals ranged from 0.4 to 0.7 millivolt for a hot junction temperature of 500°C and cold junction at 18°C. The variation from crystal to crystal did not correlate with the composition nor orientation of the crystals. The mean thermoelectric power in a 15° temperature interval was directly measured for six of the crystals. When plotted against temperature it shows two straight line portions intersecting at 460°±15°C with the higher temperature part having the smaller slope. Curve B, Fig. 4 is typical. Although these thermoelectric investigations were not very extensive they show conclusively that the degree of order affects the thermoelectric properties very slightly. The only effect is a slight change in the second derivative of the thermal e.m.f.-temperature relation, which occurs apparently very close to the temperature of completion of disorder.

Table III. *Elastic characteristics of the crystals.*

$f(l, m, n)$	$E \times 10^{-11}$ (dynes/cm²)	$1/E \times 10^{13}$ (cm²/dynes)	Atomic Percent Cu
0.143	3.62	27.6	53.65
.183	4.02	24.9	53.34
.243	6.07	16.5	55.50
.009	2.29	43.8	52.13
.193	5.39	18.7	50.89
.286	8.25	12.1	54.60
.231	6.00	16.6	50.22
.323	14.3	6.97	50.81
.162	4.18	24.1	52.16
.145	4.62	21.6	51.25

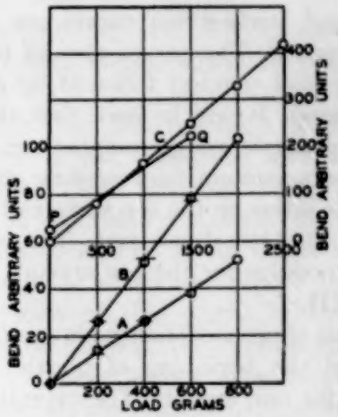

Fig. 5. Curves A and B, ordinate scale left, show load-strain relationship. Curves C and PQ, ordinate scale right, show the effect of plastic flow.

Elastic Behavior

Ten of the crystals with the most uniform and regular cross section were selected for a preliminary study of their elastic behavior. Young's modulus was measured for each crystal on the bending beam apparatus described by Hanson.[26]

[24] This deviation could be lessened if the Bragg and Williams procedure had been exactly followed. Thus, instead of using the experimental resistivity near room temperature as typical of the completely ordered state, an ideal resistivity would have been used, namely, the average resistivity of copper and zinc.

[25] T. Muto, Sci. Pap. Inst. Phys. Chem. Res. **30**, 99 (1936).

[26] The apparatus has been somewhat modified by Professor Tyndall. An improved and more sensitive optical system for observing the bending is now in use. Further-

Two typical stress-strain curves are shown in Fig. 5, A and B. The curves were all taken with increasing load (circles) followed by decreasing load (crosses). It will be seen that there is no sign of hysteresis nor permanent set. In these curves the maximum load reading corresponds to a tensile stress on the top surface of the beam of about 20×10^6 dynes/cm^2. The values for Young's modulus for the ten crystals are given in Table III.

The limit of proportionality between stress and strain and the beginning of plastic flow were obtained for one crystal. The crystal was first taken up to a load of 2500 g and on unloading it returned to zero. (See Fig. 5, curve C.) It was then again loaded to 2500 g, and the preceding readings were duplicated. An additional 500 g caused a rapid drift (plastic flow). The whole load was immediately removed,[27] and the crystal returned to a new zero as shown by the point marked P. A 1500-g load then gave the point Q. When this was removed point P was again obtained. From these results it seems clear that the limit of proportionality and the beginning of plastic flow are very close together, if not identical. The increase in the modulus (about 20 percent) shown by the decreased slope of PQ is very marked after such a small permanent deformation. The tensile stress on the upper surface of the beam for the 2500-g load is 70×10^6 dynes/cm^2. The strain is 1.4×10^{-4}. A second crystal (50.05 atomic percent copper) was strained until the maximum tensile stress on the upper surface of the beam was 80×10^6 dynes/cm^2 without, however, exceeding the proportional limit. The "yield point" determined by Elam[28] for beta-brass is of the order of 10 times the above values. This difference is not surprising in view of the fact that Elam's values are for permanent extensions sufficient to cause slip bands to appear. The extreme values of tensile

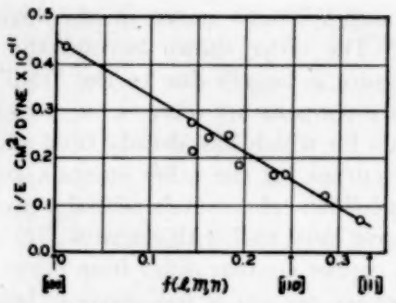

FIG. 6. Reciprocal of Young's modulus, $1/E$, *versus* $f(l, m, n)=(l^2m^2+m^2n^2+n^2l^2)$. The arrows at the bottom show directions in the lattice that correspond to certain values of $f(l, m, n)$.

stress obtained by the writer would correspond to a resolved shear stress of about 35×10^6 dynes/cm^2, i.e., half the tensile stress provided a slip plane[29] is near the most favorable orientation of 45° to the length of the specimen.

For a cubic crystal Young's modulus in a given direction may be expressed in terms of the elastic parameters, S_{11}, S_{12} and S_{44} and the direction cosines, l, m and n, as follows:

$$1/E=S_{11}-(2S_{11}-2S_{12}-S_{44})\times(l^2m^2+m^2n^2+n^2l^2), \quad (1)^{30}$$

where $(l^2m^2+m^2n^2+n^2l^2)$ is called the orientation function, $f(l, m, n)$. Since $1/E$ is linear in $f(l, m, n)$, a straight line should result when the reciprocals of the values obtained for Young's modulus are plotted against $f(l, m, n)$. Fig. 6 is such a plot for the values given in Table III. The points, with the exception of two,[31] lie within experimental error on a straight line. This is true in spite of the fact that these crystals differ widely in composition, some even being outside the beta-phase. The value of S_{11}, the intercept on the $1/E$ axis ($f=0$), is 0.448×10^{-11} cm^2/dyne. This corresponds to a Young's modulus of 2.23×10^{11} dynes/cm^2 in the [100] direction, in which direction the modulus is a minimum. The maximum value of the modulus obtained from the reciprocal of the ordinate at $f(l, m, n)=\frac{1}{3}$

more, a cylindrical roller on a flat block is used in place of one of the knife edges, since it was found that with two knife edges a frictional drag occurred. This was undoubtedly the cause of the small hysteresis observed by Hanson. The fact that no such hysteresis exists for zinc crystals when the roller is used is now definitely established. Van Allen also obtained no hysteresis when measuring Young's modulus for a zinc crystal by a direct stretch method (Thesis, State University of Iowa, 1936).

[27] The extra 500 g was acting at the most, for 10 seconds.

[28] C. F. Elam, Proc. Roy. Soc. **A153**, 273 (1935–36).

[29] Slip planes are not definitely known for beta-brass. The glide direction is probably [111] according to Elam and the slip plane possibly (110) or (112).

[30] E. Schmid and W. Boas, *Struktur und Eigenschaften der Materie XVII, Kristallplastizität.*

[31] The discrepancies for these two points are definitely greater than can be attributed to experimental error. The writer is unable to account for them.

is 19.9×10^{11} dynes/cm². This is for the [111] direction, or space diagonal. The modulus at $f=0.25$ includes among other possible directions, the face diagonal [110]. This value is 6.54×10^{11} dynes/cm². The material shows an unusually high degree of elastic anisotropy as may be seen from the large value, 8.94, of the ratio of the maximum to the minimum modulus in comparison with other metal crystals. For instance some metals of face-centered cubic structure have values of this ratio: Al 1.20; Cu 2.85; Au 2.72; Ag 2.64; alpha-brass 3.41. For body-centered cubic alpha-iron the ratio is 2.15 while tungsten (also b.c.c.) is practically isotropic.[32] Zinc, which is hexagonal, has a ratio of 3.6.[33] That there is no simple connection between the degree of anisotropy and the particular type of cubic lattice, is perhaps not surprising because of the fact that the elastic behavior does not depend primarily on the geometry of the structure, but on the electrostatic energy of the valence electrons and ions, plus an exchange energy caused by overlapping of ions.[34]

The slope of the line of Fig. 6 is obviously, from Eq. (1), equal to the combination $-(2S_{11}-2S_{12}-S_{44})$. From this slope and the value of S_{11} the value of the quantity $(2S_{12}+S_{14})$ may be computed. It is 0.28×10^{-13} cm²/dyne. The two constants S_{12} and S_{44} cannot be found separately from measurements of Young's modulus alone.

Although this determination of the elastic parameters is not complete and cannot be regarded as of high precision chiefly because of the lack of sufficiently uniform dimensions of the crystals, it is so far as the writer knows, the first attempt to study the elastic behavior of single crystals of this alloy. In spite of the disabilities mentioned, the type of stress-strain relation is clearly shown. The small (or no) dependence of the elastic parameters on the composition is very remarkable particularly when it is remembered that crystals distinctly outside the beta-phase fall in line with the others. The very large anisotropy of Young's modulus with direction of the lattice is a particularly interesting feature. It seems very likely that this is largely because of the high degree of order and that it might become considerably less above the critical temperature.

Acknowledgment

The writer wishes to express sincere appreciation to Professor E. P. T. Tyndall for suggesting this problem and for much helpful advice and many valuable suggestions throughout the work. The writer also thanks the Physics Department of the State University of Iowa for providing facilities for this investigation, Mr. J. G. Sentinella for making the molds and constructing the goniometer, and Helen H. Webb, the author's wife, for her assistance in all phases of the work.

[32] Values of cubic metals from tables in E. Schmid and W. Boas: *Kristallplastizität*, pp. 200–202.

[33] This is the ratio of $E_{90}/E_0=S_{11}/S_{33}$. E. P. T. Tyndall, Phys. Rev. **47**, 398 (1935). The max./min. ratio is slightly larger.

[34] Reference 20, Chapter IV.

Viscosity in an Expanding Bubble

EVERETT C. WESTERFIELD AND W. B. PIETENPOL
Department of Physics, University of Colorado, Boulder, Colorado

(Received June 15, 1938)

The rate of doing work per unit volume in a homogeneous medium is shown to be $dw/dt = \nabla(\mathbf{v} : \Psi)$ where $\mathbf{v}$ is the velocity vector and Ψ the stress dyadic. For an incompressible fluid this becomes $dw/dt = 2\mu\Phi : \Phi + (\rho/2)dv^2/dt$, where μ is the coefficient of viscosity, Φ the symmetric rate of strain dyadic and ρ the mass density. From this relation, it is shown that the pressure difference between the inside and outside of a steadily expanding bubble composed of an incompressible viscous fluid, is given by $p_1 - p_2 = 2\gamma(r_1^{-1} + r_2^{-1}) + 4\mu K(r_1^{-3} - r_2^{-3})$ where γ is the surface tension, r_1 and r_2 the inner and outer radii of the bubble, respectively, and K is the expansion constant r^3v for any point in the material of the bubble.

INTRODUCTION

A BULB method has been used by one of the authors[1] for the determination of the surface tension of molten glass. Under static conditions the pressure difference between the inside and outside of the bubble is balanced by the surface tension of the liquid. When, however, a bubble is expanding at a uniform rate, a portion of the pressure difference is employed in maintaining the rate of expansion against the viscous forces then introduced. After one has determined the surface tension for the static condition, one may then determine the coefficient of viscosity. Experiments are under way for the determination of the viscosity of molten glass by this method.

The theory has been developed for the general case of an expanding bubble with the assumption that the material is mobile to the extent that forces of restitution caused by what is generally termed elasticity may be neglected. The method of approach is from the standpoint of dyadics as employed by Page.[2] When we have occasion to refer to this text explicitly in the course of the paper, we will employ the abbreviation (*TP*).

RATE OF DOING WORK IN A VISCOUS FLUID

In the notation of Page (*TP*, Chap. VI) where Ψ is the stress dyadic and $\mathbf{v}$ the velocity of the medium, the force on a surface element $d\mathbf{s}$ of the volume τ will be $(d\mathbf{s})\cdot\Psi$. Since Ψ is symmetric, this may be written as $\Psi\cdot d\mathbf{s}$ and hence the rate at which the surface forces do work in the volume τ is $\int_s \mathbf{v}\cdot\Psi\cdot d\mathbf{s}$. The rate per unit volume is then given by

$$dw/dt = \lim_{\tau=0} (1/\tau)\int_s \mathbf{v}\cdot\Psi\cdot d\mathbf{s} = \nabla\cdot\overline{\mathbf{v}\cdot\Psi} \quad (1)$$

or, in terms of the Gibbs double dot product

$$dw/dt = \nabla\overline{\mathbf{v} : \Psi}. \quad (2)$$

As the body force in the medium is $\nabla\cdot\Psi$ per unit volume (*TP*, 52–1) the time rate of increase of kinetic energy per unit volume is

$$(d/dt)(\tfrac{1}{2}\rho v^2) = \mathbf{v}\nabla : \Psi, \quad (3)$$

where ρ is the density. Hence

$$dw/dt = (d/dt)(\tfrac{1}{2}\rho v^2) + \Psi : \nabla\mathbf{v}. \quad (4)$$

From (*TP* 76–12),

$$\begin{aligned}\Psi : \nabla\mathbf{v} &= -(p + \tfrac{2}{3}\mu\nabla\cdot\mathbf{v})\nabla\cdot\mathbf{v} + 2\mu\Phi : \nabla\mathbf{v} \\ &= -(p + \tfrac{2}{3}\mu\nabla\cdot\mathbf{v})\nabla\cdot\mathbf{v} + 2\mu\Phi : \Phi, \quad (5)\end{aligned}$$

since the double dot product of a symmetric with a skew-symmetric dyadic is zero, and Φ is the symmetric part of $\nabla\mathbf{v}$. Hence (4) becomes

$$\begin{aligned}dw/dt = (d/dt)(\tfrac{1}{2}\rho v^2) \\ -(p + \tfrac{2}{3}\mu\nabla\cdot\mathbf{v})\nabla\cdot\mathbf{v} + 2\mu\Phi : \Phi. \quad (6)\end{aligned}$$

For an incompressible fluid $\nabla\cdot\mathbf{v} = 0$, and (6) reduces to

$$dw/dt + \tfrac{1}{2}\rho(dv^2/dt) + 2\mu\Phi : \Phi \quad (7)$$

while, if the motion is such that the rate of change of kinetic energy is zero, the first term drops out and

$$dw/dt = 2\mu\,\Phi : \Phi. \quad (8)$$

[1] W. B. Pietenpol, Physics 7, 26 (1936).
[2] L. Page, *Introduction to Theoretical Physics* (Van Nostrand, 1935), second edition.

If, in addition, the motion of the fluid is irrotational, $\Phi = \nabla \mathbf{v}$ and (8) may be written

$$dw/dt = 2\mu(\nabla \mathbf{v}) : (\nabla \mathbf{v}). \quad (9)$$

Rate of Doing Work in an Expanding Bubble

Consider the material of a bubble of thickness $r_2 - r_1$, where r_1 is the inner radius and r_2 the outer radius of the bubble, divided into two concentric bubbles by a sphere of radius r. As the bubble expands or contracts let r vary in such a manner as to maintain the original division of material. Then for an incompressible fluid

$$(d/dt)(r^3 - r_1^3) = 3r^2 dr/dt - 3r_1^2 dr_1/dt = 0. \quad (10)$$

If the only motion of the bubble is that of radial expansion, $v = dr/dt$ for the velocity of the fluid at a distance r from the center of the bubble and

$$r^2 v = r_1^2 v_1 = K, \quad (11)$$

where K is a spatial constant. Since the vector velocity $\mathbf{v}$ at any point is directed along the radius vector $\mathbf{r}$,

$$\mathbf{v} = \mathbf{r}_0 v, \quad (12)$$

and

$$\nabla \mathbf{v} = (\nabla v)\mathbf{r}_0 + v \nabla \mathbf{r}_0, \quad (13)$$

where the zero subscript is used to denote the unit vector. From Eq. (11)

$$\nabla v = K \nabla (1/r^2) = -2K\mathbf{r}_0/r^3 = -2\mathbf{r}_0 v/r, \quad (14)$$

and from (*TP*, 79–4)

$$\nabla \mathbf{r}_0 = (1/r)(\boldsymbol{\theta}_0 \boldsymbol{\theta}_0 + \boldsymbol{\phi}_0 \boldsymbol{\phi}_0), \quad (15)$$

hence

$$\nabla \mathbf{v} = (v/r)(-2\mathbf{r}_0 \mathbf{r}_0 + \boldsymbol{\theta}_0 \boldsymbol{\theta}_0 + \boldsymbol{\phi}_0 \boldsymbol{\phi}_0) \quad (16)$$

and

$$\nabla \mathbf{v} : \nabla \mathbf{v} = 6v^2/r^2. \quad (17)$$

For a bubble expanding at a slow steady rate so that the rate of change of kinetic energy is negligible, Eqs. (9) and (17) give

$$dw/dt = 12\mu v^2/r^2 = 12\mu K^2/r^6 \quad (18)$$

as the rate per unit volume for doing work against the viscous stresses in the fluid. Integrated throughout the material of the bubble, this gives

$$dW/dt = 16\pi\mu K^2(r_1^{-3} - r_2^{-3}), \quad (19)$$

for the total rate of doing work in the bubble.

If p_1 is the gas pressure on the inside of the bubble, and p_1' the opposing pressure exerted by the surface tension on the inside of the bubble, the net pressure on the inside of the bubble is given by

$$p_1'' = p_1 - p_1' = p_1 - 2\gamma/r_1, \quad (20)$$

where γ is the surface tension. The work done per second by this pressure is

$$dW_1/dt = 4\pi p_1'' r_1^2 v_1 = 4\pi K p_1 - 8\pi K\gamma/r_1. \quad (21)$$

Similarly, the work done per second by the net pressure on the outside of the bubble is given by

$$dW_2/dt = -4\pi K p_2 - 8\pi K\gamma/r_2. \quad (22)$$

But since the work done by the net pressures must equal the work done against the internal stresses, Eqs. (19), (21) and (22) may be combined to give

$$p_1 - p_2 = 2\gamma(r_1^{-1} + r_2^{-1}) + 4\mu K(r_1^{-3} - r_2^{-3}). \quad (23)$$

If the thickness d of the bubble is small compared to the average radius, Eq. (23) may be replaced by the approximate relation

$$p_1 - p_2 = 4\gamma/r + 12\mu v d/r^2, \quad (24)$$

where r is the average radius, and v the average radial velocity of the bubble at any given instant and $p_1 - p_2$ is the pressure difference required to balance the viscous forces in a steadily expanding bubble of finite thickness. This formula is particularly applicable to bubbles of extremely viscous materials such as molten glass.

Actinoelectric Effects in Tartaric Acid Crystals*

JAMES J. BRADY AND WILLIAM H. MOORE
Oregon State College, Corvallis, Oregon
(Received October 26, 1938)

Tartaric acid crystals illuminated with light from a carbon arc exhibit a flow of current when connected to a galvanometer without the aid of an impressed battery. This actinoelectric effect is greatly dependent upon the orientation of the crystal with respect to the illuminating beam of light. It is shown that a section of the crystal can be chosen which shows a series of equipotential lines when its surface is examined with two probes while the crystal is illuminated. The measured currents are about 10^{-12} ampere, when the crystal is illuminated with the light from a carbon arc. The effect is a linear function of light intensity for the lower light intensities, but increases more rapidly for higher intensities. The effect is practically independent of temperature in the range from 20°C to −40°C. The maximum spectral response is at approximately 10,500A.

A NUMBER of experimenters[1] have shown that certain crystals, when illuminated, produce an electrical current which can be measured with an electrometer or galvanometer connected in series with the crystal without the aid of an impressed battery. According to Coblentz[2] the term actinoelectricity was used by Hankel to designate the above phenomenon about 95 years ago. Present theories[1] are not entirely satisfactory, and it appears desirable to investigate the effect in more detail.

Most of the crystals used in this investigation were chosen from a supply of commercially prepared tartaric acid crystals.[3] The results were checked, however, with crystals grown in our laboratory. The "dark resistance" of a crystal three mm thick with a cross-sectional area of approximately 50 sq. mm is 2×10^{9} ohms.

The experimental arrangement for carrying out the investigation is shown in Fig. 1. No results are reported when an external source of e.m.f. is used. A carbon arc and a 150-watt gas-filled tungsten filament lamp are used as light sources.

An FP-54 tube is used in a Brown and DuBridge[4] circuit for amplifying the actinoelectric currents. The current sensitivity of the amplifier is 10^{-14} ampere per mm deflection of the galvanometer.

The crystal is held between two brass disks with spring tension on one of the disks. The crystal holder is designed so that the light can be sent either perpendicular or parallel to the direction of the current through the crystal.

Contradictory evidence has been reported by other experimenters as to the origin of the effect. Coblentz,[2] working with molybdenite shows that the seat of the effect is at certain points along the crystal surfaces. Geiger[5] finds, in the case of argentite, no observable effect when the contacts are shielded from light and that the currents are measurable only when at least one of the electrodes is illuminated. Schneider[6] finds, in the case of argentite, that the seat of conversion of light into electronic energy occurs both at the contacts as well as at certain spots on the crystal.

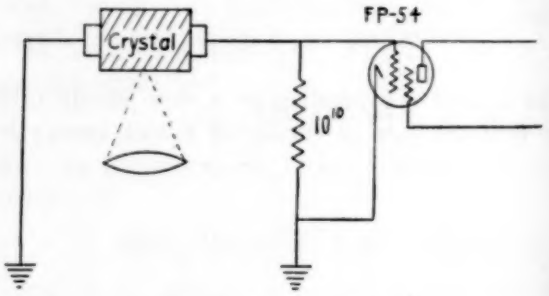

FIG. 1. Experimental set-up.

* Published with the approval of the Monographs Publication Committee, Oregon State College. Research Paper No. 13, Department of Physics, School of Science.

[1] For bibliography and a review of theories see B. Lange, *Photoelements* (Reinhold Publishing Corporation, 1938).

[2] W. W. Coblentz, Scientific Papers of Nat. Bur. of Standards, No. 486, April (1924).

[3] Maximum limits of impurities: SO_3—0.01 percent; Ca—0.001 percent; Fe—0.001 percent; other H. M.—0.000 percent.

[4] H. Brown and L. A. DuBridge, Rev. Sci. Inst. **4**, 532 (1933).

[5] P. H. Geiger, Phys. Rev. **22**, 461 (1923).

[6] W. A. Schneider, Phys. Rev. **31**, 82 (1928).

The experiments with tartaric acid crystals show none of the irregular variations in current as the light beam is moved over the surface of the crystal as reported for instance by Coblentz.[2] There were no "sensitive spots" found in the case of a good clear single crystal although the response in many cases varied in a *regular manner* as the surface was explored with a light beam of approximately one mm diameter.

Figure 2 represents the way in which the current varies with the time of illumination when the light beam is at right angles to the flow of the current. The maximum deflection is reached within the period of the galvanometer and then drops down to a final value. This final current remains constant even though the crystal is illuminated for one-half hour or more. As soon as the light is cut off, the current immediately reverses and then drops to zero in the manner indicated by the curve. The decrease in current which takes place a few seconds after the light is turned on is obviously caused by the building up of a space charge or polarization within the crystal which limits the flow of electrons. When

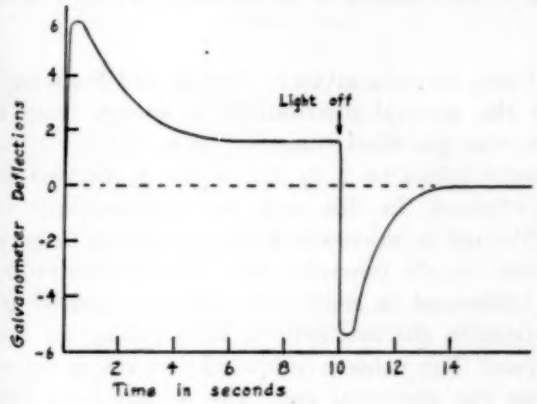

FIG. 2. Variation of actinoelectric current with time of illumination.

the light is turned off, the space charge is neutralized by the rush of electrons in the opposite direction. The residual current, which remains constant after the light has been shining on the crystal for some time, indicates that electrons enter and leave the crystal through the electrodes.

Crystals which appear to have flaws and are not very transparent give results which are notably different from those from good clear crystals. The current, in these crystals, starts out in one direction just after the light is turned on, quickly reverses, and then slowly reaches a maximum (approximately after one minute) in the opposite direction.

Figure 3 represents a single crystal of tartaric acid. When the light beam is parallel to the direction of the current (longitudinal effect), the following results are recorded. With the *c* axis vertical, the electrodes against the orthopinacoid

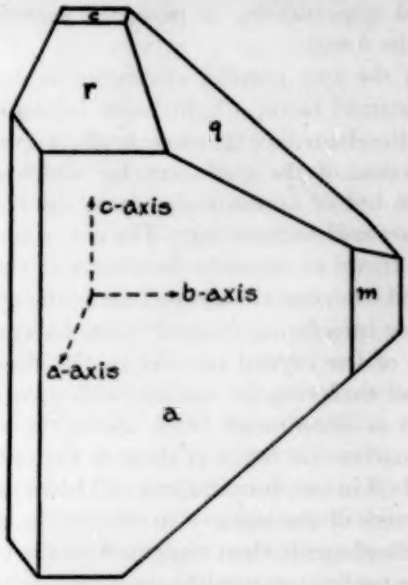

FIG. 3. A monoclinic crystal of tartaric acid with the crystal faces labeled according to crystallographic notation. *a*—orthopinacoid; *q*—clinodome; *c*—basalpinacoid; *r*—orthodome.

faces, and the clinodome face to the right looking at the illuminated orthopinacoid face, the electrons in the crystal flow in the same direction as the light energy. In this case, a residual current remains after long periods of illumination. When the crystal is turned through 180° about the *c* axis so that the opposite orthopinacoid face is turned toward the light, the electron flow is still in the direction of light propagation. When the crystal is turned from this position through 180° about the *b* axis, the electron flow is still in the direction of light propagation, but no residual current remains after 30 sec. or more of illumination. If the crystal is now turned through 180° about the *c* axis, the electrons flow in a direction *opposite* to the direction of light propagation. In this case, no residual current remains. These

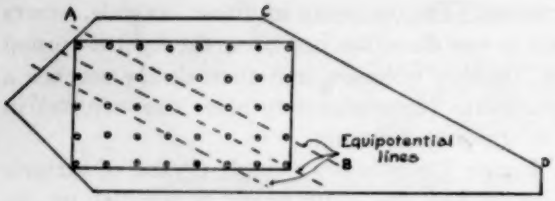

FIG. 4. A section of the crystal cut parallel to the clinodome face.

results are surprising because the crystal, to all outward appearances, is perfectly symmetrical about the *b* axis.

With the two parallel electrodes against the orthopinacoid faces, a light beam falling on the upper clinodome face (transverse effect) produces a deflection of the galvanometer which is just equal to but of opposite sign from the response of the lower clinodome face. The electrons in the crystal travel in opposite directions as the light is shifted from one clinodome face to the other.

A very interesting study is made by cutting a section of the crystal parallel to the clinodome face and exploring its surface with two probes while it is illuminated from above the surface with a carbon arc lamp. A sheet of Cellophane is marked off in two-mm squares and holes made at the corners of the squares to receive the probes. The Cellophane is then cemented to the crystal, and the probes are used to measure the current between two points on the crystal surface as the probes are inserted into the holes in the Cellophane. No current is observed when the two probes are placed anywhere on the line *AB* (Fig. 4). The same is true for all lines parallel to *AB*. These lines are very nearly parallel to the side *CD*. Appreciable galvanometer deflections were noted when one probe was placed at a point on the line *AB* and the other probe was placed at a point on one of the other equipotential lines.

Light Intensity Investigation

The way in which the current varies as a function of light intensity is shown in Fig. 5. The initial value of the current (Fig. 2) is used. The experimental arrangement shown in Fig. 6 is used to obtain this curve. The light intensity is varied by changing the number of glass plates interposed between the carbon arc and the crystal. The light reflected from the glass plate *A* falls on a light shielded photronic cell which is connected to a galvanometer. The light intensity falling on the photronic cell is in a region where the response of the cell is linear. The light intensity falling on the crystal is then directly proportional to the deflections of the photronic cell galvanometer. The curve is similar to that obtained by Schneider[6] for the actinoelectric effects in argentite.

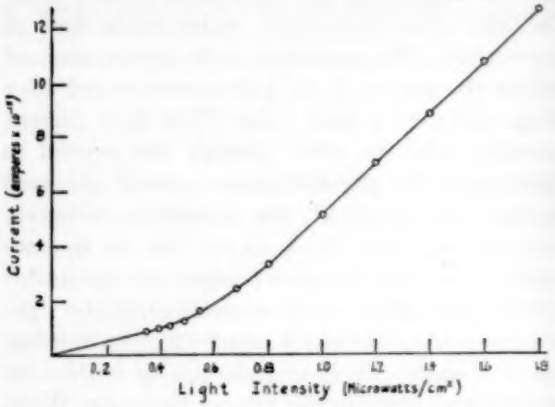

FIG. 5. The variation of the actinoelectric current with light intensity.

From the data given by Barnes and Forsythe[7] for the spectral distribution in energy from a 100-watt gas-filled tungsten lamp, the total intensity falling on a sq. cm at one m distance is determined. In this way the thermocouple is calibrated in microwatts/cm² of radiant energy falling on the junction. After the thermocouple is calibrated in microwatts/cm², it is used to determine the intensity of light falling on the crystal. This value is compared with the response from the photronic cell. The output from the photronic cell is then used to measure the light intensities in microwatts/cm².

Effect of Temperature

In order to study the effect of temperature on the current response, a crystal is mounted in an evacuated Pyrex tube to prevent moisture from collecting on the crystal as its temperature is lowered. The glass tube is covered with tinfoil except for the portion near the electrodes and is

[7] B. T. Barnes and W. E. Forsythe, J. Opt. Soc. Am. **26**, 313 (1936).

then surrounded with solid carbon dioxide. The results show no effects of temperature greater than experimental error in the range from −40 to +30°C.

This is in agreement with the findings of Coblentz[2] for molybdenite.

Spectral Response

Figure 7 shows the way in which the actinoelectric current varies with the wave-length of the light. A carbon arc is used as a light source and is dispersed by means of a double-prism monochromator. The arc has a maximum intensity at approximately 8500A. The energy distribution of the light from the monochromator is determined by means of a thermocouple designed for this purpose. The actinoelectric currents are then corrected for the energy distribution, and the currents are plotted on an equal energy scale. Because of the small galvanometer deflections the monochromator slits must be widened so the wave-length band has a width of 300A at 5500A.

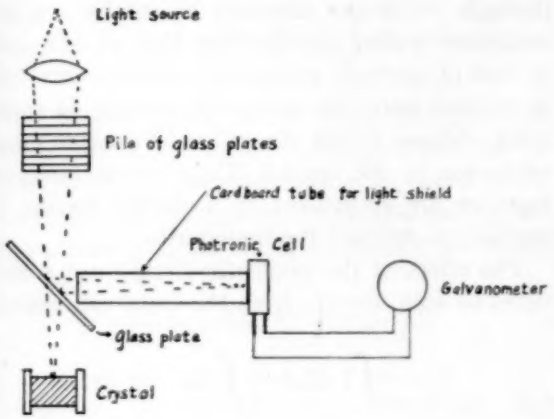

FIG. 6. The experimental set-up for measuring the variation of current with light intensity.

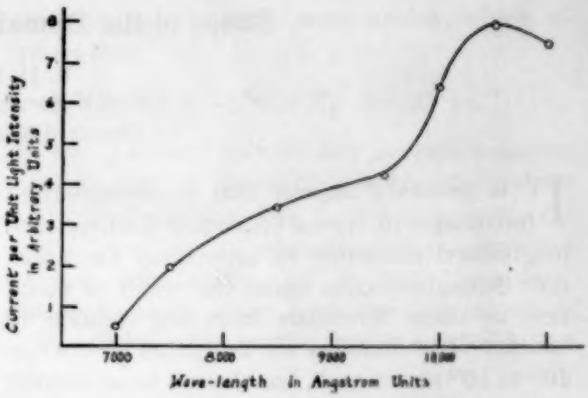

FIG. 7. Spectral response curve.

The maximum response can be seen to be at approximately 10,500A. The light is in a direction perpendicular to the electron flow through the crystal in this case. The actinoelectric response is linear with light intensity for the intensities emerging from the monochromator.

In conclusion, the authors wish to express their thanks to Dr. W. D. Wilkinson of the Geology Department of Oregon State College for orienting the crystals. The senior author wishes to express his appreciation to the Physics Department of the University of California for the loan of the monochromator and to the National Academy of Sciences for the grant-in-aid which made possible the purchase of some of the apparatus used in this research.

Shape of the Domains in Ferromagnetics

E. H. KENNARD
Cornell University, Ithaca, New York
(Received November 28, 1938)

IT is generally agreed that a demagnetized ferromagnetic crystal consists of domains each magnetized uniformly to saturation, the apparent demagnetization being the result of variation in these directions from one domain to another. The domains are estimated to contain 10^{12} to 10^{15} atoms each, but there is no agreement as to their shape. The common assumption that they are roughly cubical can scarcely be justified. It seems worth while to restate the objection to this assumption in a more concrete form; then the condition which must be satisfied by the equilibrium positions of domain boundaries in an ideal cubical crystal will be thrown into a new form.

In a demagnetized iron crystal one-sixth of the domains are commonly assumed to be magnetized to saturation in each of the directions parallel to the three axes. Now if such a domain were more or less round or cubical in form, it would necessarily be surrounded by a local field of the order of I_0, the intensity of magnetization within a domain; this becomes evident upon recalling the formulas for a sphere. This local field might happen to be offset at some points by fields due to other sources, but the cancellation cannot be universal; for over the part of the surface where one domain abuts upon another in which the direction of magnetization differs by a right angle or more, there is a sheet of poles of density roughly equal to I_0, and hence a jump in the normal component of H roughly equal to $4\pi I_0$. In an iron crystal, with $I_0=1800$, the resulting local fields would be of the order of 2000 oersteds. Yet it is observed that an applied field of less than 10 oersteds suffices to magnetize the crystal as a whole to saturation. The conclusion seems inescapable that cubical domains could not be stable; they would tend to alter each other's magnetization so as to become lined up into rows forming long slender domains of larger size. Thus we reach by elementary reasoning the old conclusion that *the domains in iron, and presumably in all ferromagnetic crystals, must have the form either of slender filaments or of thin plates, magnetized longitudinally.*[1] The plate form was suggested for cobalt by Landau and Lifschitz.[2]

The domain boundaries are assumed to be so located as to minimize the total energy due to the Weisz-Heisenberg or quantum field and to magnetic interaction. Considering only cubic crystals, let us assume all fields to be weak enough so that each domain is magnetized sensibly along one axis. Then the quantum energy varies only because there is an excess of it in the domain boundaries, proportional to their area. Presumably there will be a transition layer, through which the direction of the local magnetization varies rapidly from that of one axis to that of another; additional excess energy will be present here due to the occurrence of spins lying oblique to the directions of easiest magnetization in the crystal. These excess energies together are equivalent to a *surface tension* T tending to contract the boundaries.

The effect of the magnetic energy can sometimes be seen directly from the usual expression,

$$U=-\int \mathbf{I}\cdot\mathbf{H}_0 d\tau+\int (\mathbf{H}_I^2/8\pi)d\tau,$$

where $\mathbf{I}$ is the magnetization and $\mathbf{H}_I$ the field due to it (both macroscopic, but on the scale of the domains), and $\mathbf{H}_0$ is the field due to all other sources. In the absence of $\mathbf{H}_0$ the magnetic forces will cause the domains to shift so as to obliterate $\mathbf{H}_I$. But in many situations a criterion involving only conditions at a single point on the boundary is more useful.

To obtain this, suppose that unit area of a boundary, with principal curvatures C' and C'', shifts a distance δs normal to itself. Then by surface-tension theory the boundary energy is

[1] Cf. R. H. de Waard, Phil. Mag. **4**, 641 (1927); F. Bloch, Zeits. f. Physik **74**, 295 (1932).
[2] L. Landau and E. Lifschitz, Physik Zeits. Sowjetunion **8**, 153 (1935).

increased by $(C'+C'')T\delta s$. The increase in magnetic energy is

$$\delta U = -\int \mathbf{H}_0\cdot\delta\mathbf{I}d\tau - \tfrac{1}{2}\delta\int \mathbf{I}\cdot\mathbf{H}_I d\tau = -\int \mathbf{H}\cdot\delta\mathbf{I}d\tau,$$

where $\mathbf{H}=\mathbf{H}_0+\mathbf{H}_I$, and the last expression results from the following transformations, in which we introduce the potential due to I, so that $\mathbf{H}_I=-\nabla\Omega$, $\nabla^2\Omega=-\text{div. }\mathbf{H}_I=4\pi\text{ div. I}$, and then carry out integrations by parts as in the divergence theorem, the integrated terms vanishing always at infinity:

$$\int \mathbf{I}\cdot\delta\mathbf{H}_I d\tau = -\int \mathbf{I}\cdot\nabla\delta\Omega d\tau = \int \delta\Omega\text{ div. I}d\tau$$

$$= \int \delta\Omega\nabla^2\Omega d\tau/4\pi = \int \Omega\,\nabla^2\delta\Omega d\tau/4\pi$$

$$= \int \Omega\text{ div. }\delta\mathbf{I}d\tau = \int \mathbf{H}_I\cdot\delta\mathbf{I}d\tau.$$

Now at any point in the transition layer $\delta I_\perp = -I_\perp'\delta s$, $\delta\mathbf{I}_\parallel = -\mathbf{I}_\parallel'\delta s$; subscripts denote, respectively, the perpendicular component in the direction of δs and the vector parallel component, and primes indicate the space derivative. Hence

$$\delta U = \delta s\int (\mathbf{H}_\parallel\cdot\mathbf{I}_\parallel' + H_\perp I_\perp')dz$$

integrated through the transition layer. But $\mathbf{H}_\parallel'=0$, and $H_\perp' = -4\pi I_\perp'$ by Gauss' law; thus, if subscripts 2 and 1 indicate values on the two sides of the boundary,

$$\int \mathbf{H}_\parallel\cdot\mathbf{I}_\parallel' dz = \mathbf{H}_\parallel\cdot\int \mathbf{I}_\parallel' dz = \mathbf{H}_\parallel\cdot(\mathbf{I}_{\parallel 2}-\mathbf{I}_{\parallel 1});$$

$$\int H_\perp I_\perp' dz = -\int H_\perp H_\perp' dz/4\pi$$

$$= -(H_{\perp 2}^2 - H_{\perp 1}^2)/8\pi = \tfrac{1}{2}(H_{\perp 2}+H_{\perp 1})(I_{\perp 2}-I_{\perp 1}).$$

Hence we can write, since $\mathbf{H}_\parallel = (\mathbf{H}_{\parallel 2}+\mathbf{H}_{\parallel 1})/2$,

$$\delta U = \tfrac{1}{2}(\mathbf{H}_1+\mathbf{H}_2)\cdot(\mathbf{I}_2-\mathbf{I}_1)\delta s.$$

The condition for equilibrium is now that the total change in energy must vanish, which requires that

$$\tfrac{1}{2}(\mathbf{H}_1+\mathbf{H}_2)\cdot\mathbf{I}_1 = \tfrac{1}{2}(\mathbf{H}_1+\mathbf{H}_2)\cdot\mathbf{I}_2 + (C'+C'')T.$$

If the quantity on the left in this equation exceeds that on the right, the boundary shifts away from medium No. 1, and vice versa. (C' and C'' are positive when they mean convexity toward domain No. 2.) A *plane* boundary, therefore, shifts away from the side on which $\frac{1}{2}(\mathbf{H}_1+\mathbf{H}_2)\cdot\mathbf{I}$ is the greater, and is in equilibrium when

$$\tfrac{1}{2}(\mathbf{H}_1+\mathbf{H}_2)\cdot\mathbf{I}_1 = \tfrac{1}{2}(\mathbf{H}_1+\mathbf{H}_2)\cdot\mathbf{I}_2.$$

Here $\frac{1}{2}(\mathbf{H}_1+\mathbf{H}_2)$ represents the mean field, due to all other sources than free poles on the part of the boundary under consideration; for equilibrium of a *plane* boundary this mean field must be equally inclined to I in the two adjacent domains.

The magnitude of the surface tension is not definitely known. According to Bloch[3] the transition layer between domains represents a compromise between the tendency of the quantum forces to decrease the gradient of the local magnetization and the tendency of the crystal forces to turn all spins into the direction of a crystal axis, and T should be of the order of the work required to turn them halfway from one axis to

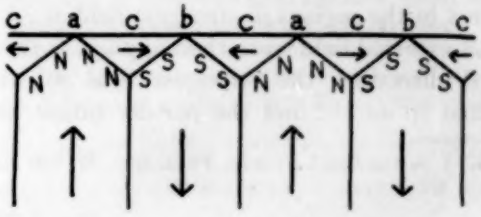

FIG. 1.

another in a layer about 30 crystal spacings thick. In iron this would make $T=2\times10^6\times30\times3\times10^{-8}=0.18$ erg/cm², roughly. If the surface tension is really of this order of magnitude, the shape of the domain boundaries must be determined largely by the local magnetic fields.

The rules obtained above are useful in making qualitative studies. It is readily verified that cubical domains would tend, because of magnetic

[3] F. Bloch, *Handbuch der Radiologie*, Vol. 6, Part 2 (1934), p. 481.

interaction, to change as suggested above. Equilibrium in an ideal crystal seems, moreover, to require that the domains extend to the surface; for any domain ending in the interior tends to shrivel up, both because of the surface tension and because of magnetic action. The field due to the domain itself tends to collapse its sides, and the field due to the poles at one end tends to pull in the other end. In an actual crystal, however, there appears to exist a certain resistance to the motion of domain boundaries, so that it might be sufficient for a domain to minimize its own magnetic field by tapering very gradually to a point, or to a sharp edge.[4]

At the surface, again, the magnetization will adjust itself so as to keep the local fields within bounds. A possible arrangement below a surface perpendicular to one crystal axis seems to be as suggested in Fig. 1. If the surface tension were absent, the magnetization, shown by arrows, would be carried round through triangular prisms lying parallel to the surface, with their oblique faces at 45° to the axis (as suggested for cobalt by Landau and Lifschitz[2]), and there would be no free poles at all. In reality, however, the boundaries must be pulled up a little by their surface tension, with the production of free poles as shown. The local fields due to such poles might be the cause of the powder patterns that are often observed; a magnetic colloid would collect in the regions of strongest field at $ccc\cdots$. If an external field were then applied in the upward direction, the strongest field might be shifted to $aa\cdots$, and the powder ridges would occur there; whereas in a reverse field they would be at $bb\cdots$. Thus the ridges in the presence of a field would be in locations halfway between the no-field positions and twice as far apart; this is just what is observed.[5]

The application of the field would also change the domains somewhat, of course. In the figure an upward field would broaden those under $aa\cdots$ and should probably tend to make their tops dome-shaped, with an increase in the pole strength; whereas the tops of the domains under $bb\cdots$ would become more peaked, with a decrease in the pole strength there, or even a reversal of its sign. These changes would intensify the phenomena just described, at least so long as the field did not become too strong.

Even if the effect of surface tension is negligible, an imperfection in the triangular prisms might result from the resistance which is observed to impede the motion of domain boundaries. It is not so easy, however, to understand how the plate-like domains can turn square corners as freely as they must do to fit the powder patterns. Furthermore, isotropic demagnetization is hard to imagine, for spindles and plates lying in all three directions can scarcely fit together without gaps. In a demagnetized crystal, do the shortest dimensions of all domains perhaps lie in the same plane? If so, the observed magnetization curve should differ according as the crystal is demagnetized by use of a parallel or a perpendicular field. This point might be worth testing experimentally.

[4] K. J. Sixtus and L. Tonks, Phys. Rev. **37**, 930 (1931).

[5] W. C. Elmore, Phys. Rev. **51**, 982 (1937); **53**, 757 (1938).

LETTERS TO THE EDITOR

Prompt publication of brief reports of important discoveries in physics may be secured by addressing them to this department. Closing dates for this department are, for the first issue of the month, the eighteenth of the preceding month, for the second issue, the third of the month. Because of the late closing dates for the section no proof can be shown to authors. The Board of Editors does not hold itself responsible for the opinions expressed by the correspondents.

Communications should not in general exceed 600 words in length.

On the Interchange Energy of Two Free Electrons

In this note, a comparison is made of the Coulomb and interchange energies for a system consisting of two free electrons moving arbitrarily with respect to each other.

The following equation given by Dirac[1] represents the perturbing energy for a system of similar particles, and contains the expressions for Coulomb and interchange energies.

$$V = V_{11} - \tfrac{1}{2}\sum_{r<s} V_{rs}\{1+(\sigma_r, \sigma_s)\}, \tag{1}$$

where V is the perturbing energy, σ is the spin dynamical variable, and the subscript rs refers to an interchange of the r and s electrons. For any permutation, P, the following equation is given:

$$V_P = (P\alpha|\,V\,|\alpha) = \int\int (P\alpha|\,q')dq'(q'|\,V\,|q'')dq''(q''|\,\alpha)$$

where α refers to the states and q to the coordinates of the electrons.

In order to evaluate the integrals involved in Eq. (1), the wave functions are replaced by wave packets representing free electrons. If we choose the coordinate system so that one electron is at the origin, and the other is at the point r_0 on the z axis; and assume that the uncertainty is the same for both electrons, and the same in all directions, we find, after integrating:

$$V_{11} = (e^2/r_0)\ \text{erf}\ (r_0/2^{\frac{1}{2}}\sigma), \tag{2}$$

$$V_{12} = (e^2h/\pi^{\frac{1}{2}}\sigma^3 m v_0)\exp[(-r_0^2/2\sigma^2)-\lambda^2]\int_0^{\lambda}\exp(t^2)dt, \tag{3}$$

$$V = V_{11} - V_{12},$$

where V_{11} is the Coulomb energy, V_{12} is the interchange energy, r_0 is the distance between the electrons, v_0 is the relative velocity between the electrons, $\lambda = 2^{\frac{1}{2}}m\pi v_0\sigma/h$; and σ is the uncertainty.

Having evaluated V_{11} and V_{12}, we may now determine V for several interesting cases.

When the positions of both electrons are known exactly, i.e., when the uncertainty, σ, is equal to zero, V equals e^2/r_0. Thus in this case the interchange energy is zero and the total perturbing energy is simply the Coulomb energy.

When the distance, r_0, between the electrons is large, the interchange energy is negligible compared to the Coulomb energy, i.e., V_{12}/V_{11} approaches zero, as r_0 approaches infinity. Thus the interchange energy diminishes as the relative velocity between the electrons increases. From this it is seen, as would be expected, that the interchange energy is dependent upon the time during which the electrons are in the neighborhood of each other.

Finally, since V_{12} is a maximum when v_0 is zero (r_0 and σ remaining fixed), it is interesting to calculate V for this case. It is found by making $\lambda \to 0$ in Eq. (3), that

$$V = (e^2/r_0)\ \text{erf}\ (r_0/2^{\frac{1}{2}}\sigma) - (e^2 2^{\frac{1}{2}}/\sigma\pi^{\frac{1}{2}})\exp(-r_0^2/2\sigma^2).$$

Figure 1 shows the variation of V_{11}, V_{12} and V, for various values of r_0/σ.

From curve I it is seen that the interchange energy is of considerable importance when the uncertainty of position of the electrons is of the order of magnitude of the distance between them. However, as the wave packets, representing the electrons, become separated, the Coulomb energy approaches the classical Coulomb energy, and the interchange energy approaches zero.

I wish to thank Dr. Boris Podolsky, University of Cincinnati, for suggesting this problem, and for many helpful discussions.

CARL A. LUDEKE*

Graduate School,
University of Cincinnati,
Cincinnati, Ohio,
November 30, 1938.

* Now at John Carroll University, Cleveland, Ohio.

[1] P. A. M. Dirac, *Quantum Mechanics*, second edition, p. 228, Eq. (38).

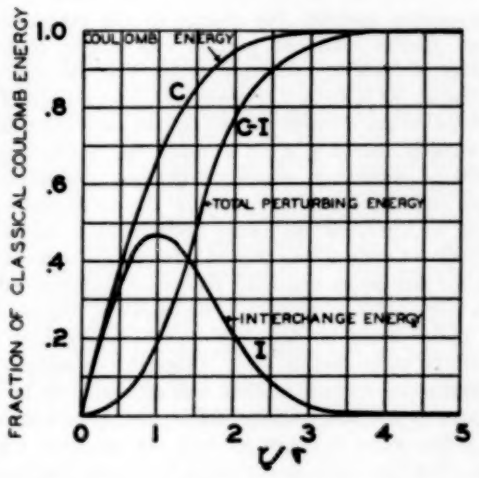

FIG. 1. Energy relations for two electrons at rest relatively to each other. C = Coulomb energy/classical Coulomb energy = $V_{11}/(e^2/r_0)$; I = Interchange energy/classical Coulomb energy = $V_{12}/(e^2/r_0)$; $C-I$ = Total perturbing energy/classical Coulomb energy = $V/(e^2/r_0)$.

Cosmic Rays and Radioactive Potassium

It is probably well to put on record the results of an experiment completed last spring. As A. K. Brewer has pointed out,[1] the present abundance of radioactive K^{40} and its known life indicate that practically all the Ca and A now existing on the earth must have been produced by its disintegration. This conclusion seems unavoidable unless the supply of K^{40} has been replenished in some way. Several nuclear physicists stated to the writer their belief that K^{40} is formed from K^{39} by the absorption of a neutron, one source of which would be cosmic rays. For such an hypothesis the present intensity of cosmic rays seems inadequate, but two facts give it a certain plausibility, namely, that radioactivity seems to be confined to the outer crust of the earth and that, although there is no evidence of large differences in the radioactivity of potassium samples, it is true that most of those tested are from sources which have been near the surface of the earth during a large part of geologic time. It was suggested to the writer that we investigate this idea since the necessary equipment for testing small amounts of potassium was available here.

For this purpose Dr. H. J. Fraser of the geology department procured for us samples from an old geological formation in Canada in which a continuous mass of granite extends from the surface to great depths. The rock from which these samples was taken had not been subjected to the action of water and we can state with certainty that, during geologic time, it has never been closer to the surface than it now lies. A piece of granite from the greatest depth, 2500 feet, was given to Mr. D. K. Beavon, who under the direction of Dr. E. H. Swift of the Chemistry Department, prepared a 22-mg sample of KCl from it.

The counter on which the measurements were made was the one used for determining the radioactivity of the separated isotopes of rubidium.[2, 3] It is a cylindrical counter one cm in diameter and three cm long with an aluminum wall 0.00125 cm thick. The sample was fused as uniformly as possible on the inner surface of a half-cylinder of platinum foil of one cm radius and two cm length, which, for counting, was swung into position concentric with the counter so that all parts of the sample were equidistant from its center. The bare foil when in place gave the standard background count of one per minute, which 20 mg of ordinary KCl should increase to about two per minute. It was calculated that with such thin samples errors due to absorption with uneven distribution would be negligible. Redistribution of the samples confirmed this conclusion by leaving the count unchanged. Similar sized samples of chemically pure KCl and of KCl specially prepared from K_2SO_4 to avoid radioactive contamination, were mounted in the same way. Alternate fifteen-minute counts were made on the sample and a standard screen, until at least 400 counts on each were recorded. Such a set constitutes a "run." Repeated runs were made on all samples, sometimes with a moistening with HCl and redistribution between runs. The C.P. and the specially prepared specimens gave nearly identical counts, but the Canadian sample ran consistently lower. The two final samples were turned over to Mr. J. S. Billheimer for analysis. He found the comparison sample to be pure KCl but the Canadian sample contained about 20 percent of impurity, probably sodium. When correction was made for the impurity, the Canadian sample was found to be about ten percent less radioactive than the laboratory samples. Since the probable error of the experiment is about ten percent, we conclude that the amount of radioactive potassium produced by cosmic rays is unimportant and probably zero.

W. R. SMYTHE

California Institute of Technology,
Pasadena, California,
December 23, 1938.

[1] A. K. Brewer, Ind. and Eng. Chem. **30**, 893 (1938).
[2] W. R. Smythe and A. Hemmendinger, Phys. Rev. **51**, 178 (1937).
[3] A. Hemmendinger and W. R. Smythe, Phys. Rev. **51**, 1052 (1937).

Photoconductivity of Metal Films

R. S. Bartlett[1, 2] in 1925, while working at this laboratory, showed that a photoconductive effect could be observed in thin films of copper, platinum, palladium and bismuth sputtered on glass. On exposure to ultraviolet light at liquid-air temperatures, decreases in resistance up to sixteen parts in one million were recorded. At room temperature, and with frequencies of incident light lower than the ultraviolet range, no effect was noticeable.

To establish whether this effect could be detected in conductors of bulk metal, a further experiment has recently been completed on fine ribbons of copper, platinum and palladium. The illumination was with x-rays in order to insure that appreciable absorption took place throughout the entire thickness of the conductor.

Ribbons approximately 0.01 mm in thickness, 1 mm wide and from 2 to 3 meters in length were rolled from fine wires of the materials mentioned, and wound upon frames so that the majority of the surface could be exposed to an x-ray beam (molybdenum target). At room temperature the resistance of the element was measured by a potentiometer method. No change in the resistance of amount greater than one part in one million could be detected at this temperature when the element was illuminated. At liquid-air temperature, fluctuations of the resistance of the element caused by temperature changes and various parasitic e.m.f.'s made the potentiometer method of detecting resistance changes unsuitable. A shutter was therefore interposed in the x-ray beam and rotated to interrupt the beam 1000 times a second. A steady direct current was passed through the element and the e.m.f. across its terminals fed to an amplifier-oscillograph circuit. No alternating component of frequency of 1000 cycles could be detected on the oscillograph with any of the three metals used. Although the accuracy of the alternating current method was estimated to be only one part in 250,000, because the elements were at most only a few ohms in resistance and the available e.m.f.'s across their terminals limited to a few volts, the method was still sensitive enough to have detected changes in resistance of the order of magnitude of those observed by Bartlett.

The conclusion therefore may be made that either (1) the photoconductive effect present in thin films of these metals sputtered on glass surfaces is a property of the bulk metal which can be caused by radiation of the ultraviolet range only, or (2) that the effect is not a property of bulk metal but is restricted to films alone and is related to their structure,—the effect may be an external photoelectric current passing between discontinuous patches of the film.

The latter alternative would seem to be supported experimentally by recent work by Lovell,[3] and Lovell and Appleyard[4] on the resistance of thin films of the alkali metals.

THOMAS C. WILSON

Sloane Physics Laboratory,
Yale University,
New Haven, Connecticut,
January 6, 1939.

[1] R. S. Bartlett, Phys. Rev. **26**, 247 (1925).
[2] A. T. Waterman, Phys. Rev. **22**, 259 (1923).
[3] A. C. B. Lovell, Proc. Roy. Soc. **A157**, 311 (1936).
[4] A. C. B. Lovell and E. T. S. Appleyard, Proc. Roy. Soc. **A158**, 718 (1937).

On the Upper Limit of the β-Spectrum of ThC″ and ThB

In 1937 Lyman[1] published a paper in which, from the character of the β-spectrum near the upper limit, he points to the existence of a neutrino rest mass different from zero. Subsequently a number of investigators, such as Alichanian, Alichanow and Dzelepow[2] and also Alichanian and Nikitin,[3] undertook a thorough study of the upper limit of the β-spectra.

According to the last authors, the difference between the experimental value for the upper limits and that deduced from the theory of Konopinski and Uhlenbeck[4] determines the magnitude μ_0 of the mass of the neutrino, i.e.

$$W_0-(E_0/511+1)=\mu_0,$$

where W_0 is the extrapolated value of the limiting energy (in mc^2) while E_0 is the experimental value of this energy in kv.

If so, it has to be assumed that the β-decay of different elements is characterized by different values of μ_0 or else to associate each elementary process of β-decay with an odd number of neutrinos, as has been suggested by G. Breit.[5]

However, in our opinion both alternatives are equally unsatisfactory. The comparison of the shape of the experimental β-spectra with that given by Konopinski and Uhlenbeck (KU) has shown that the substitution of the value W_0 (obtained by extrapolating the KU plots) in the expression for the distribution of electrons according to their energies in the β-spectra does not lead to a closer agreement of the experimental β-spectrum with the calculated one. More satisfactory results can be obtained by taking W_0' between the limits

$$(1+E_0/511)<W_0'<W_0.$$

The computations with the experimental results obtained by Alichanian and Zavelsky[6] for ThC″ and ThB are shown in Figs. 1 and 2.

The solid curves refer to the experimental β-spectra for ThC″ and ThB. They are in fairly good agreement with

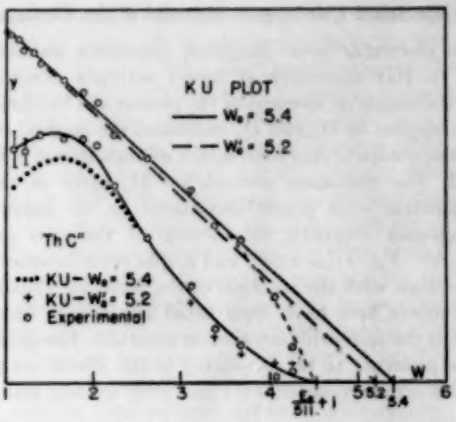

FIG. 1. Konopinski-Uhlenbeck plots and experimental results for ThC″.

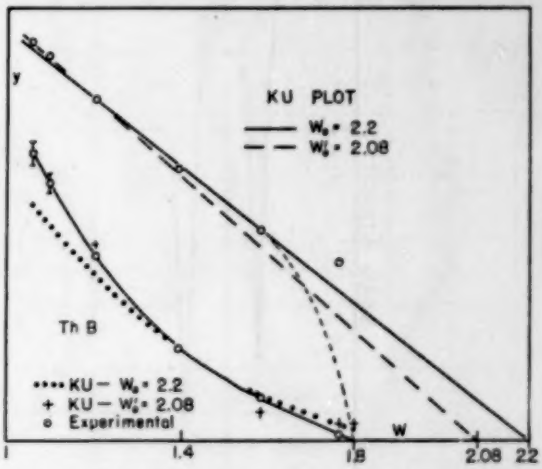

FIG. 2. Konopinski-Uhlenbeck plots and experimental results for ThB.

those obtained when substituting W_0' in the KU theoretical spectrum. The dotted lines show the results obtained by substituting W_0. The existence of the above disagreement has been already pointed out by the author[7] for ThB, RaE and ThC″.

The following conclusions may be drawn:

1. The equation given by Konopinski and Uhlenbeck must be considered as an empirical equation $[f(z,W)(W_0'-W)^4\sim N]$, requiring a suitable choice of the value W_0', distinct from that obtained by extrapolating the KU plots.

2. The assumption that the difference $W_0-(E_0/511+1)$ determines the rest mass of the neutrino, as expressed by certain authors, is not sufficiently justified.

A. ZAVELSKY

L. Tenteleva 24, Apt. 9
Leningrad 95, U.S.S.R.,
December 14, 1938.

[1] E. M. Lyman, Phys. Rev. **51**, 1 (1937).
[2] A. I. Alichanian, A. I. Alichanow and B. S. Dzelepow, Phys. Rev. **53**, 766 (1938).
[3] A. I. Alichanian and S. J. Nikitin, Phys. Rev. **53**, 767 (1938).
[4] E. J. Konopinski and G. Uhlenbeck, Phys. Rev. **48**, 7 (1935).
[5] G. Breit, Rev. Sci. Inst. **9**, 3, 63 (1938).
[6] A. I. Alichanian and A. Zavelsky, C. R. l'USSR, **17**, 467, 469 (1937).
[7] A. Zavelsky, Information at the 3rd All-Union Symposium on Nuclear Problems, in October, 1938 (Russian).

An Electrical Quadrupole Moment of the Deuteron*

The molecular beam magnetic resonance method[1] applied to HD molecules at liquid nitrogen temperature gives the magnetic moment of the proton and the deuteron. When applied to H_2 and D_2 molecules the method reveals the close groups of sharp resonance minima shown in Figs. 1 and 2. The resonance minima for H_2 agree in number and location with predictions based on the assumption of spin-spin magnetic interaction of the two protons $(\mu_1\cdot\mu_2/r^3-3(\mu_1\cdot r)(\mu_2\cdot r)/r^5)$ and a spin-orbit interaction of the protons with the rotation of the molecule $(2\mu_P\bar{H}I\cdot J)$. All symbols here have their usual significance except $\bar{H}$ which is the spin-orbit interaction constant. The only state of the molecule to be considered is the lowest rotational state of orthohydrogen: $J=1$ and total nuclear spin $I=1$. The nine energy levels which arise from these interactions and from the external magnetic field give six possible transitions for the nuclear spin because $\Delta M_N=\pm 1$. The pattern can be accounted for completely on the basis of the known value of the proton moment ($\mu_P=2.78$) with the known value of the internuclear distance and a value for $\bar{H}$ of 27 gauss.

In the case of D_2 the deep central minimum arises from the states with $I=2$ and $J=0$. The six smaller peaks arise from the states with $J=1$ and $I=1$. The states with $J=2$ are not abundant enough at these low temperatures for observation. Since the internuclear distance in the D_2 molecule is the same as in H_2 and the mass is twice as great the spin-orbit interaction constant $\bar{H}$ is half as great. The deuteron magnetic moment ($\mu_D=0.853$) is 0.307 times

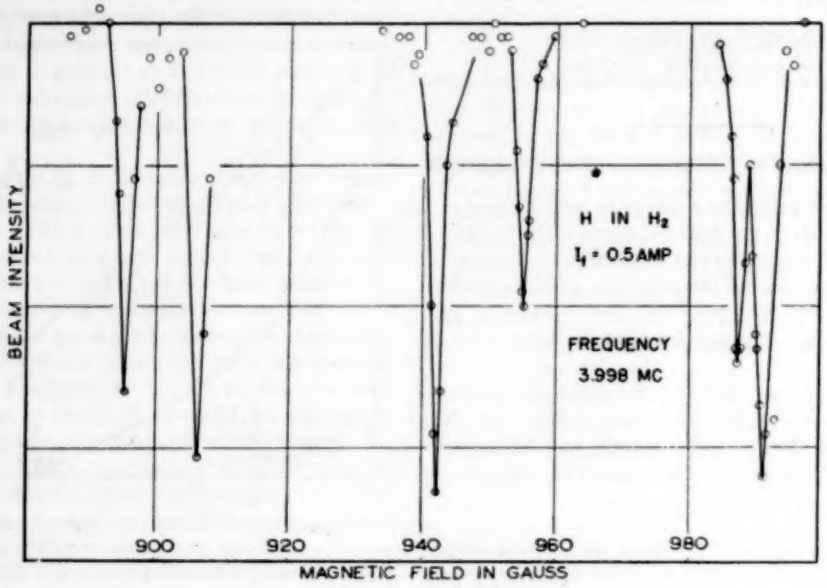

FIG. 1. Resonance minima for H in H_2.

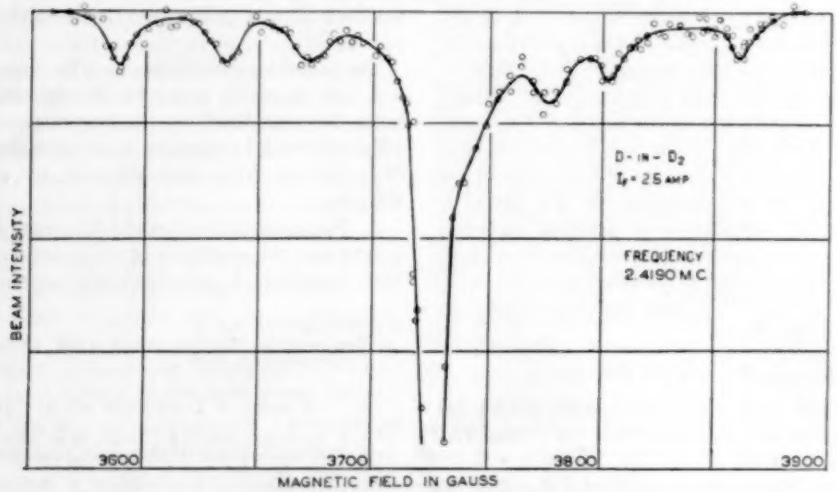

FIG. 2. Resonance minima for D in D_2.

that of the proton and therefore the magnetic spin-spin interaction is proportionately smaller. It was expected that the theory of the resonance minima for H_2 when applied to D_2 should give the locations of the minima from the constants given above. The displacements of the minima from the center should be much less than those of H_2. However experiment shows the displacements to be six times greater than the predicted values.

This effect can be accounted for by the presence of an electrical quadrupole moment in the deuteron. The interaction energy which gives rise to the large displacements is that of the nuclear quadrupole moment with the gradient of the molecular electric field. This form of interaction contributes to the nine energy levels exactly as the spin-spin and therefore appears as a larger spin-spin interaction.

To prove that the large displacements in D_2 are of nuclear origin rather than molecular, similar experiments were performed on the proton and the deuteron in the HD molecule. The group of resonance minima for H was narrow as expected and that for D had large displacements as in D_2. Furthermore, the experimentally evaluated spin-orbit interaction constant for D_2 is one-half as great as that for H_2 as predicted. We therefore believe that the apparent large spin-spin interaction is not magnetic, nor is it of molecular origin and must be a nuclear effect which behaves like a quadrupole moment.

To obtain the magnitude of this quadrupole moment one must know the molecular electric field. This value can be calculated from the various wave functions which have been suggested for the hydrogen molecule. The result of such a calculation by Dr. A. Nordsieck with Wang wave functions when combined with our data yields a quadrupole moment $Q=(3z^2-r^2)_{Av}$ of about 2×10^{-27} cm^2. The chief source of error lies in the inaccuracy of the wave functions.

The sign of the quadrupole moment may also be inferred from our measurements in two ways. Present indications are that it is positive, that is, the charge configuration is prolate along the spin axis. Full details of these experiments will be published later in this journal.

We are greatly indebted to Dr. Nordsieck for making available to us the results of his calculations and to Dr. Brickwedde of the National Bureau of Standards for preparation of the sample of pure HD used in the experiments. The experiments were supported in part by a grant from the Research Corporation.

J. M. B. KELLOGG
I. I. RABI
N. F. RAMSEY, JR.
J. R. ZACHARIAS

Columbia University,
Hunter College (JRZ),
New York, New York,
January 15, 1939.

* Publication assisted by the Ernest Kempton Adams Fund for Physical Research of Columbia University.

[1] J. M. B. Kellogg, I. I. Rabi, N. F. Ramsey and J. R. Zacharias, Bull. Am. Phys. Soc. Vol. 13, No. 7, Abs. 24 and 25.

Thermal Dilatation of Superconductors

In recent years there has been much speculation as to the underlying cause of the superconducting state of metals, and many experiments have been performed to investigate possible abrupt changes in other physical properties of materials in passing through the transition temperature. In 1925 Sizoo and Onnes[1] reported that the application of pressure lowered the transition temperatures for tin and indium, which indicated that metals may expand on passing into the superconducting state. This possibility was investigated by McLennan, Allen and Wilhelm[2] in 1931. They measured the thermal dilatation of lead and Rose's metal in the neighborhood of their respective transition temperatures, but when they plotted the thermal dilatation against the temperature they obtained essentially smooth curves and, hence, concluded that there was no discontinuity in the thermal dilatation at the transition temperature. As recently as 1934[3] and 1935[4] their work was still being quoted as providing evidence that no discontinuity exists in this region. As a matter of fact, when their data are plotted on a magnified scale, as illustrated in Fig. 1, we see that there appears to

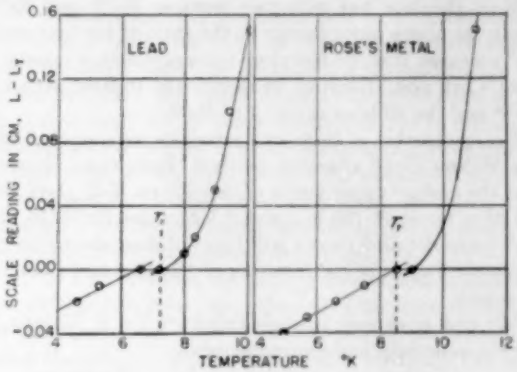

FIG. 1. Thermal expansion curves.

be a discontinuity which is just within the range of resolution of their apparatus. Since the magnitude of the apparent discontinuity is of the order of one unit in their last significant figure, their experiments cannot be accepted as definitely demonstrating its existence. The mutual consistency of the two curves, however, does seem to indicate that the discontinuity is real, and makes it appear desirable to repeat the experiment with somewhat more refined apparatus and to obtain a larger number of points in the immediate neighborhood of the transition temperature. From their report, the Toronto group seem to have pushed the sensitivity of the optical lever almost to its limit, however, there is the possibility of developing other methods such as one involving the displacement of interference fringes for monochromatic light reflected from mirrors attached to the ends of a superconducting metal rod.

E. C. WESTERFIELD

University of Colorado,
Boulder, Colorado,
May 12, 1938.

[1] G. J. Sizoo and H. Onnes, Communications from the Physical Laboratory of Leiden, No. 180b.
[2] J. C. McLennan, J. F. Allen and J. O. Wilhelm, Trans. Roy. Soc. Canada **25**, Sec. 3, 1–12 (1931).
[3] E. F. Burton, *Superconductivity* (Toronto, 1934).
[4] H. G. Smith and J. O. Wilhelm, Rev. Mod. Phys. **7**, 240 (1935).

β-Radioactivities of Rhenium

On bombarding rhenium with slow neutrons, Fermi and his co-workers[1] found a β-activity with half-life 20 hours, and Kurtschatow and his collaborators[2] obtained 20-hour and 85-hour activities. Pool, Cork and Thornton[3] found that the bombardment of rhenium gives rise to an 18-hour period, which they ascribed to Re^{186} obtained through neutron loss Re^{187} $(n,2n)$ Re^{186}.

We repeated the experiments by bombarding metallic rhenium with slow neutrons (through paraffin) from Be+D and fast neutrons from Li+D (up to about 17 Mev) produced in the cyclotron in our laboratory. In both cases we obtained activities having half-lives 16 hours and 90 hours, respectively, which correspond to the two periods above-mentioned. The ratio, however, of the initial intensities corrected for the infinite activation time, or $R = I(90\text{ hr.})/I(16\text{ hr.})$, was 1.2 for slow neutrons from Be+D and 17 for fast neutrons from Li+D.

Now rhenium has only two isotopes Re^{185} and Re^{187}. From the above large change in the ratio of the intensities for two cases, it seems therefore more probable, contrary to Pool, Cork and Thornton, to ascribe the 16-hour period to Re^{185} and the 90-hour activity to Re^{186}.

Energy spectra of these two activities were studied with the Wilson cloud chamber method. Both emit electrons and the energy upper limits reduced from K-U plots were 1.2 Mev for Re^{186} (90 hr.) and 2.5 Mev for Re^{185} (16 hr.).

A more detailed report will be published shortly in the Scientific Papers of the Institute of Physical and Chemical Research.

We wish to express our best thanks to Dr. Y. Nishina for his valuable help and encouragement.

K. SINMA
F. YAMASAKI

Nuclear Research Laboratory,
Institute of Physical and Chemical Research,
Tokyo, Japan,
December 29, 1938.

[1] E. Fermi *et al.*, Proc. Roy. Soc. **149**, 522 (1935).
[2] B. Kurtschatow *et al.*, Physik. Zeits. Sowjetunion **8**, 589 (1935).
[3] M. L. Pool, J. M. Cork and R. L. Thornton, Phys. Rev. **52**, 239 (1937).

The Effect of Hydroxyl Ion Concentration (or of pH) on the Film Potentials of Multilayers

When an *X* multilayer of calcium stearate is built upon a subphase of metal, the resultant increment of film potential may be as high as 100 Mv per layer if the aqueous subsolution upon which the monolayer is spread initially is made alkaline to a *p*H of 9.4 by the addition of ammonia.[1] With potassium ions instead of ammonium ions the film potentials are lower, and of the order of 60 Mv per layer.[2]

An experiment carried out by us in March, 1938, gave evidence of the effect of *p*H upon film potentials and suggested the more definite work described in this letter. In the earlier experiment the *p*H of the aqueous subsolution was brought to 9.4 by the use of ammonia, but this is volatile. As long as the *p*H was close to 9.4, the increment of potential per layer due to the taking up of positive ions by the outside of the multilayer was of the order of 85 Mv, but when the *p*H fell below this, the film potential also dropped, and in some instances to zero. If after such a drop the *p*H was restored to 9.4, the increment of the film potential was immediately restored to a large value, as for example 300 Mv per layer. (The increase in magnitude above 100 Mv per layer is due to an increased thickness of the multilayer underneath.)

In order to secure additional and conclusive evidence it seemed that *X* films should be built at a low *p*H if possible. An interruption in the work gave us the advantage that during this interval Goranson and Zisman discovered how to produce *X* films on ebonite at a *p*H of 6.3, and it seemed that their technique could be used for deposition upon a metal.

In our work the speed of dipping was 5 cm per minute, with an interval of 30 seconds between each down and up trip but only a short interval when the slide was in the air. Several trends are evident in Fig. 1.

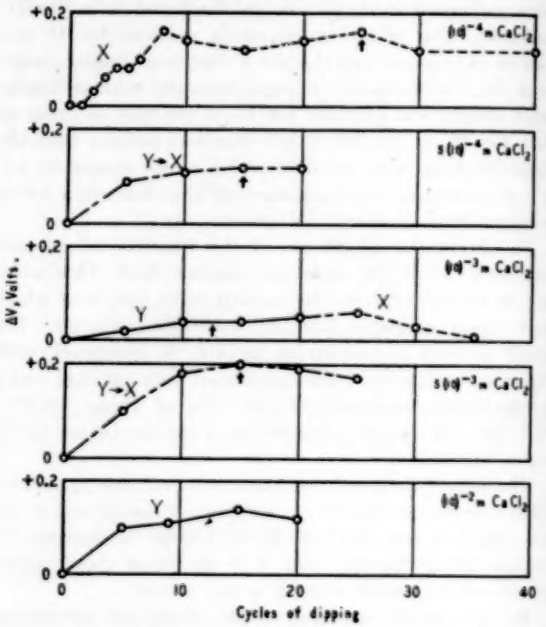

FIG. 1. Variation of film potentials with number of layers. ———— *Y* deposition; —— — —— *Y* changing to *X* deposition; — — — — — *X* deposition. The arrow marks the optical thickness at which the film gave an orange interference color with the electric vector of polarized white light perpendicular to the plane of incidence and with the angle of incidence about 80°.

(1) The film potentials of the calcium stearate *X* multilayers on gold at *p*H 6.3 do not increase linearly with the number of layers, but reach a value of about +0.1 or +0.2 volt in a few layers, as with the *Y* type of deposition. After this the increment per *X* layer is almost zero (±). For similar *X* layers on ebonite at this *p*H, Goranson and Zisman report a charge which increases rapidly with the number of layers.

(2) At a *p*H of 6.3, $(10)^{-4}$m $CaCl_2$ gives the *X* type of deposition; $(10)^{-3}$m $CaCl_2$ gives the *Y* type of deposition. An intermediate molarity gives a deposition which may start with the *Y* type and change over to the *X* type. The contact angle changes continuously from about 0° to about 90° as the type of deposition changes from *Y* to *X*.

The increase in calcium concentration has no definite effect on the film potential at this low *p*H.

(3) The experiments described in this letter, when compared with those at a *p*H of 9.4, prove that the *p*H of the solution is one of the primary factors which determine the film potential.

The data of Langmuir and Schaefer[3] indicate that our monolayer at $(10)^{-4}$m Ca^{++} consists of 27 molecules of stearic acid to 73 of calcium stearate. We have used still higher concentrations of the ion in the solution to increase its proportion in the film. It is of interest to determine the relation between the concentration of the hydroxyl ion in the solution, the Ca^{++} ion in the monolayer, and the film potential of the *X* multilayer.

WILLIAM D. HARKINS
RICHARD W. MATTOON

George Herbert Jones Laboratory,
University of Chicago,
Chicago, Illinois,
January 14, 1939.

[1] William D. Harkins and Richard W. Mattoon, Phys. Rev. **53**, 911 (1938).
[2] Eliot F. Porter and Jeffries Wyman, Jr., J. Am. Chem. Soc. **60**, 1083 (1938).
[3] Irving Langmuir and Vincent J. Schaefer, J. Am. Chem. Soc. **58**, 284 (1936).

Chemical Separation of Nuclear Isomers

Many examples of nuclear isomers are now known, and it is of interest to have methods to find possible genetic relationships between the isomeric states of the same nucleus. For instance, this can be readily accomplished by standard methods if the lower level has a longer life than the upper. But for the opposite case the problem is much more difficult because a transient equilibrium is reached soon and the only apparent period is that of the parent.

An actual *separation* of two genetically related isomers of a nucleus can be performed by the following artifice in some cases: Consider the case in which the element having the isomers can give compounds suitable for the application of the Szilard-Chalmers[1] method of concentration and prepare initially such a compound from a mixture of the two isomers. When the isomer in the upper state decays to the lower state the nucleus emits a gamma-ray and recoils. The energy of recoil may be sufficient to knock the decayed atom out of the compound and the daughter activity may then be separated as in the Szilard-Chalmers method.

However, if the energy of the transition gamma-ray is of the order of magnitude of 100 kv, as one might expect,[2-4] the recoil for elements of medium and high atomic weight would not be sufficient to break an ordinary chemical bond. Fortunately the gamma-ray is highly internally converted and the recoil from the conversion electron is higher than that from the corresponding gamma-ray so that recoil energies comparable to chemical bond energies are obtained.

Even if the recoil energy is insufficient to break the bond, the method does not necessarily fail because the energy given to the bond may suffice to create an activated condition within the molecule such that it may undergo chemical reaction upon collision with some other kind of molecule deliberately introduced for this purpose. The daughter activity will then be found in the product of the chemical reaction.

We have used this method to separate the 18-minute and 4.4-hour isomers of Br^{80}. The separation was fairly complete and showed definitely that the 18-minute period is formed from the 4.4-hour period.

About one liter of ethyl bromide was irradiated for three hours with slow neutrons from the Berkeley cyclotron and the radioactive bromine was removed as solid sodium bromide. Radioactive tertiary butyl bromide was synthesized by saturating tertiary butyl alcohol with hydrobromic acid generated from the sodium bromide. Five grams of the butyl bromide were introduced into 200 cc of aqueous methyl alcohol (75 mole-percent methyl alcohol) at 0°C where it underwent chemical reaction with both the methyl alcohol and the water liberating hydrobromic acid. In this manner the butyl bromide molecules which contain a bromine nucleus which has recoiled can react to liberate hydrobromic acid. Under the experimental conditions chosen this type of activation occurs much more frequently than the spontaneous activation due to thermal agitation, and hence there is a large enrichment of the radioactivity of the lower isomeric state (18 minutes) in the reaction products. The chemical reaction was allowed to proceed for about three times the radioactive half-life of the lower state and then, after first extracting the unreacted butyl bromide with benzene, silver bromide was precipitated from the aqueous methyl alcohol.

In Fig. 1, *a*, is shown the decay curve of such a concentrate effected four hours after the end of the bombardment. The first reading was taken 27 minutes after the precipitation of the silver bromide. The activity evidently has two periods, a short one of 18-minute half-life shown in curve *b*, due to the recoil atoms, contaminated with an activity

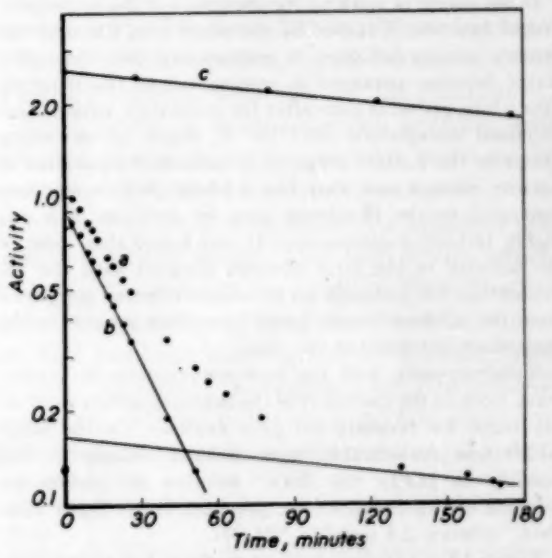

FIG. 1. (*a*) Decay curve of bromine extracted from 4-hour activity of Br^{80}. (*b*) Curve *a* corrected for long-lived tail (18-minute half-life). (*c*) Decay curve of the bromine activity from which the extraction was made.

decaying in the same manner as the starting substance, whose decay is shown in curve *c*. This small long-lived tail, which we followed for 24 hours, arises from the bromide liberated in the spontaneous chemical reaction. By repeating the experiment, but with an elapse of 26 hours between the end of the bombardment and the beginning of the chemical reaction, a decay very similar to curve *a* was obtained. These two runs also showed that the upper state (parent substance) was decaying with a half-life of approximately four hours. By comparing curves *b* and *c*, and by taking into account that curve *b* started 27 minutes after the end of the chemical reaction, it can be seen that most of the nuclei in the upper state decay by falling to the lower state from which the observed disintegration electrons are emitted.

DeVault and Libby have applied our method of separation to other bromine compounds and will report their findings shortly.

We wish to thank Professor E. O. Lawrence for his interest and encouragement in this work. Thanks are also due to the Research Corporation for continued support.

E. SEGRÈ
R. S. HALFORD
G. T. SEABORG

Radiation Laboratory,
Department of Physics,
Department of Chemistry,
University of California,
Berkeley, California,
January 13, 1939.

[1] L. Szilard and J. A. Chalmers, Nature **134**, 462 (1934).
[2] W. Weizsäcker, Naturwiss. **24**, 813 (1936).
[3] B. Pontecorvo, Phys. Rev. **54**, 542 (1938).
[4] E. Segrè and G. T. Seaborg, Phys. Rev. **54**, 772 (1938).

Evidence for Gamma-Radioactivity of 4.5-hour Br^{80} from Radiobromate

In the course of work on the chemistry of the decomposition of bromoform caused by the recoil from the neutron-capture gamma-radiation, it was noticed that the radioactive bromine persisted in coming out of the molecule over a long period of time after the irradiation ceased. This remained unexplained until Dr. E. Segrè (cf. preceding Letter to the Editor) proposed a method of separation of nuclear isomers and that the 4.5-hour Br^{80} isomer was converted to the 18-minute form by emission of a soft highly forbidden gamma-ray. It was found that most of the activity in the later extracts decayed with the 18-minute half-life although no 18-minute bromine not grown from the 4.5-hour isomer could have been present in the bromoform extracted at the time.

Simultaneously with the later experiments on bromoform, work on the chemistry of the neutron-capture gamma-ray recoil for bromate ion gave evidence for the effect which was considerably more definite because it was possible to purify the BrO_3^- solution completely for bromine of lower valence by precipitation of AgBr from BrO_3^- solution 2.5 molal in NH_4OH.

Figure 1A is a typical decay curve for a AgBr precipitate

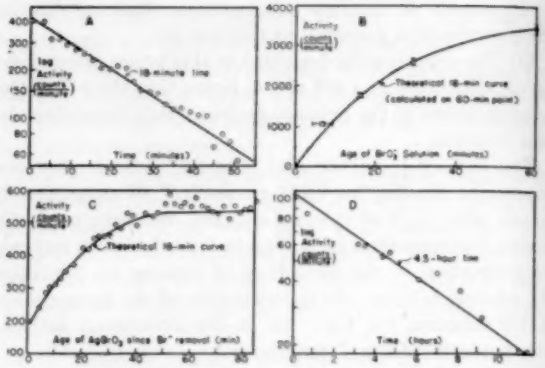

FIG. 1. Growth and decay curves. A, decay of AgBr precipitate; B, growth curve for AgBr precipitates; C, growth curve for $AgBrO_3$ purified for Br^-; and D, decay of AgBr activity with 4.5-hour mother BrO_3^-.

obtained from a mother BrO_3^- solution which had stood several hours so the 18-minute activity originally present when removed from the neutron source (200 mg $RaBr_2$+Be powder) could have been present to less than five percent of the activity found. Apparently very little of the 4.5-hour activity was present in these precipitates. Figure 1B is a plot of the activities of AgBr precipitates obtained from a single mother BrO_3^- solution which had stood various times since its last purification for Br^-. The solid line is the theoretical 18-minute growth curve. Figure 1C is a plot of the activity of a $AgBrO_3$ precipitate (obtained by acidifying the ammoniacal solution) which was purified for Br^- at zero time. The solid line is the 18-minute growth superimposed on an initial activity of 160 counts per minute. This initial activity must have been due to 18-minute Br^{80} still remaining in the BrO_3^- after the activation by the kick from the electron ejected by the converted soft gamma-ray or to beta-radiation from the 4.5-hour body itself, or to both. However, the curve does show that unless the 4.5-hour beta-rays are softer than about 500 kv (this was determined by the thickness of the sample and the wall of the counter) at least 75 percent of the 4.5-hour body must decay by the gamma-emission process. Further, in view of the fact that experiments with BrO_3^- showed the efficiency of the much more powerful neutron gamma-ray recoil in destroying the ion to be only 80 percent approximately, it seems probable that most, if not all, of the initial 25 percent activity is due to retention of 18-minute activity in the BrO_3^- rather than to 4.5-hour beta-emission. Of course this indicates that the 4.5-hour body is practically a pure gamma-ray emitter, unless it has beta-radiation softer than about 500 kv.

Figure 1D shows the activities of AgBr precipitates obtained at various times from a given mother BrO_3^- solution. The solid line is the theoretical 4.5-hour decay curve.

DON C. DEVAULT
W. F. LIBBY

Department of Chemistry,
University of California,
Berkeley, California,
January 14, 1939.